

**Synthesis of ZnO Nanorods by Microwave Irradiation of Precursor Solution and
Study of their Process Parameters**

by

Munira Sultana

MASTER OF PHILOSOPHY IN PHYSICS



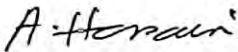
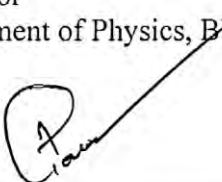
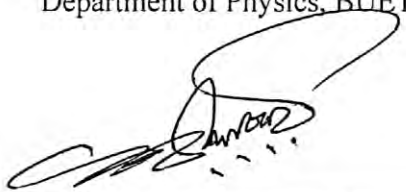
Department of Physics

BANGLADESH UNIVERSITY OF ENGINEERING AND TECHNOLOGY

June, 2021

The thesis titled “Synthesis of ZnO Nanorods by Microwave Irradiation of Precursor Solution and Study of their Process Parameters” submitted by Munira Sultana, Roll No.: 0417143010P, Session: April 2017, has been accepted as satisfactory in partial fulfillment of the requirement for the degree of MASTER OF PHILOSOPHY IN PHYSICS on 30 June, 2021.

BOARD OF EXAMINERS

- 
1. Dr. Mohammad Jellur Rahman (Supervisor)
Associate Professor
Department of Physics, BUET, Dhaka-1000
Chairman
- 
2. Dr. Md. Rafi Uddin
Professor and Head
Department of Physics, BUET, Dhaka-1000
Member
(Ex-officio)
- 
3. Dr. A. K. M. Akther Hossain
Professor
Department of Physics, BUET, Dhaka-1000
Member
- 
4. Dr. Md. Feroz Alam Khan
Professor
Department of Physics, BUET, Dhaka-1000
Member
- 
5. Muhammad Shahriar Bashar
Principal Scientific Officer
Institute of Fuel Research & Development
Bangladesh Council of Scientific and Industrial Research
Dhaka-1205
Member
(External)

CANDIDATE'S DECLARATION

It is hereby declared that this thesis or any part of it has not been submitted elsewhere for the award of any degree or diploma.

.....

Munira Sultana

Acknowledgements

At the very first, I express my satisfaction to praise the almighty Allah who has given me the strength and opportunity to complete my thesis work success.

It is my privilege to offer my heartiest gratitude and profound respect to my supervisor Dr. Mohammad Jellur Rahman, Associate Professor, Department of Physics, Bangladesh University of Engineering Technology (BUET), for providing me the opportunity to work in such an emerging field of research. I am indebted to him for his continuous guidance, suggestions and kind supervision throughout the research work. His boundless enthusiasm, ambition and innovative thoughts for scientific problems inspired me in pursuing the whole investigation. I consider myself lucky to be a member of his team.

I am grateful to Professor Dr. Md. Rafi Uddin, Head of the Department of Physics for his kind permission for providing me the necessary facilities and administrative support to carry out this research work. I am also thankful to all other faculty members of the Department for giving inspiration during the work.

I would like to acknowledge sincerely the financial support provided by the Committee for Advanced Studies and Research (CASR), BUET, to fulfill this research work.

I would like to thank all of my fellow lab mates. Working with them during all these years has truly been a wonderful experience. I would like to especially thank Md. Mahmud Hasan for his constant help and support.

I would take the opportunity to express my appreciation to Solar Energy Technology Laboratory, Bangladesh Council of Industrial Research (BCSIR), for the dedicated support in this research work regarding the characterization of the samples.

Finally, I would like to extend my sincere thanks to all my family members for their unlimited love and blessing. This dissertation would never have been possible without their moral support and affection.

Abstract

Zinc oxide (ZnO) nanorods in the form of hexagonal prismatic shape have been successfully synthesized by a simple one step microwave assisted irradiation process using a customized domestic microwave oven. The effects of different process parameters such as microwave power, precursor reagents, synthesis time, precursor concentration etc. have been studied. The morphological, structural and optical properties of the ZnO nanorods are studied using scanning electron microscopy, powder X-ray diffraction and UV-Visible spectroscopies. ZnO nanorods with the smallest diameter of 300 nm has been synthesized using zinc nitrate precursor. The average diameter increases from 300 to 500 nm and the average length varies from 1.8 to 3.5 μm with the increase in precursor concentration and synthesis time. The best length to diameter ratio of the synthesized ZnO nanorods was obtained with an optimum concentration of 15 mM and synthesis time of 20 min using the customized system with basic precursor solution. All the samples have strong absorption in the UV region and the band gap values varies between 3.28 to 3.30 eV, very near to the standard value of 3.40 eV for ZnO at room temperature. XRD spectra confirms the hexagonal wurtzite structure of the ZnO nanorods and EDAX study confirms their purity. The nanorods has a higher dielectric constant value at room temperature in the lower frequency region, which decreases with increasing frequency.

CONTENTS

	Page No
Candidate's Declaration	iii
Acknowledgements	iv
Abstract	v
Contents	vi
List of Figures	viii
List of Tables	xiii
List of Abbreviations	xiv

CHAPTER 1 INTRODUCTION

1.1 Introduction	1
1.2 Objectives	3
1.3 Outline of the Thesis	4

CHAPTER 2 LITERATURE REVIEW AND THEORETICAL ASPECTS

2.1 Literature Review on Synthesis of ZnO Nanostructures	5
2.2 Basic Growth Mechanisms	18

CHAPTER 3 EXPERIMENTAL DETAILS

3.1 Synthesis of ZnO	21
3.1.1 Preparation of precursor solutions	21
3.1.2 Microwave treatment	23
3.1.3 Sample collection	25
3.2 Analysis Techniques	25
3.2.1 Scanning electron microscopy	25
3.2.2 X-ray diffraction	27

3.2.3	Energy dispersive X-ray spectroscopy	29
3.2.4	Ultraviolet-visible spectroscopy	30
3.2.5	Dielectric properties	32

CHAPTER 4

RESULTS AND DISCUSSION

4.1	Surface Morphology	34
4.1.1	Effect of microwave power	34
4.1.2	Effect of precursor	41
4.1.3	Precursor concentration effect	42
4.1.4	Effect of synthesis time	47
4.1.5	Effect of surfactant	52
4.1.6	Effect of heat treatment	53
4.2	Elemental Analysis	54
4.3	Structural Property	58
4.4	Optical Property	61
4.5	Dielectric Property	64

CHAPTER 5

SUMMARY AND CONCLUSIONS

5.1	Summary	67
5.2	Conclusions	69
5.3	Future Scopes	69
	References	70

List of Figures

Figure No.		Page No.
Fig. 2.1	Illustration of the growth mechanism of fluorine doped ZnO at different Au sputtering times (a) 10 s, (b) 15 s, and (c) 20 s.	5
Fig. 2.2	Morphology of the synthesized nanostructure varies with pH of the precursor.	6
Fig. 2.3	ZnO nanorods grown on Si substrate with seed layer.	7
Fig. 2.4	SEM images of ZnO nanorods grown in (a) 75 mM, (b) 0.1 M, and (c) 0.2 M solution, at fixed preheating and post-heating time of 10 min each. The insets reveal the cross section of the ZnO nanorods.	7
Fig. 2.5	SEM image of the ZnO nanorods synthesized in presence of anionic surfactant.	8
Fig. 2.6	White light emission due to excitation with blue light.	9
Fig. 2.7	Room temperature PL spectrum of different morphologies of ZnO. (a) Nanoparticles, (b) Nanorods and (c) Nanosheet.	9
Fig. 2.8	UV–Vis absorption spectra of different morphologies of ZnO. (a) Nanoparticles, (b) Nanorods, and (c) Nanosheets and in the inset (blue shift).	10
Fig. 2.9	Absorption spectra of ZnO nanorods with different pH values.	11
Fig. 2.10	SEM images and diameter of hexagonal ZnO nanorods grown at 90°C various concentrations (a) 15, (b) 20, (c) 25, (d) 30 and (e) 35 mM precursor concentration for 180 min.	11
Fig. 2.11	PL spectra of the ZnO nanorods at room temperature.	12
Fig. 2.12	EDX spectrum for the ZnO nanorods generated at 20 min of reaction time showing presence of Si.	13
Fig. 2.13	SEM image of nanoforest synthesized using microwave irradiation.	14
Fig. 2.14	Aspect ratio of ZnO structures as a function of time exposure for different (a) microwave power inputs and (b) furnace temperatures.	14
Fig. 2.15	SEM images of pristine ZnO NCs obtained via (a) conventional synthesis and (b) microwave-assisted route.	15

Fig. 2.16	Antibacterial activity of ZnO/QR nanohybrids, <i>E. coli</i> are exposed to 80 µg/ml ZnO/QR.	16
Fig. 2.17	SEM image of free-standing ZnO nanowires formed on a SnO ₂ substrate by electrodeposition.	17
Fig. 2.18	Phase stability diagrams for the ZnO (s)-H ₂ O system at 25 °C as a function of precursor concentration and pH.	19
Fig. 3.1	Schematic diagram of the customized microwave oven for synthesis of ZnO nanorods.	21
Fig. 3.2	Photograph of the customized microwave oven.	22
Fig. 3.3	Placement of hard paper board at proper height.	23
Fig 3.4	Locating the hot spot position within the microwave chamber, the exact hotspot location on the hard paper board.	23
Fig. 3.5	Different steps of the synthesis process: (a) filtered solution before microwave treatment, (b) white solution after microwave treatment, (c) finally collected sample after repeating same process (at least three times).	24
Fig. 3.6	Schematic diagram of a scanning electron microscope with the steps of image formation.	26
Fig. 3.7	A schematic representation of Bragg's law.	28
Fig. 3.8	The structural as well as phase identification measurements were carried out by an X-ray diffractometer (GBC-XRD, EMMA) with a step size of 0.02 deg. using a Cu_K _{α1} (λ = 1.54062 Å) radiation source operated at 35.5 kV and 28 mA.	28
Fig. 3.9	Morphological and elemental analysis were done by a SEM with EDX (Carl Zeiss, EVO 18).	30
Fig. 3.10	A schematic diagram of an UV-Visible spectrophotometer.	31
Fig. 3.11	The optical measurements were made using an UV-VIS-NIR (Hitachi, UH4150) spectrophotometer coupled with an integrating sphere.	32
Fig. 3.12	The dielectric property was measured using an impedance analyzer (Wayne Kerr, 6500B series).	33
Fig. 4.1	Morphology of the synthesised nanorods using ZAH at 50% microwave power.	34

Fig. 4.2	SEM images of the synthesized ZnO nanorods using ZAH precursor at (a) 30% and (b) 50% microwave power.	35
Fig. 4.3	SEM images ZnO nanorods formed by heating an equimolar (50 mM) mixture of HMT and ZAH at 70% microwave power.	36
Fig. 4.4	SEM images ZnO nanorods formed by heating an equimolar (50 mM) mixture of HMT and ZNH at 30% microwave power.	36
Fig. 4.5	SEM images ZnO nanorods formed by heating an equimolar (50 mM) mixture of HMT and ZNH, (a) at 50%; (b) at 70% microwave power.	37
Fig. 4.6	Particle size distribution for (a, c, e) diameter and (b, d, f) length of ZnO nanorods formed by heating an equimolar (50 mM) mixture of HMT and ZAH (a) and (b) at 30%; (c) and (d) at 50%; (e) and (f) at 70% microwave power.	38
Fig. 4.7	Particle size distribution for (a, c, e) diameter and (b, d, f) length of ZnO nanorods formed by heating an equimolar (50 mM) mixture of HMT and ZNH (a) and (b) at 30%; (c) and (d) at 50%; (e) and (f) at 70% microwave power.	39
Fig. 4.8	The average (b) length and (a) diameter of ZnO nanorods formed by heating an equimolar (50 mM) mixture of HMT and ZAH using different microwave power.	40
Fig. 4.9	The average (a) length and (b) diameter of ZnO nanorods formed by heating an equimolar (50 mM) mixture of HMT and ZNH using different microwave power.	40
Fig. 4.10	Variation of aspect ratio with microwave power.	40
Fig. 4.11	SEM image of ZnO nanorods formed by heating an equimolar (50 mM) mixture of HMTA and (a) ZAH, (b) ZNH, with 50% microwave power.	42
Fig. 4.12	SEM images ZnO nanorods formed by heating an equimolar mixture of HMT and ZNH with (a) 5 mM and (b) 10 mM precursor concentration.	43
Fig. 4.13	SEM images ZnO nanorods formed by heating an equimolar mixture of HMT and ZNH, (a) 15 mM; (b) 50 mM precursor concentration.	44

Fig. 4.14	Particle size distribution of ZnO nanorods formed by heating an equimolar mixture of HMT and ZNH, (a) and (b) 5 mM; (c) and (d) 10 mM; (e) and (f) 15 mM; (g) and (h) 50 mM precursor concentration.	45
Fig. 4.15	The average (a) length and (b) diameter of ZnO nanorods of ZnO nanorods formed by heating an equimolar mixture of HMT and ZNH with different precursor concentration.	46
Fig. 4.16	Variation of aspect ratio with precursor concentration.	46
Fig. 4.17	SEM images ZnO nanorods formed by heating an equimolar mixture of HMT and ZNH for (a) 5 min; (b) 7 min.	48
Fig. 4.18	SEM images ZnO nanorods formed by heating an equimolar mixture of HMT and ZNH for (a) 10 min; (b) 20 min.	49
Fig 4.19	SEM images ZnO nanorods formed by heating an equimolar mixture of HMT and ZNH for 30 min.	50
Fig. 4.20	Particle size distribution of (a, c) diameter and (b, d) length of the ZnO nanorods formed by heating an equimolar mixture of HMT and ZNH for (a) and (b) 5 min, (c) and (d) 7 min.	50
Fig 4.21	Particle size distribution: Variation of (e, g, i) diameter and (f, h, j) length of the ZnO nanorods formed by heating an equimolar mixture of HMT and ZNH for (e) and (f) 10 min; (g) and (h) 20 min; (i) and (j) 30 min.	51
Fig. 4.22	The average (a) diameter and (b) length of ZnO nanorods of ZnO nanorods formed by heating an equimolar mixture of HMT and ZNH for different synthesis time.	51
Fig. 4.23	Variation of aspect ratio with synthesis time.	52
Fig. 4.24	Effect of addition of surfactant on the morphology of the ZnO nanorods.	53
Fig. 4.25	Effects of heat treatment on the size of ZnO nanorod: (a) as synthesized, and treated at (b) 500 °C (c) 700 °C (d) 900 °C.	54
Fig. 4.26	Elemental analysis of the ZnO nanorods synthesized using ZAH at (a) 30%, (b) 50% and (c) 70% microwave power.	55
Fig. 4.27	Elemental analysis of the ZnO nanorods synthesized using ZNH at (a) 30%, (b) 50% and (c) 70% microwave power.	56

Fig. 4.28	Elemental analysis of the ZnO nanorods synthesized different synthesis time: (a) 5 min, (b) 7 min, (c) 10 min, (d) 15 min, (e) 20 min and (f) 30 min.	57
Fig. 4.29	XRD spectra of the ZnO nanorods synthesized (a) with different precursors, (b) at different concentrations.	59
Fig. 4.30	XRD spectra of the ZnO nanorods synthesized for different synthesis time.	60
Fig. 4.31	UV-visible spectra of the ZnO nanorods obtained from different microwave powers.	62
Fig. 4.32	UV-visible spectra of the ZnO nanorods obtained from different (a) precursor concentrations and (b) synthesis time.	63
Fig. 4.33	Variation of dielectric constant of the ZnO nanorods with frequency.	65
Fig. 4.34	Variation of dielectric loss of the ZnO nanorods with frequency.	66

List of Tables

Table 4.1	Average length and diameter of ZnO nanorods after adding surfactant.	52
Table 4.2	Elemental analysis of the nanorods produced using ZAH precursor with varying microwave power.	54
Table 4.3	Elemental analysis of the nanorods produced using ZNH precursor with different microwave power.	55
Table 4.4	Elemental analysis of the ZnO nanorods with varying synthesis time.	57
Table 4.5	Different structural parameters of the ZnO nanorods obtained from XRD studies.	60
Table 4.6	Energy band gap of the ZnO nanorods.	64

List of Abbreviations

PL	Photoluminescence
UV	Ultraviolet
HMTA	Hexamethylene Tetraamine
ZNH	Zinc Nitrate Hydrated
ZAH	Zinc Acetate Hydrated
SEM	Scanning Electron Microscope
CRT	Cathode Ray Tube
NA	Numerical Aperture
KeV	Kilo Electron Volt
XRD	X-ray Diffraction
EDX	Energy Dispersive X-ray
Vis	Visible range
LED	Light Emitting Diode
CCD	Charge-couple Device
NIR	Near Infrared Range
JCPDS	Joint Committee on Powder Diffraction Standards
FWHM	Full Width at Half Maximum

CHAPTER 1

INTRODUCTION

1.1 Introduction

Zinc oxide (ZnO) is a promising photonic material for UV blue devices like short wavelength light emitting and laser diodes. It shows a high degree of surface activity leading to potential applications in the field emission displays, gas sensors, nano resonators, nano cantilevers, etc., which have important applications in nano systems and biotechnology [1–4]. Some important properties ZnO such as the electronic structure, conductivity, melting temperature, mechanical properties, etc. can be modified by controlling the size of the particles. However, the major challenges in synthesis of such nanocrystals are to control their size, shape and morphology. ZnO can be formed into a wide variety of nanostructures such as nanorods, nanowires, nanotubes, etc. using a range of growth techniques and therefore opening a wide door for potential applications [5–9]. Several methods ranging from vapor phase processes to solution route have been investigated for the synthesis of ZnO nanostructures [10–13]. Solution-based techniques include a low-cost benchtop alternative to vapor phase processes and are more attractive for its commercial scale-up. It is also possible to introduce additives like surfactants to control the reaction conditions. But, these solution-based hydrothermal processes usually require longer synthesis time ranging from 1.5 to 17 hours. [14–17]. Sahoo et al. [14] synthesized undoped and Mg doped ZnO nanorods by sol gel and hydrothermal method. Undoped and 5% Mg doped ZnO nanorods were grown on cleaned glass substrates by simple low-cost spin coating technique followed by a low temperature hydrothermal method with 5 hours synthesis time. Napi et al. [15] sputter deposited the gold nanoparticles on glass substrates before hydrothermal reaction to reduce the synthesis time and it was reported that gold nanoparticles could reduce the synthesis time notably. Whereas, Zhao et al. [16] varied the pH of precursor solution and they found that the morphology of the nanostructures changes with pH of the solution. The precursor solution was transferred into a Teflon-lined stainless steel autoclave and heated at 120 °C. Jang et al. [17] varied the pH of the precursor solution within a range of 9.0 – 11.8 and also observed the optical and structural properties of the synthesized nanostructures. They reported that, ZnO

nanostructures were fabricated at $\text{pH} > 10.0$ had good optical properties and low defect content. The hydrothermal reaction was carried on at 95°C for 2 hours. All these processes have long synthesis time, which may hinder their commercialization. As an alternative of the chemical baths the microwave-assisted heating process can drastically reduce the time required for the synthesis of ZnO micro and nanostructures.

The effect of process parameters on the size distribution of ZnO nanostructure and related variation in their photoluminescence (PL) property was studied by several researchers [18–20]. Zhu et al. [18] successfully synthesized high density ZnO-nanorod arrays (rod length $1.59\ \mu\text{m}$) via a microwave-assisted solution-phase method using zinc chloride and ammonia solution as reactants. In this process, a laboratory purpose microwave oven was used for microwave irradiation and the synthesis time ranges from 10 to 40 min only. The influence of concentration of ammonia solution, work power, and microwave irradiation time on the morphology and size of final products were carefully investigated in this report. The room temperature photoluminescence spectrum of the synthesized ZnO-nanorod arrays shows a blue emission at 469 nm. Rana et al. [19] used a domestic microwave oven (850 watts, 2.45 GHz) for the growth of ZnO nanostructures. They designed a pressurized reaction vessel from the quick synthesis of ZnO nanorods. This customized reaction vessel helps to raise solution temperature well above the boiling point and the synthesis time was only few minutes.

Fang and Liu [20] synthesized (002) oriented ZnO nanorod arrays with different diameters and lengths on silicon substrate via the rapid microwave-assisted hydrothermal method with the help of magnetron sputter deposited ZnO seed layer. The size and surface density of the nanorods can be controlled individually by adjusting process parameters including precursor concentrations, heating temperature, and heating time. They reported that, the photoluminescence performance of the nanorods is closely dependent on the mean size of the rods. Also, reducing rod diameter leads to decreased UV emission and visible emission intensity ratio, which has been attributed to the increased impurities or defects on the nanorod surface.

ZnO nanorods were also synthesized via seed mediated microwave assisted method [21,22], microwave assisted single step precipitation [23,24] or as films onto different substrates [25,26]. Most of these microwave-assisted reactions were demonstrated

using laboratory purpose microwave reactors with controlled temperature and power level modes. Those microwave reactors consist of circular cavity, containing a waveguide that delivers single-mode microwaves with high energy density for uniform sample heating. On the other hand, domestic ovens have multimode heating property with hot and cold spots within the microwave oven chamber. In a microwave oven, the microwaves from the transmitter are reflected by the metallic walls of the oven, which creates standing wave with nodes and antinodes. Therefore, high and low electric field intensity spots are formed inside the microwave oven. Food on a carousel has to be rotated to minimize the effect of cold spots. The high electric field intensity causes hotter spots compared to the low intensity spots. A substance gets heated by the microwaves due to the collision among the molecular dipoles. Therefore, the polar solvents like water or alcohol get heated more rapidly. Researchers reported the synthesis of ZnO nanorods using expensive single mode microwave reactors [20,23], which required higher energy density per unit volume of the sample. Though, in some studies cost-effective domestic microwave assisted methods to synthesis ZnO nanostructures were discussed [27,28], the highest possible energy density positions were not identified to get the best cost benefit ratio. If the hot spot within the microwave chamber can be identified, effective heating of the reaction vessel could be ensured. Along with proper customization of the domestic microwave oven, efficient synthesis of ZnO nanorods at a very short synthesis time would be possible.

1.2 Objectives

Objectives of this research are-

- To develop a facile single-step and cheap method to synthesis ZnO nanorods.
- To synthesis ZnO nanorods of high aspect ratio with high surface activity via microwave assisted chemical route.
- To observe the surface morphology of the synthesized ZnO nanorods.
- To measure the diameter and length of the nanorods.
- To study the effect of different process parameters including precursor concentration, temperature and synthesis time on the size of the nanorods.

1.3 Outline of the Thesis

- The basic properties of the ZnO are described in **Chapter 1**. A brief introduction to the background and motivation for this research work are discussed. Also, how this research work is different and unique compared to the previous relative research work are clarified. Main objectives of investigation are also discussed.
- In **Chapter 2**, literature review on the previous research work on the synthesis of ZnO nanorods are presented. Moreover, the basic growth mechanisms of ZnO nanorods in hydrothermal method are described using step by step chemical reactions.
- The experimental setup, the method of customization of a domestic microwave oven for microwave irradiation are described in **Chapter 3**. Detail about the experimental steps is provided. A brief introduction to the characterization techniques is also discussed.
- In **Chapter 4**, different properties of the prepared ZnO nanorods are presented, which are investigated with different characterization techniques.
- **Chapter 5** includes the summary and conclusions of this research work with possible fields of their applications. Also, a number of future works are suggested.

CHAPTER 2

LITERATURE REVIEW AND THEORETICAL ASPECTS

2.1 Literature Review on Synthesis of ZnO Nanostructures

Napi et al. [15] discovered a synthesis method for fluorine doped ZnO that is easier to grow with shorter reaction time. For that the gold nanoparticles were sputter deposited (10 s, 15 s, and 20 s) on the glass substrates before hydrothermal reaction (3 hours, 6.5 hours, and 10 hours). It is clear from Fig. 2.1 that Au nanoparticles grown with longer sputter deposition time facilitates the growth of higher density of fluorine doped ZnO nanorod. Also, Au nanoparticles could promote the growth of nanorods in shorter time.

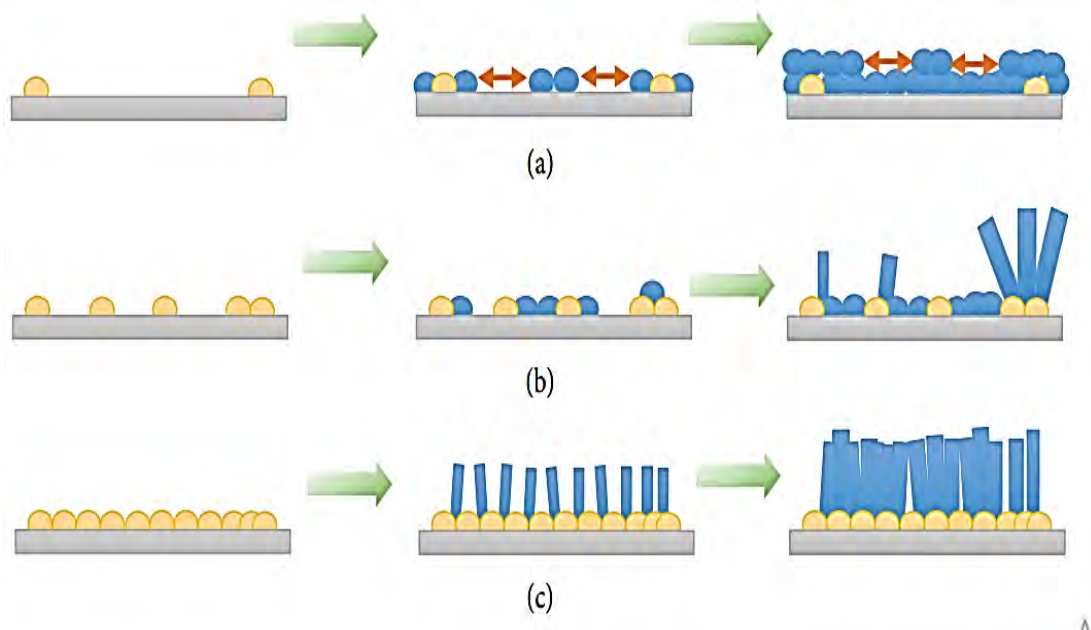


Fig. 2.1: Illustration of the growth mechanism of fluorine doped ZnO at different Au sputtering times (a) 10 s, (b) 15 s, and (c) 20 s [15].

Zhao et al. [16] reported that, ZnO microstructures varied with pH (from 11 to 14) of the precursor solution. Fig. 2.2 shows the synthesized ZnO microstructures with twining-hexagonal prism, twining-hexagonal disk, sphere, flower-like shape. These different shaped ZnO microstructures were obtained using 17 hours long hydrothermal processes.

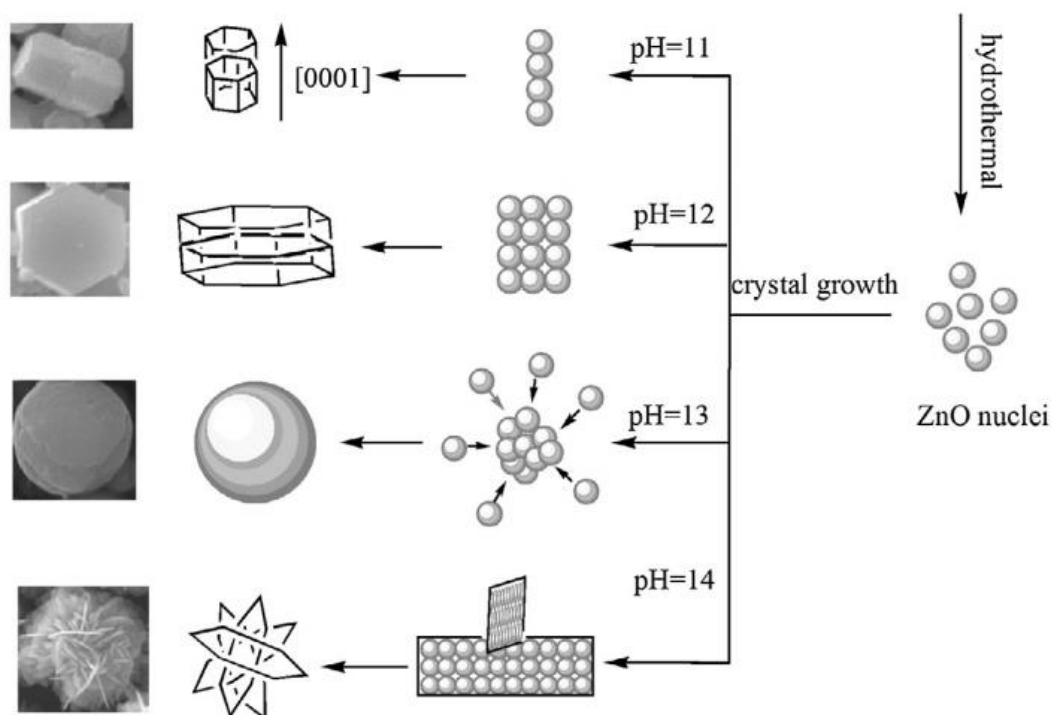


Fig. 2.2: Morphology of the synthesized nanostructures varies with pH of the precursor [16].

Microwave assisted synthesis of ZnO nanostructures became famous, as it can reduce the synthesis time for hydrothermal process from several hours to few minutes only. Fang et al. [20] successfully prepared ZnO nanorod arrays with different diameters and lengths. For that, a seed layer was fabricated on silicon substrate before microwave assisted synthesis of ZnO nanorods. The size and surface density of the nanorods can be controlled individually by adjusting process parameters including precursor concentrations, temperature and heating time. They used WX-4000 microwave digestion system and heated the precursor solution at various temperatures from 60 to 110°C for various time from 5 to 40 min. Fig. 2.3 shows the SEM image of the synthesized ZnO nanorods.

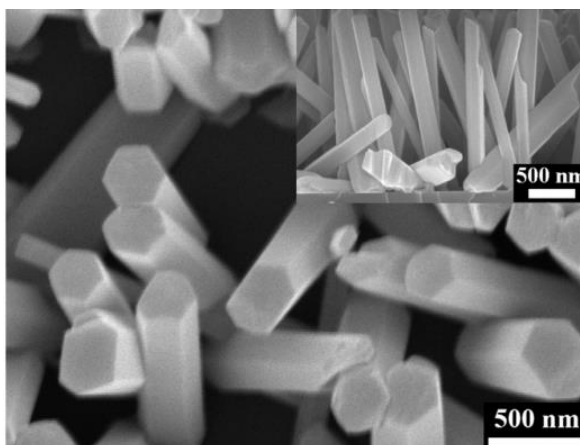


Fig. 2.3: ZnO nanorods grown on Si substrate with seed layer [20].

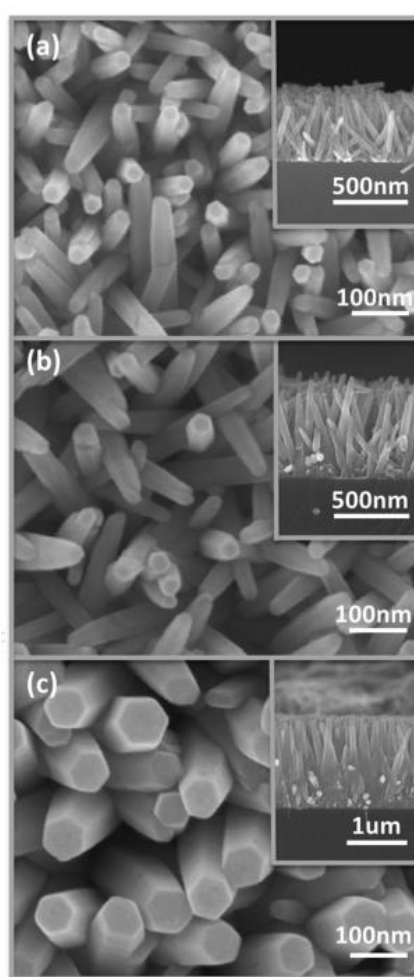


Fig. 2.4: SEM images of ZnO nanorods grown in (a) 75 mM, (b) 0.1 M, and (c) 0.2 M solution, at fixed preheating and post heating time of 10 min each. The insets reveal the cross section of the ZnO nanorods [21].

Chae et al. [21] presented a microwave-assisted growth of ZnO nanorods using a preheating hydrothermal method under tailored preheating and post heating growth

conditions. The parameters such as solution concentration, preheating time, and post heating time, were changed to optimize ZnO nanorods growth. Fig. 2.4 shows the variation in morphology of the synthesized ZnO nanorods with solution concentration with fixed preheating and post heating time.

Barreto et al. [23] reported that, addition of an anionic surfactant, sodium di-2-ethylhexyl-sulfosuccinate (AOT) to the reaction media allowed the synthesis of smaller particles and a significant increase in UV absorption, and a well-defined maximum at 374 nm was observed. They also used a laboratory purpose microwave reactor as a source of microwave irradiation. The synthesis time varied from 5 to 20 min, instead of hours. Fig. 2.5 shows the SEM image of ZnO nanorods synthesized in presence of sodium di-2-ethylhexyl-sulfosuccinate.

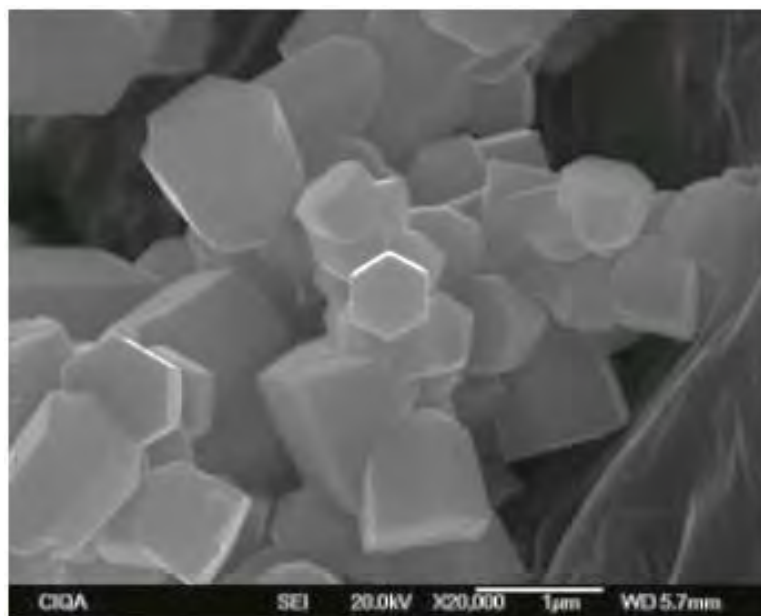


Fig. 2.5: SEM image of the ZnO nanorods synthesized in presence of anionic surfactant [23].

The reactor was placed inside a 2.45 GHz domestic microwave oven with disc rotation of 4 rpm. Brahma et al. [25] fabricated ZnO coatings (1-3 μm) with a short synthesis time (1-5 min) using microwave irradiation from a domestic microwave oven (2.45 GHz). The growth process is simple, economic, less cumbersome, environmentally benign, and that uses environment friendly precursors as starting materials. The coatings obtained are uniform over the entire area of the substrate and the density of nucleation and the growth rate are significantly high. Luminescence could be tuned from strong visible light emission to an enhanced UV emission, when the nature of

surfactants varies from polymeric to ionic and nonionic. White light emission could be achieved from these ZnO coatings by exciting with a blue laser, as shown in Fig. 2.6.

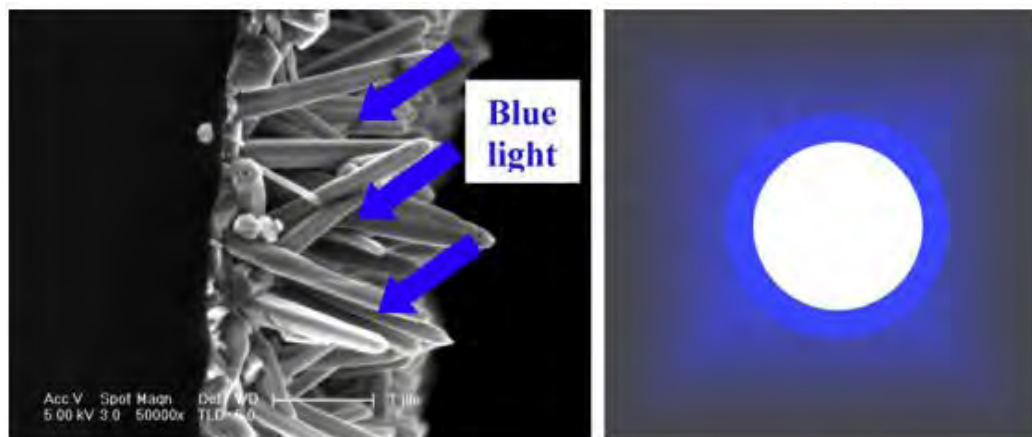


Fig. 2.6: White light emission due to excitation with blue light [25].Fig.

Agarwal et al. [29] synthesized nanoparticles, nanorods, nanosheet using hydrothermal process in an oven for 24 hours. They have discovered that the optical properties can be tuned by changing the size and morphology of ZnO nanostructures.

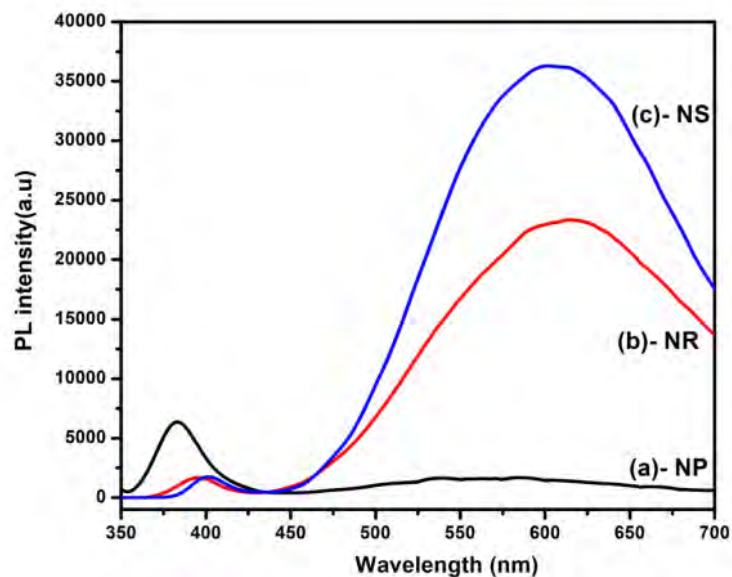


Fig. 2.7: Room temperature PL spectrum of different morphologies of ZnO. (a) Nanoparticles, (b) Nanorods and (c) Nanosheet [29].

It was clearly observed from the PL spectrums in Fig. 2.7, the luminescence intensity was maximum in the UV region for nanoparticles. Whereas, the maximum intensity for nanorods or nanosheets is found in the visible region. The UV–Vis absorption results show a blue shift in the characteristic absorption peaks, shown in Fig 2.8 and there is also a decrease in the crystallite size of the nanostructures. The optical band gap was calculated and was found to increase with a decrease in average crystallite size, attributed to the quantum confinement effect. It is also observed from the results that the optical properties are strongly affected by the size, morphology as well as by the synthesis methods of ZnO nanostructures.

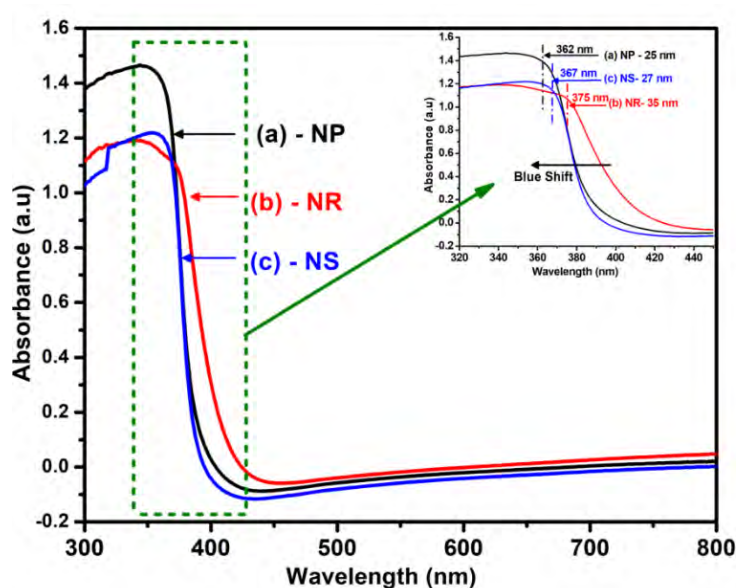


Fig. 2.8: UV–Vis absorption spectra of different morphologies of ZnO. (a) Nanoparticles, (b) Nanorods, and (c) Nanosheets and in the inset (blue shift) [34].

Alver et al. [30] were successful to grow ZnO nanorod array on glass substrate using hydrothermal process. They reported that, due to higher precipitation rate, at pH 4 and 10 no film deposition was observed on glass slides. Hydrothermal growth was carried out at 95 °C in a sealed beaker placed on a hotplate for 2 hours and then cooled down to room temperature. Fig. 2.9 shows that pH does not influence too much the band gap energy of the ZnO rod arrays. The size of the ZnO nanorods strongly depends on pH of the precursor solution. Kurda et al. [31] deposited a ZnO seed layer on glass substrate before growing ZnO nanorod array using hydrothermal process. The ZnO seed layer deposited on glass was immersed in the solution, where the glass was face down, and the reaction vessel was kept at 90°C for 60, 90, 120, 150, 180 min.

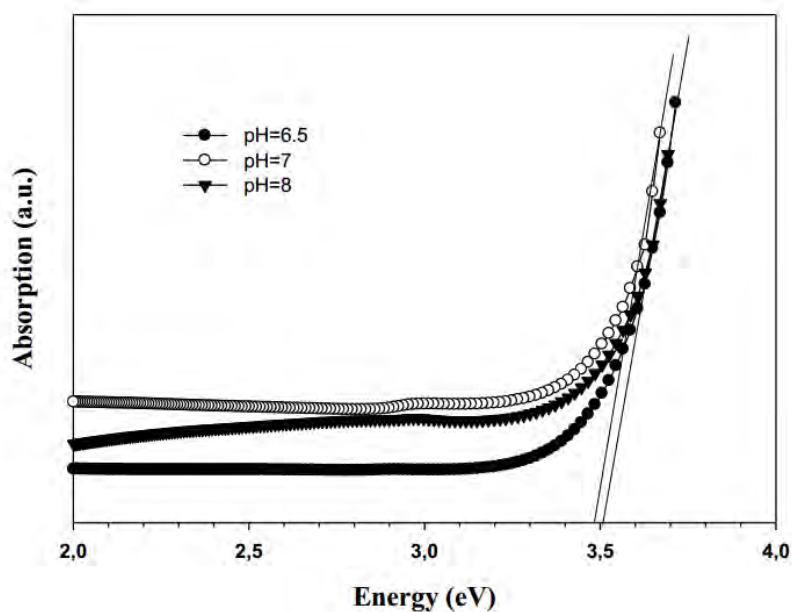


Fig. 2.9: Absorption spectra of ZnO nanorods with different pH values [30].

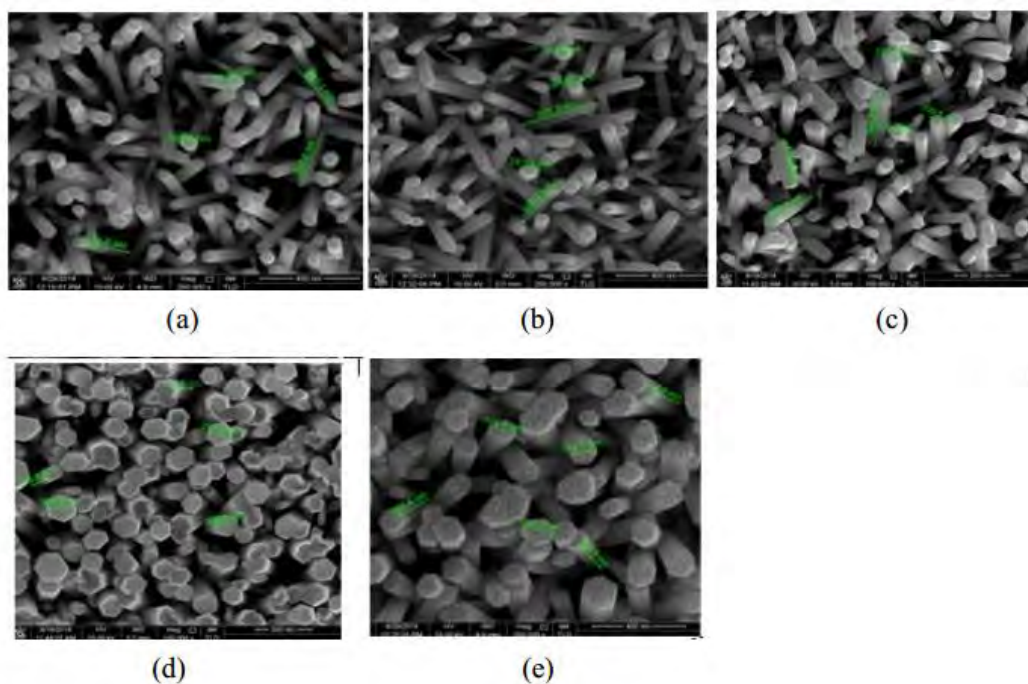


Fig. 2.10: SEM images and diameter of hexagonal ZnO nanorods grown at 90°C various concentrations (a) 15, (b) 20, (c) 25, (d) 30 and (e) 35 mM precursor concentration for 180 min [31].

The average diameter and average length of the ZnO nanorods obtained from the FESEM. They observed that the average diameter and length strongly depends on the precursor concentration and synthesis time. Fig. 2.10 shows how the precursor concentration effects the average diameter of the synthesized ZnO nanorods. In this

case, precursor concentration was varied from 15 to 35 mM keeping the synthesis time fixed at 180 min.

Yuan et al. [32] fabricated ZnO nanorods on the ZnO seed layers coated ITO substrates ranging in various times from 1.5 to 5 hours. have been fabricated from aqueous solutions at low temperature. They found that the diameter of ZnO nanorods increased with increasing growth time below 3 hr. The maximum optical transmission in the visible for the well-aligned ZnO nanorod arrays grown in 1.5 hours. was obtained. Whereas, Lin et al. [33] synthesized ZnO nanorods on Si substrates by performing a hydrothermal process for 13 hours. They used bare Si substrates without any ZnO seed layer on it and discovered a successful process for the growth of ZnO nanorods.

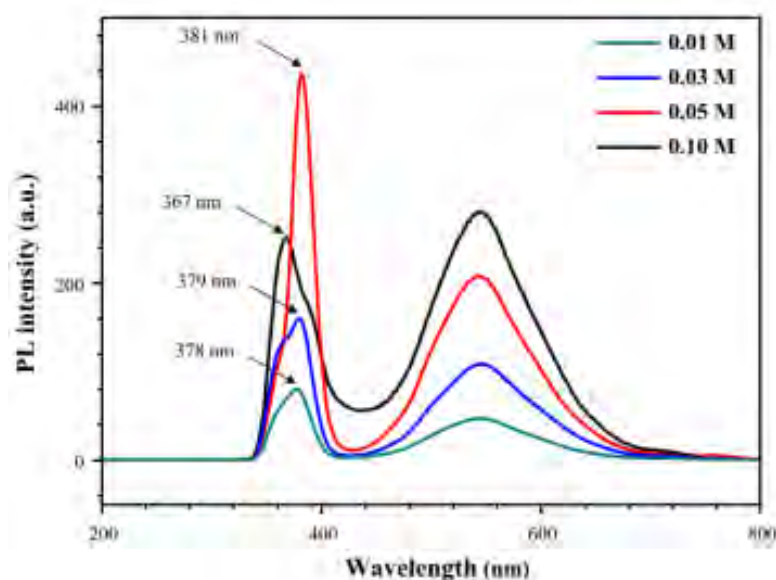


Fig. 2.11: PL spectra of the ZnO nanorods at room temperature [33].

Fig. 2.11 shows PL spectra in arbitrary unit measured from the ZnO nanorods synthesized with four different precursor concentrations using this process; a UV band and a very broad visible band falling into the region between 480 and 600 nm can be observed.

Majithia et al. [39] used single mode microwave cavity of the CEM Discover system for microwave irradiation. In single mode microwave reactor, the sample is placed at the antinodes of the standing electromagnetic wave. A contactless IR sensor and the

Intelligent pressure device, each of which are integrated in the CEM Discover system, are used to monitor temperature and pressure respectively in the reaction vessel [34].

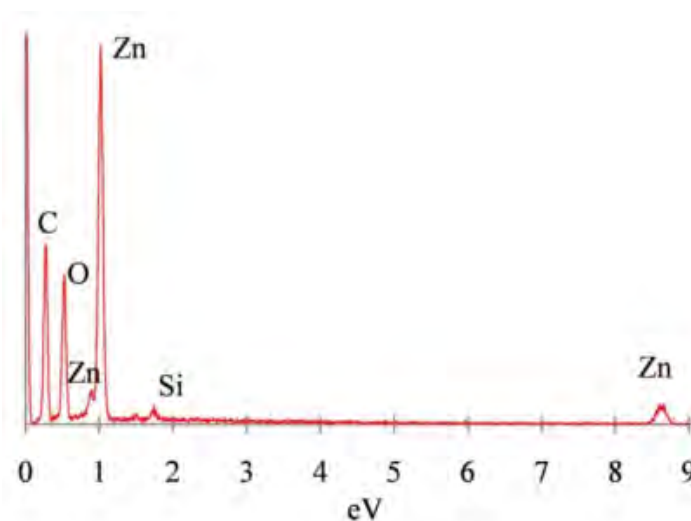


Fig. 2.12: EDX spectrum for the ZnO microstructures generated at 20 min of reaction time showing presence of Si [34].

Results presented in this work also show presence of zinc silicate caps on ZnO microstructures, which is confirmed from the EDX spectra in Fig. 2.12. In the current system, longer reaction times could be used for the synthesis of nanofilms of hemimorphite (zinc silicate hydroxide), a material with interesting optoelectronic properties. The generation of zinc silicates can be avoided at lower temperatures (~ 100 °C). However, high-quality faceted ZnO microstructures were generated only at higher temperatures of 170 °C.

Some researcher tried to use domestic microwave oven for microwave irradiation to make the synthesis process cost effective. As, the domestic ovens are designed to serve different purpose, they have certain limitations during laboratory purpose use. Customization of domestic oven usually done to minimize the limitations and to ensure efficient heating of the precursors. Ghosh et al. [35] used a microwave assisted process that takes less than 4 hours, whereas conventional two step hydrothermal synthesis of nanoforest takes 25 h to attain comparable dimensions. They fabricated well-spaced and thinner nanorod arrays with controlled conditions in microwave assisted synthesis to enable branch formation. Rapid and uniform seed deposition to main rods by forced seeding method was successfully used, as shown in Fig. 2.13. This seeding technique required only 5 min whereas dipping technique requires at least an hour.

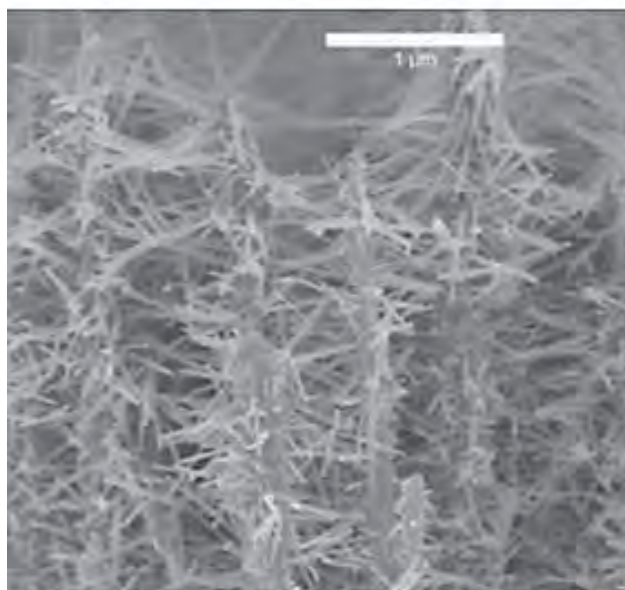


Fig. 2.13: SEM image of nanoforest synthesized using microwave irradiation [35].

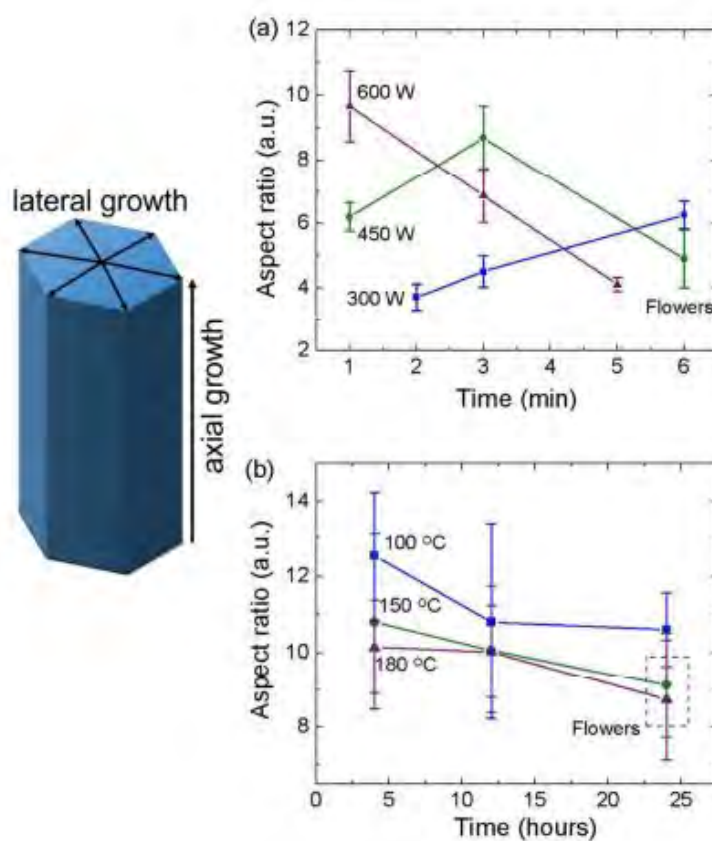


Fig. 2.14: Aspect ratio of ZnO structures as a function of time exposure for (a) different microwave power inputs and (b) furnace temperature [36].

ZnO nanorod arrays were grown on a seed layer deposited using spin coating method on Si substrates. The seed layer was annealed before hydrothermal process and the

growth was carried out in a domestic 850 W microwave oven. Preheated solution was utilized as an accelerator to increase the aspect ratio of the ZNRs and reduce the fabrication time. Pimentel et al. [36] reported a comparative study of the synthesis of ZnO nanostructures using either microwave irradiation with low cost domestic microwave equipment and conventional heating, both under hydrothermal conditions. Fig. 2.14 shows the variation of aspect ratio with synthesis time for both synthesis methods.

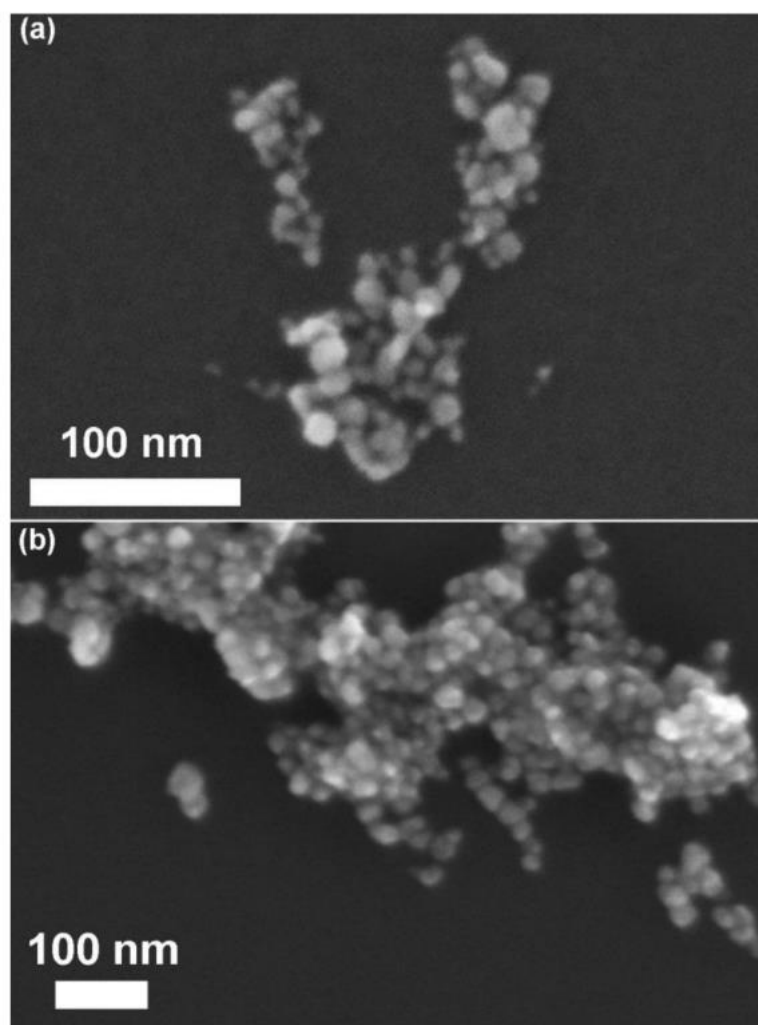


Fig. 2.15: SEM images of pristine ZnO NCs obtained via (a) conventional synthesis and (b) microwave-assisted route [37].

The similarities between the physical properties of the ZnO nanostructures synthesized under both routes indicate that microwave synthesis is time and energy saving methodology which can be largely employed for the production of ZnO nanostructures with a high potential for practical applications. Garino et al. [37] synthesized colloidal

ZnO nanocrystals (ZnO NCs) using microwave irradiation and optimized for biological applications as shown in Fig. 2.15. They also prepared ZnO NCs using conventional hydrothermal approach and compared the properties of the two families of NCs. After that through a deep statistical analysis, it was in fact possible to estimate that the ZnO NCs, obtained via microwave synthesis, show more reproducible and reliable results for biological application.

Yalcin produced ZnO nanoflakes (ZnO-Nfs) by using microwave-assisted techniques and investigated their dielectric properties. These ZnO-Nfs can be used gas and humidity sensing applications [38].

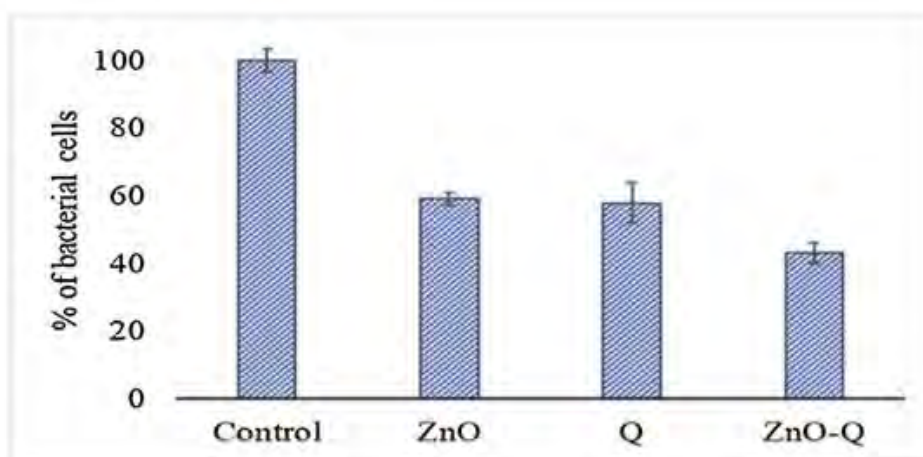


Fig. 2.16: Antibacterial activity of ZnO/QR nanohybrids, *E. coli* are exposed to 80 $\mu\text{g/ml}$ ZnO/QR [39].

Sadhukhan et al. [39] reported a method for microwave-induced synthesis of fluorescent ZnO nanorods and their usage as a cargo material to carry hydrophobic drug, quercetin. In this study, it was found that ZnO/QR can induce profound cytotoxic effect via the combinatorial ROS enhancement effects of ZnO and free QR in cancer cells. Apart from its anticancer effect, ZnO and ZnO/QR showed profound antibacterial activity. The bar diagram in Fig. 2.16 shows the comparative antibacterial activity.

In some studies researchers showed how to control the density of the seeded ZnO nanowire arrays for applications such as field emission [40,41], and direct current nanogenerators [42,43]. In simple terms, controlling the seed layer thickness can control the nanowire density [40–43]. Zheng et al. [44] used Electrochemical deposition technique for achieving uniform large area synthesis of ZnO

nanostructures, because it exerts a strong external driving force to make the reactions take place, even if they are non-spontaneous. Izaki et al. [45] showed that, the growth of ZnO nanostructures can occur on a general substrate, flat or curved, without any seeds, as long as the substrate is conductive. Yu et al. [46] discovered effect of an external electric field and observed better nanowire alignment and stronger adhesion to the substrate have been observed.

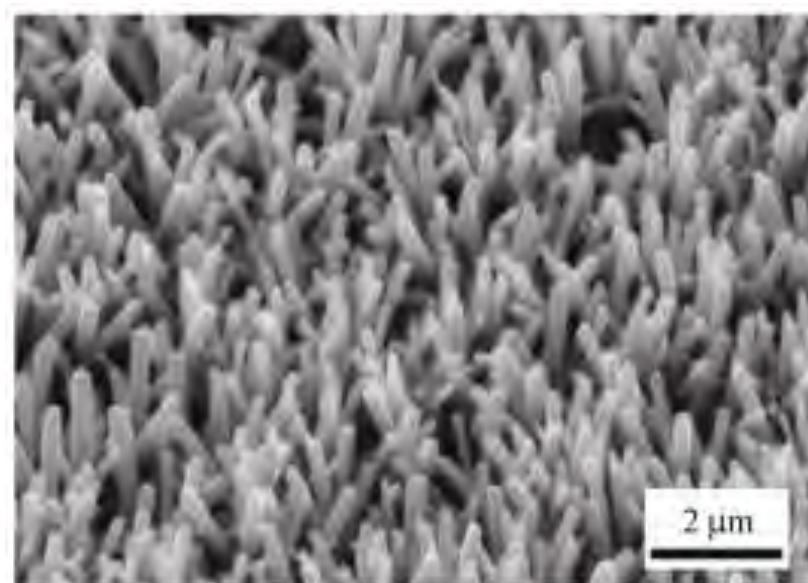


Fig. 2.17: SEM image of free-standing ZnO nanowires formed on a SnO₂ substrate by electrodeposition [47].

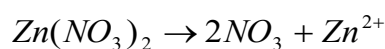
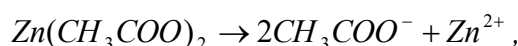
ZnO nanowires can be grown by electrodeposition methods in combination with templates. Anodic aluminium oxide (AAO), polycarbonate membranes, nano-channel glass, and porous films self-organized from di-block copolymers are most commonly used templates. Zheng et al. [47] used anodic aluminium membrane (AAM) as template due to its simplicity and capability of large area fabrication. The template can be chemically dissolved after nanowire growth, leaving behind the free-standing nanowires (shown in Fig. 2.17).

Conventional hydrothermal process is the most common method for synthesis of ZnO nanostructure. Hydrothermal is a chemical reaction-based process and ZnO nanostructures can be easily synthesized by heating the precursor solution. Another main advantage of wet chemical methods is that, using ZnO seeds in the form of thin films or nanoparticles. ZnO nanowires with high density were synthesized on ZnO seeds [48–51]. ZnO nanowires can be also grown on arbitrary substrates, such as Si

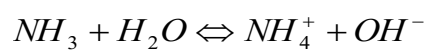
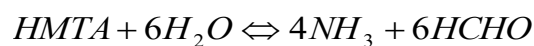
wafers flat [48] and pillar array [49], polydimethylsiloxane (PDMS) [50], fibres [51], [52]. Also, it is very easy to add any surfactant or chemical agent to control the reaction condition as well as size and morphology of the synthesized ZnO nanostructures.

2.2 Basic Growth Mechanisms

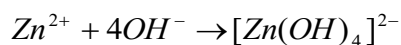
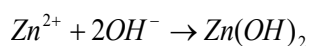
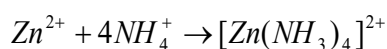
When zinc source precursor is added into distilled water, it dissociates into zinc ion, Zn^{2+} , as follows:



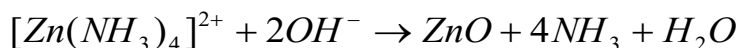
These Zn^{2+} ions provided by $Zn(CH_3COO)_2$ or $Zn(NO_3)_2$ required for building up the ZnO nanorods. In this facile synthesis method use hexamethylene tetramine (HMTA) and NH_3 is the product of the decomposition of HMTA. Later, NH_3 hydrolyses into ammonium ions, NH_4^+ and hydroxide ions, OH^- .



NH_3 produces a basic alkaline environment that is necessary for the formation of $Zn(OH)_2$. It coordinates with Zn^{2+} to stabilize the aqueous Zn^{2+} . The Zn^{2+} ions react with OH^- and NH_4^+ ions and depending on the concentration of Zn^{2+} and pH value, may lead to the formation of tetraaminezincate ions $[Zn(NH_3)_4]^{2+}$, zinc hydroxide $[Zn(OH)_2]$ or tetrahydroxozincate ions $[Zn(OH)_4]^{2-}$ [53].



ZnO nuclei are crystallised when heated using microwave [20,23, 27,28], as a result of the reaction of $[Zn(NH_3)_4]^{2+}$ complex ions and OH^- ions.



$[Zn(OH)_4]^{2-}$ have an octahedral geometry, start to agglomerate in the solution. When the aggregates reach around 150 ions, wurtzite-structured ZnO domains are nucleated in the central region of the aggregates. Thus, the core of aggregate comprises Zn^{2+} and O^{2-} ions only, while the surface still mainly consists of Zn^{2+} and OH^- ions. A nanometre-sized core of the wurtzite-structured ZnO comes into play when around 200 ions aggregates.

Further growth carry on as a result of dehydration of Zn^{2+} and OH^- ions [53].

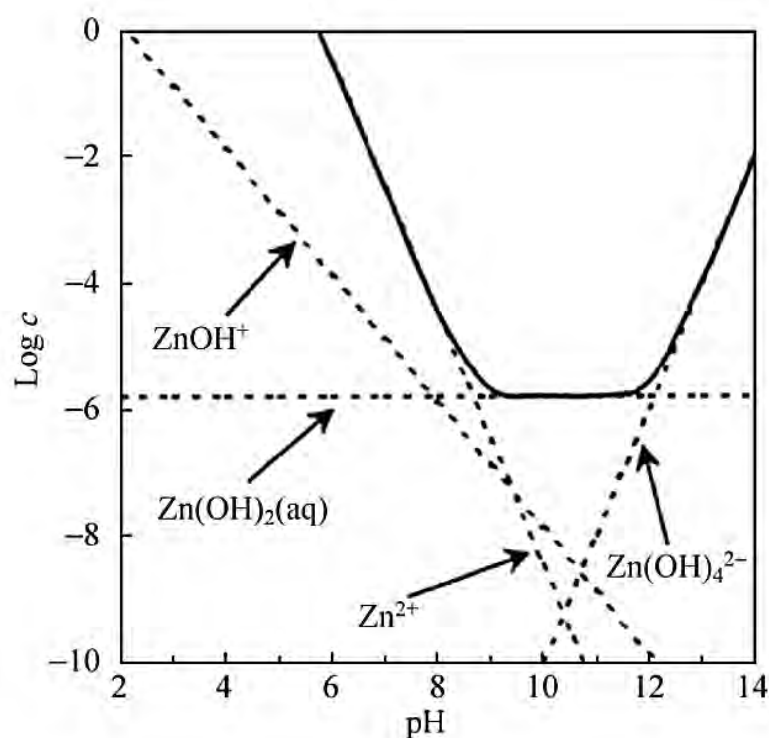
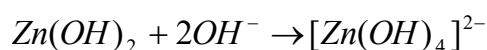
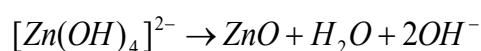


Fig. 2.18: Phase stability diagrams for the ZnO (s)–H₂O system at 25 °C as a function of precursor concentration and pH [54].

When more ammonia is available in the solution, more OH^- ions and NH_4^+ ions leads to the formation of ZnO [55].

The wurtzite structure of ZnO grown along the c-axis has high-energy polar planes, i.e., $\pm(0001)$, with alternating Zn^{2+} -terminated and O^{2-} -terminated surfaces [53]. As a

result, the available growth units easily adsorb on these high-energy polar surfaces. Such a process is repeated over time, leading to a fast growth along the $\pm[0001]$ directions. As no complexing agent was used to alter the growth direction, it can be assumed that ZnO nanorods are synthesised at the preferential growth direction in $[0001]$ [53]. Phase stability diagrams for the ZnO (s)–H₂O system at 25 °C as a function of precursor concentration and pH is shown in Fig. 2.18, where the dashed lines denote the thermodynamic equilibrium between the Zn²⁺ soluble species and the corresponding solid phases [54].

CHAPTER 3

EXPERIMENTAL DETAILS

3.1 Synthesis of ZnO

3.1.1 Preparation of precursor solutions

In this experiment a very low-cost microwave oven (Model: P90D23ATP-Q8Eco+) is used, which can facilitate 10 power levels to be adjusted. Fig. 3.1 shows the schematic diagram of the customized microwave oven. A two-neck quartz bottle was used as sample vessel, one neck was used to connect with condenser and the other was used to insert a K-type thermocouple to record the temperature. The sample vessel was associated with a condenser to prevent the dry out of solvent during synthesis process.

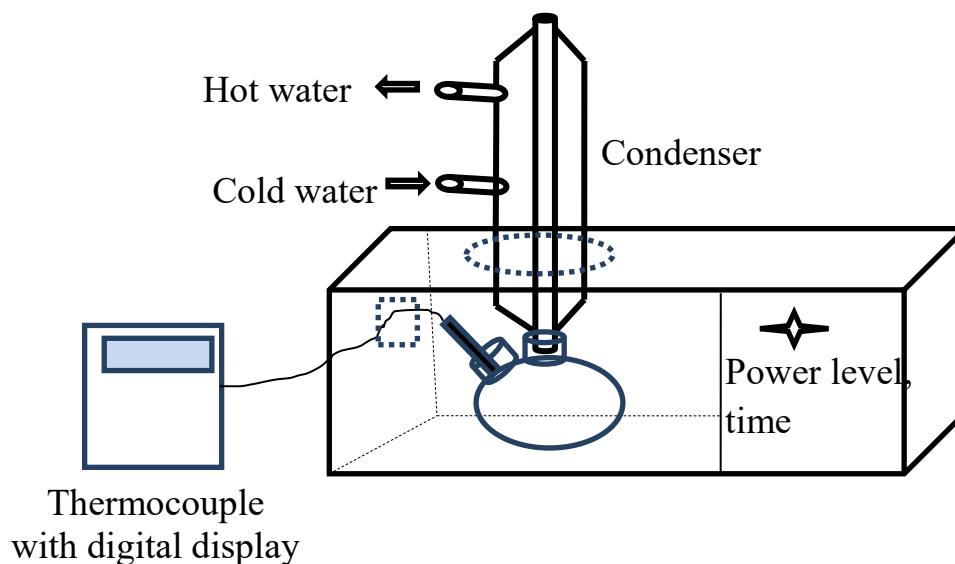


Fig. 3.1: Schematic diagram of the customized microwave oven for synthesis of ZnO nanorods.

This microwave oven operates by pulse-width modulation where the magnetron can be switched on-off and the time interval can be controlled to determine the average cooking power. In this experiment 50% of the full power level is used. It was observed that, an average temperature of 100°C was obtained after 9 min of heating. But only 5 min is required to reach the average temperature 100°C with 100% power level. As the solvent in this experiment was distilled water, average stable temperature does not increase with the increase of synthesis time. Only the power level of the microwave oven is conjectured to affect the initial temperature rise ramp to obtain

stable synthesis temperature. Fig. 3.2 shows the real picture of the customized microwave oven.



Fig. 3.2: Photograph of the customized microwave oven.

To synthesis ZnO nanorods, zinc acetate, $\text{Zn}(\text{CH}_3\text{COO})_2 \cdot 2\text{H}_2\text{O}$ (ZAH: Merck India), zinc nitrate, $\text{Zn}(\text{NO}_3)_2 \cdot 6\text{H}_2\text{O}$ (ZNH: Merck India) and hexamethylene tetraamine, $(\text{C}_6\text{H}_{12}\text{N}_4)$ (HMTA: Loba Chemie) of analytical grade are used. Equimolar solution of ZAH or ZNH precursor salt are mixed with HMTA in 100 ml distilled water and stirred for 1 hour at room temperature using a magnetic stirrer. The clear solution is then filtered using a filter paper to remove any dust particle or undissolved salt. Then the clear filtered solution is placed into the customized microwave oven (Eco+ P90D23ATP-Q8, 2450 MHz, 900 W, 23 L) for microwave treatment.

3.1.2 Microwave treatment

In this work, a domestic microwave oven is customized for the microwave assisted synthesis of ZnO nanorods. For that the hot spots within the microwave oven chamber are located at first for efficient heating of the precursor. A hard paper board was placed inside the microwave oven and operated the oven with 100% power for few minutes. Fig. 3.3 shows pictorial demonstration of the hot spot locating setup. The paper board got burnt on hotspot areas (Fig. 3.4). The largest burn area was found at a slightly left position from the microwave oven chamber center. This large hotspot was selected to place the reaction vessel, which ensures efficient and uniform heating of small volume of solution in the reaction vessel.



Fig. 3.3: Placement of hard paper board at proper height.



Fig. 3.4: Locating the hot spot position within the microwave chamber, the exact hotspot location on the hard paper board.

substance gets heated through microwaves due to the collision among molecular dipoles. Hence the polar solvents like water or alcohol get heated more rapidly. There are reports on the synthesis of ZnO nanorods using expensive single mode microwave reactors, that required higher energy density per unit volume of the sample. Though, some reports also show that cost-effective domestic microwaves can also be used for the synthesis of ZnO nanorods, but the highest possible energy density positions were not identified to get the best cost benefit ratio. In this work, the hot spot position within the microwave chamber is identified first, which ensures effective heating of the reaction vessel and repeatability of the synthesis process. It is to mention that the same experiments have been repeated three times which give the same results.

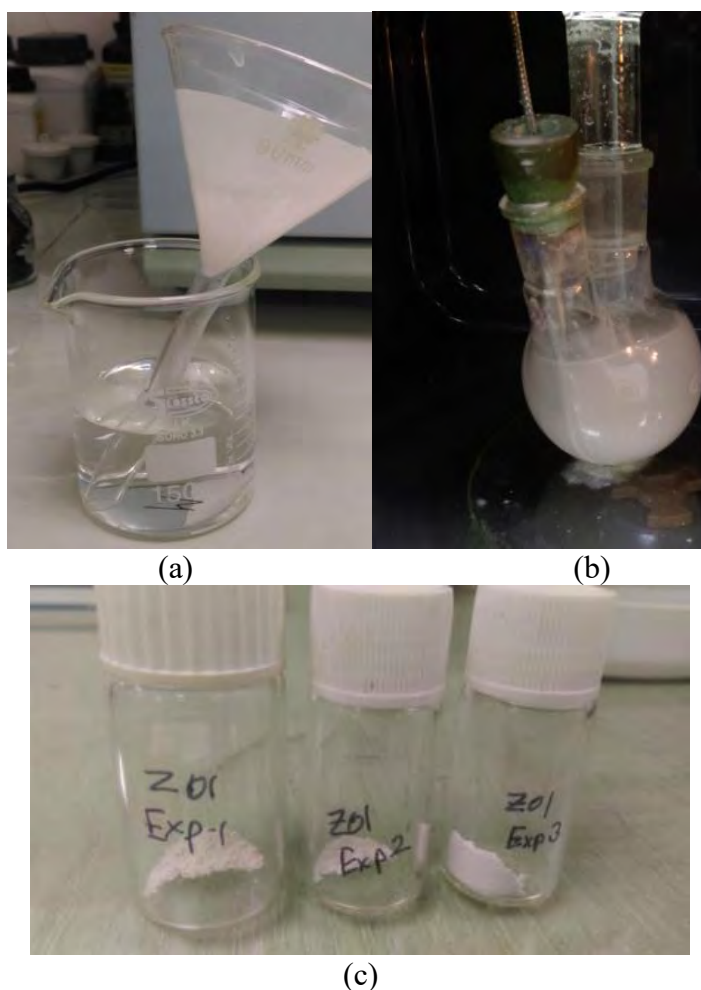


Fig. 3.5: Different steps of the synthesis process: (a) filtered solution before microwave treatment, (b) white solution after microwave treatment, (c) finally collected sample after repeating same process (at least three times).

It is demonstrated that fast synthesis of ZnO nanorods is possible using the customized domestic microwave oven. The effect of different process parameters on the morphological, structural and electrical properties of the synthesized ZnO nanorods is studied in this research work.

Microwave power was varied from 30%-70%, to observe the effect of microwave power variation on ZnO nanoparticles morphology. Also, the molar concentration of the Precursor concentration was varied from 15 to 50 mM. Synthesis time was varied from 5 to 20 min keeping the molar concentration and microwave power same, to observe the effect of time variation on the size of the ZnO nanorods. After microwave treatment the solution becomes milky white with white precipitation as shown in Fig. 3.5.

3.1.3 Sample collection

When the reaction was finished, the solution was cooled to room temperature. Then the white precipitate was wash with distilled water and centrifuged at 10000 rpm for several times. Finally, the collected white precipitate was dried in oven at 80°C for overnight.

3.2 Analysis Techniques

3.2.1 Scanning electron microscope

A Scanning Electron Microscope (SEM) is a type of electron microscope that produces images of a sample by scanning it with a focused beam of electrons as shown in Fig. 3.6. Electrons emitted from electron gun pass through of series of lenses to be focused and scanned across the sample. The incident or primary electron beam causes secondary electrons to be emitted from the sample and these are ultimately accelerated from 10 to 12 kV. They are most commonly detected with an Everhart-Thornley (ET) detector. The basic component of this detector is a scintillation material that emits light when struck by energetic electrons accelerated from the sample to the detector. The light from the scintillator is channelled through a light pipe to photomultiplier, where the light incident on a photocathode produces electrons that are multiplied, creating the very high gains necessary to drive the CRT. High potentials of 10 to 12 kV are necessary for efficient light emission by the scintillator. The electron beam is generally scanned in a raster scan pattern, and the beam's position is combined with the detected

signal to produce an image. SEM can achieve resolution better than 1 nanometre. Specimens can be observed in high vacuum, in low vacuum, in wet conditions (in environmental SEM), and at a wide range of cryogenic or elevated temperatures. All microscopy techniques have a finite limit beyond which they are unable to resolve any features. For optical microscopy this limit is given by:

$$d = 0.61 \frac{\lambda}{NA}$$

Where, d is the resolvable distance, λ is the wavelength of the light, and NA is the numerical aperture of the lens used for imaging. Using real numbers for NA and a wavelength on the lower end of the visible spectrums yields a minimum resolvable distance of about 100-200 nm.

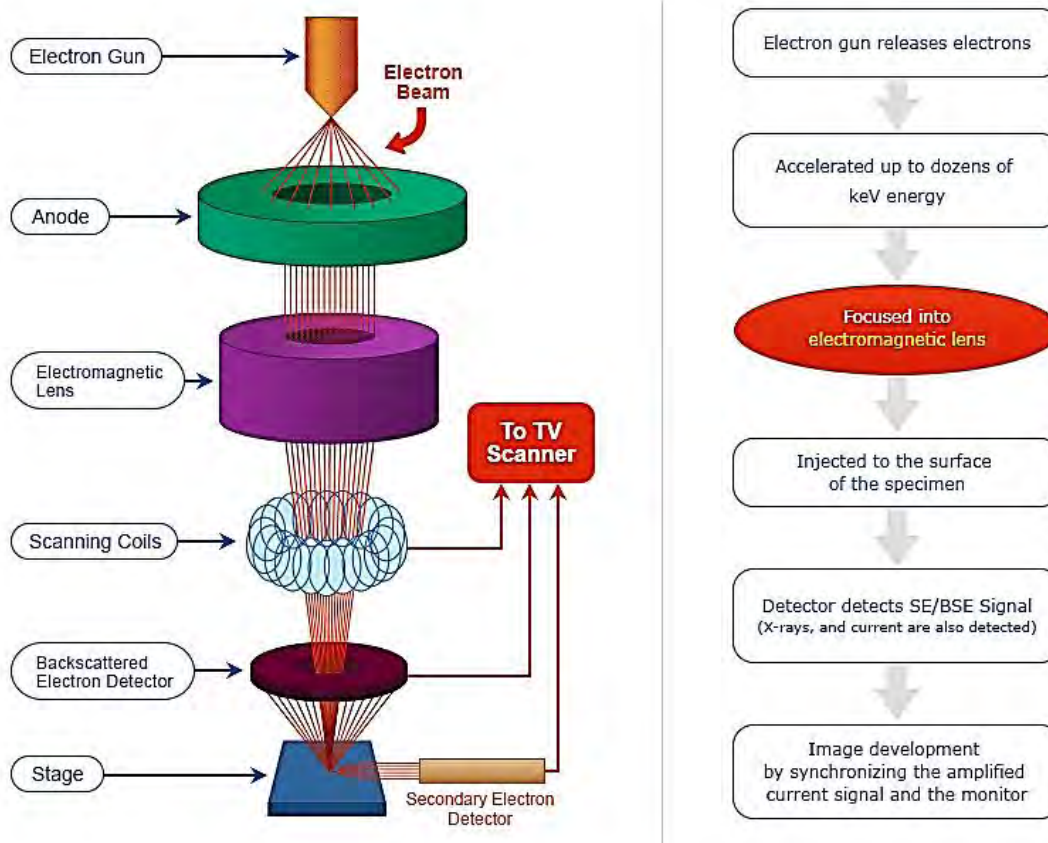


Fig. 3.6: Schematic diagram of a scanning electron microscope with the steps of image formation.

An SEM, on the other hand, uses electrons rather than light at energies of about 10-30 keV. The use of electrons has two main advantages over optical microscope:

- Much larger magnifications are possible since electrons wavelengths are much smaller than the photon wavelengths and
- The depth of the field is much higher (suitable for studying rough surfaces)

3.2.2 X-ray diffraction

Crystals are regular arrays of atoms. X-Ray Diffraction (XRD) is a technique used to characterize the crystal structure of materials. X-rays are a form of energetic electromagnetic radiation of wavelength 10^{-10} - 10^{-11} m, of comparable size to the spacing of atoms within a solid. Atoms scatter X-ray waves, primarily through the atom's electrons. Just as an ocean wave striking a lighthouse produces secondary spherical waves emanating from the lighthouse. So, an X-ray striking an electron produces secondary spherical waves emanating from the electron. This phenomenon is known as elastic scattering, and the electron (or lighthouse) is known as the scatterer. A regular array of scatterers produces a regular array of spherical waves as shown in Fig. 3.7. Although these waves cancel one another out in most directions through destructive interference, they add constructively in a few specific directions, determined by Bragg's law:

$$2d \sin \theta = n\lambda$$

Here d is the spacing between diffracting planes, θ is the incident angle, n is any integer, and λ is the wavelength of the beam. These specific directions appear as spots on the diffraction pattern called reflections. Thus, XRD results from an electromagnetic wave (the X-ray) impinging on a regular array of scatterers (the repeating arrangement of atoms within the crystal). The position of the resultant maxima in scattering intensity may be used to deduce crystal plane spacing and hence the structure of an unknown sample.

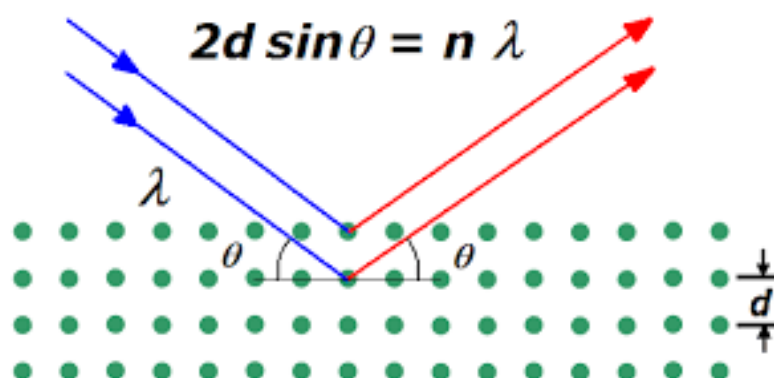


Fig. 3.7: A schematic representation of Bragg's law.



Fig. 3.8: The structural as well as phase identification measurements were carried out by an X-ray Diffractometer (GBC-XRD, EMMA) with a step size of 0.02 deg. using a $\text{Cu_K}\alpha_1$ ($\lambda = 1.54062 \text{ \AA}$) radiation source operated at 35.5 kV and 28 mA.

X-ray diffractometers consist of three basic elements: an X-ray tube, a sample holder and an X-ray detector as shown in Fig. 3.8. X-rays are generated in a cathode ray tube by heating a filament to produce electrons, acceleration the electrons toward a target by applying a voltage, and bombarding the target material with electrons. When electrons have sufficient energy to dislodge inner shell electrons of the target material, characteristic X-ray spectra are produced. These spectra consist of several

components, the most common being K_α and K_β . K_α consists, in part, of $K_{\alpha 1}$ and $K_{\alpha 2}$. $K_{\alpha 1}$ has a slightly shorter wavelength and twice the intensity as $K_{\alpha 2}$. The Specific wavelengths are characteristic of the target material (Cu, Fe, Mo, Cr). Filtering, by foils or crystal monochromators, is required to produce monochromatic X-rays needed for diffraction. $K_{\alpha 1}$ and $K_{\alpha 2}$ are sufficiently close in wavelength such that a weighted average of the two is used. Copper is the most common target material for single-crystal diffraction, with $\text{Cu}K_\alpha$ radiation $\lambda = 1.5418 \text{ \AA}$. These X-rays are collimated and directed onto the sample. As the sample and detector are rotated, the intensity of the reflected X-rays is recorded. When the geometry of the incident X-rays is recorded. When the geometry of the incident X-rays impinging the sample satisfies the Bragg Equation, constructive interference occurs and a peak in the intensity occurs. A detector records and processes this X-ray signal and converts the signal to a count rate which is then output to a device such as a printer or computer monitor.

The geometry of an X-ray diffractometer is such that the sample rotates in the path of the collimated x-ray beam at an angle θ while the X-ray detector is mounted on an arm to collect the diffracted X-rays and rotates at an angle of 2θ . The instrument used to maintain the angle and rotate the sample is termed a goniometer. For typical powder patterns, data is collected at 2θ from -5° to 70° , angles that are present in the X-ray scan.

3.2.3 Energy-dispersive X-ray spectroscopy

Energy-Dispersive X-ray Spectroscopy (EDX), is an analytical technique used as shown in Fig. 3.9 for the elemental analysis or chemical characterization of a sample. It relies on an interaction of some source of X-ray excitation and a sample. Its characterization capabilities are due in large part to the fundamental principle that each element has a unique atomic structure allowing unique set of peaks on its X-ray emission spectrum. To stimulate the emission of characteristic X-rays from a specimen, a high-energy beam of charged particles such as electrons or protons, or a beam of X-rays, is focused into the sample being discrete energy levels or electron shells bound to the nucleus. The incident beam may excite an electron in an inner shell, ejecting it from the shell while creating an electron hole where the electron was. An electron from an outer, higher-energy shell then fills the hole, and the difference in

energy between the higher energy of the X-rays emitted from a specimen can be measured by an energy-dispersive spectrometer. As the energies of the X-rays are characteristic of the difference in energy between the two shells and of the atomic structure of the emitting element, EDX allows the elemental composition of the specimen to be measured.



Fig. 3.9: Morphological and elemental analysis were done by an SEM with EDX (Carl Zeiss, EVO 18).

3.2.4 Ultraviolet-visible spectroscopy

Ultraviolet-Visible Spectroscopy (UV/Vis) refers to absorption spectroscopy or reflectance spectroscopy in the ultraviolet-visible spectral region. The instrument used in ultraviolet-visible spectroscopy is called a UV/Vis spectrophotometer as shown in Fig. 3.10. It measures the intensity of light passing through a sample (I), and compares it to the intensity of light before it passes through the sample (I_0). The ratio I/I_0 is called the transmittance, and is usually expressed as a percentage ($\%T$). The absorbance, A is based on the transmittance:

$$A = 2 - \log(T\%)$$

The UV-visible spectrophotometer as shown in Fig. 3.11 can also be configured to measure reflectance. In this case, the spectrophotometer measures the intensity of light reflected from a sample (I), and compares it to the intensity of light reflected from a reference material (I_0) (such as a white tile). The ratio I/I_0 is called the reflectance, and is usually expressed as a percentage (% R).

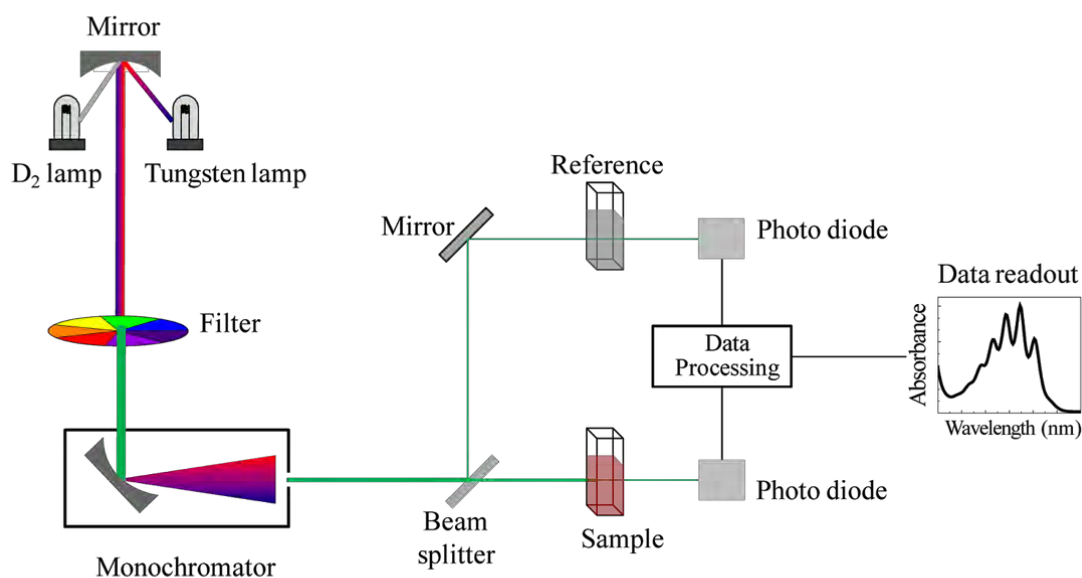


Fig. 3.10: A schematic diagram of an UV-Visible spectrophotometer.

The basic parts of a spectrophotometer are a light source, a holder for the sample, a diffraction grating in a monochromator or a prism to separate the different wavelength of light, and a detector. The radiation source is often a Tungsten filament (300-2500 nm), a deuterium arc lamp, which is continuous over the ultraviolet region (190-400 nm), Xenon arc lamp, which is continuous from 160-2000 nm; or more recently, light emitting diodes (LED) for the visible wavelengths. The detector is typically a photomultiplier tube, a photodiode, a photodiode array or a charge-coupled device (CCD). Single photodiode detectors and photomultiplier tubes are used with scanning monochromators, which filter the light so that only light of a single wavelength reaches the detector at one time. The scanning monochromator moves the diffraction grating to “step-through” each wavelength so that its intensity may be measured as a function of wavelength. Fixed monochromators are used with CCDs and photodiode arrays. As both of these devices consists of many detectors grouped into one or two-dimensional

arrays, they are able to collect light of different wavelengths on different pixels or groups of pixels simultaneously.



Fig. 3.11: The optical measurements were done using an UV-Vis-NIR (Hitachi, UH4150) spectrophotometer coupled with an integrating sphere.

3.2.5 Dielectric properties

The study of frequency dependent electrical properties is very essential in science and technology. A material that can store energy when a voltage is applied causing electric polarization is known as dielectric property. The dielectric material is an insulator or a very poor conductor of electric current. When dielectrics are placed in an electric field, practically no current flows in them because of their zero-electron mobility. When electric polarization occurs in the dielectric, the positive and the negative charges are displaced in the direction opposite to the electric field. The capacitance of a capacitor filled with dielectric material is greater than in vacuum. Dielectric property of the samples was measured using a 6500B Wayne Kerr impedance analyzer as shown in Fig. 3.12.



Fig. 3.12: The dielectric property was measured using an impedance analyzer (Wayne Kerr, 6500B series).

CHAPTER 4

RESULTS AND DISCUSSION

4.1 Surface Morphology

ZnO nanorods synthesized in this research work have twinning hexagonal prismatic shape, which is very commonly formed by wet chemical methods. Fig 4.1 clearly depicts the shape of the synthesized nanorods. Xu et al. [53] defined this shape as two joined hexagonal prisms connected by a common basal plane forming a twinning growth relationship.

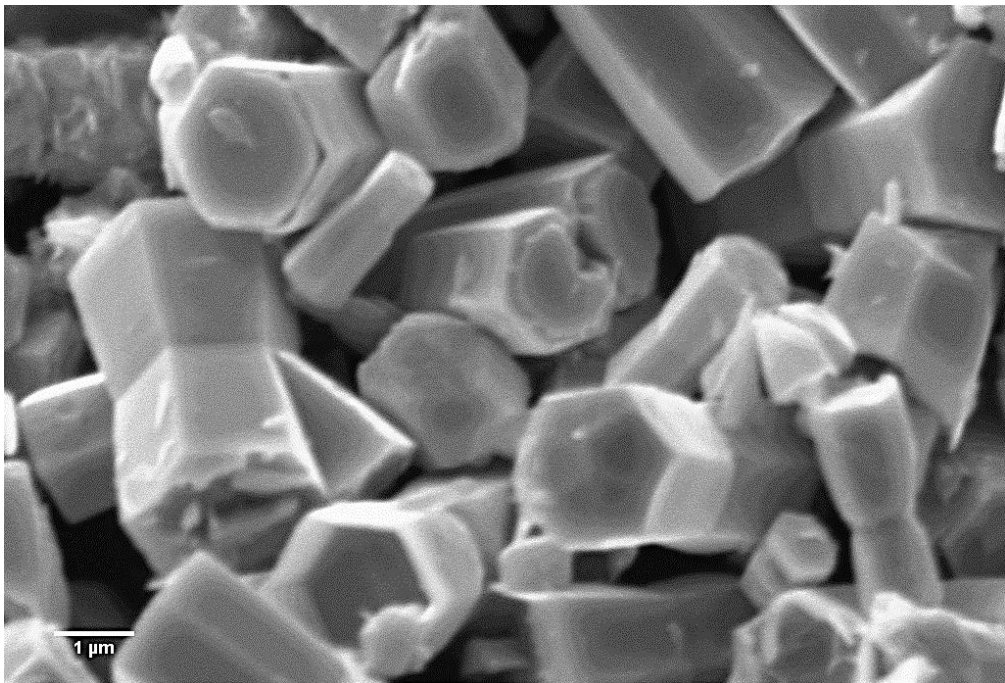


Fig. 4.1: Morphology of the synthesized nanorods using ZAH at 50% microwave power.

4.1.1 Effect of microwave power

The microwave system employed to synthesize the ZnO particles allows setting a constant synthesis time. In order to analyse the microwave power effect on the final morphology of the ZnO nanorods, synthetic reactions were carried out within the microwave power range 30%-70%. ZAH or ZNH was used as the precursor salt. The SEM images are shown in Figs. 4.2 to 4.5.

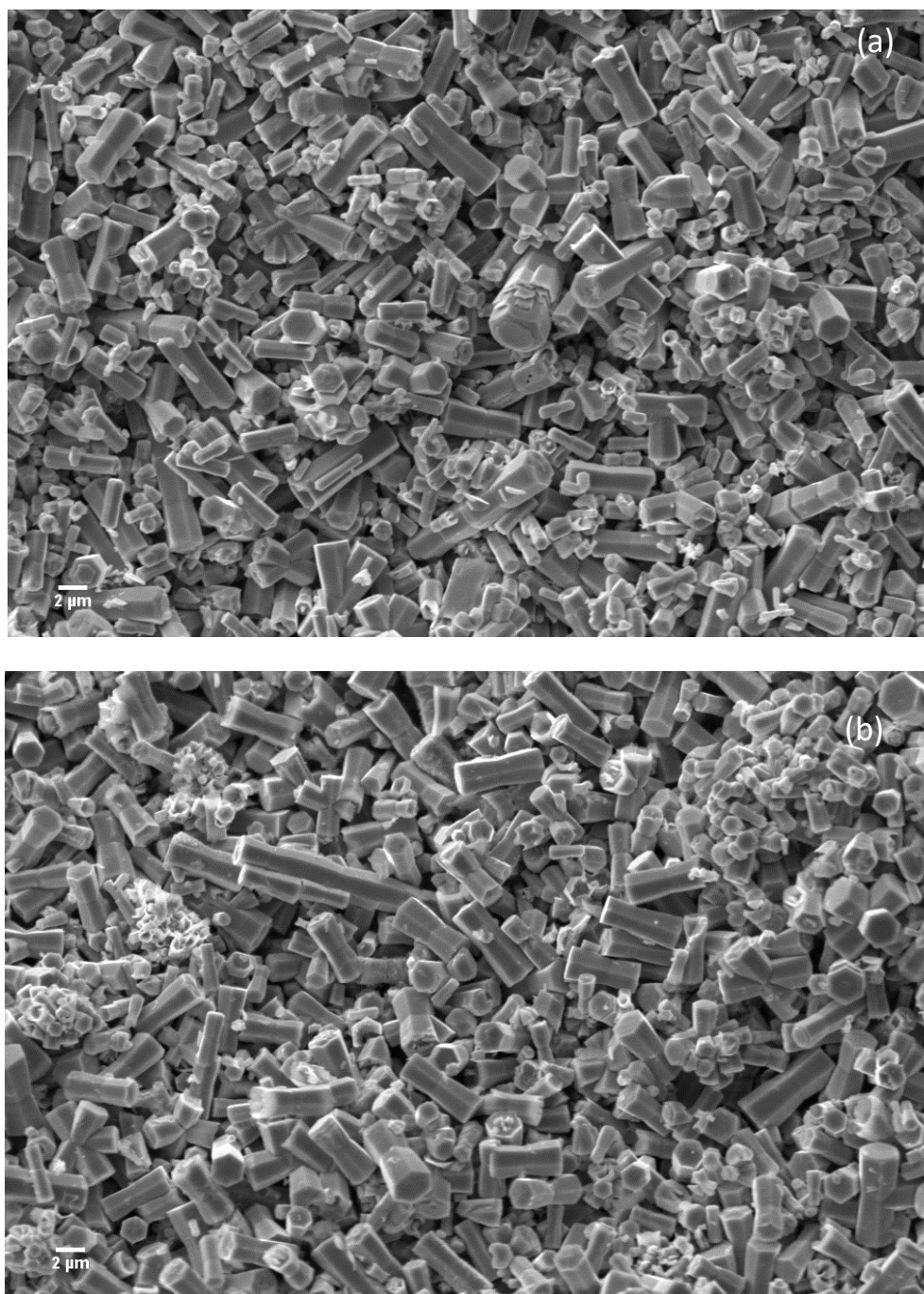


Fig. 4.2: SEM images of the synthesized ZnO nanorods using ZAH precursor at (a) 30% and (b) 50% microwave power.

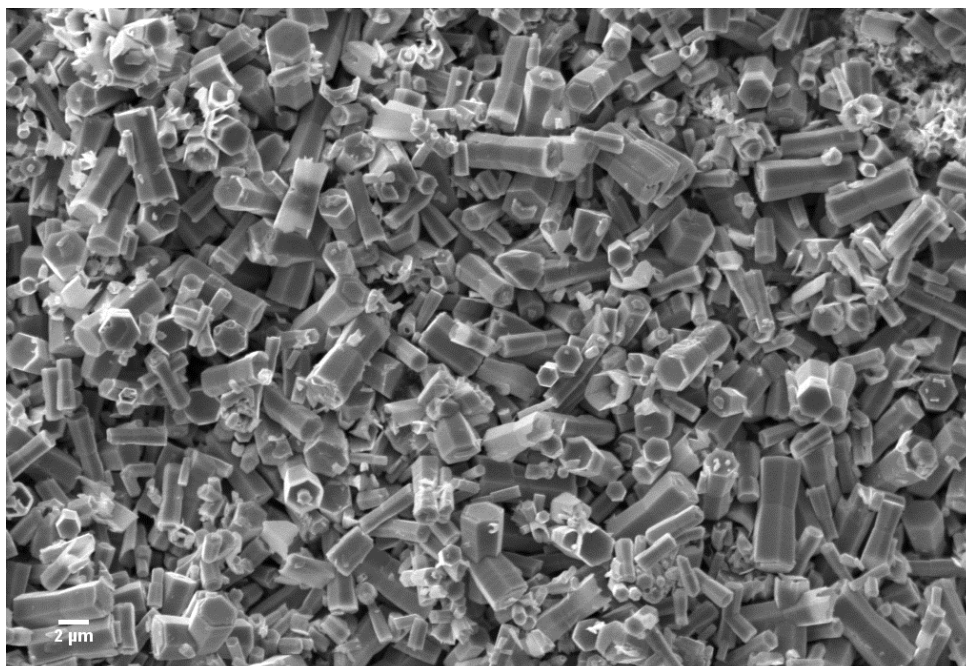


Fig. 4.3: SEM images ZnO nanorods formed by heating an equimolar (50 mM) mixture of HMT and ZAH at 70% microwave power.

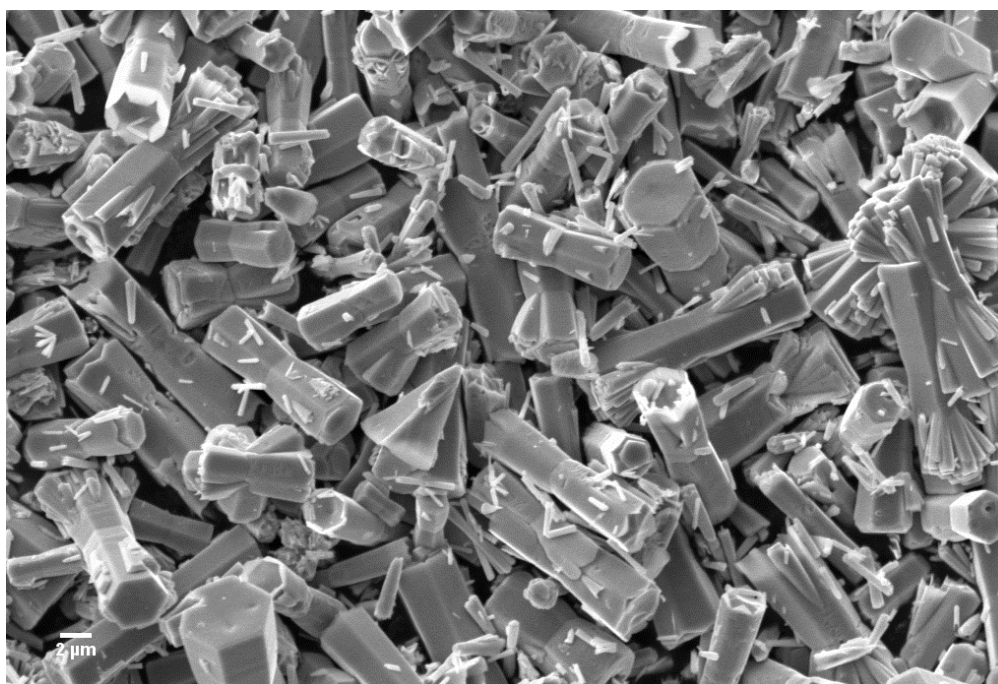


Fig. 4.4: SEM images ZnO nanorods formed by heating an equimolar (50 mM) mixture of HMT and ZNH at 30% microwave power.

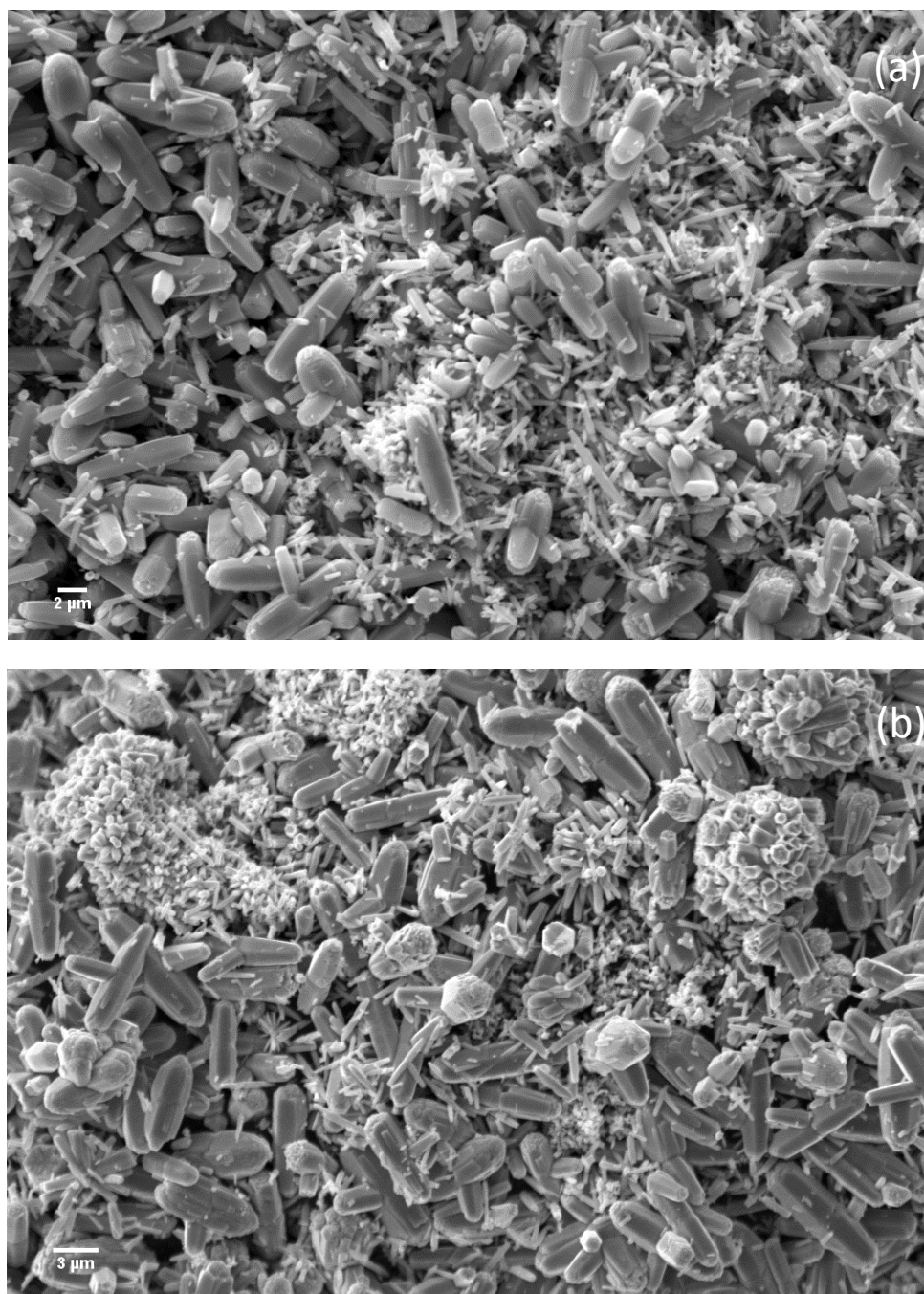


Fig. 4.5: SEM images ZnO nanorods formed by heating an equimolar (50 mM) mixture of HMT and ZNH, (a) at 50%; (b) at 70% microwave power.

Homogenous morphological distribution of bi-hexagonal rod-like structure can be observed, when ZAH is used as precursor. The morphological difference due to microwave power variation is more prominent in case of hexagonal prismatic type nanorods formed using ZNH precursor. The variation in particle size with microwave power is easily visible. Average diameter and length of the nanorods were calculated using Gaussian distribution.

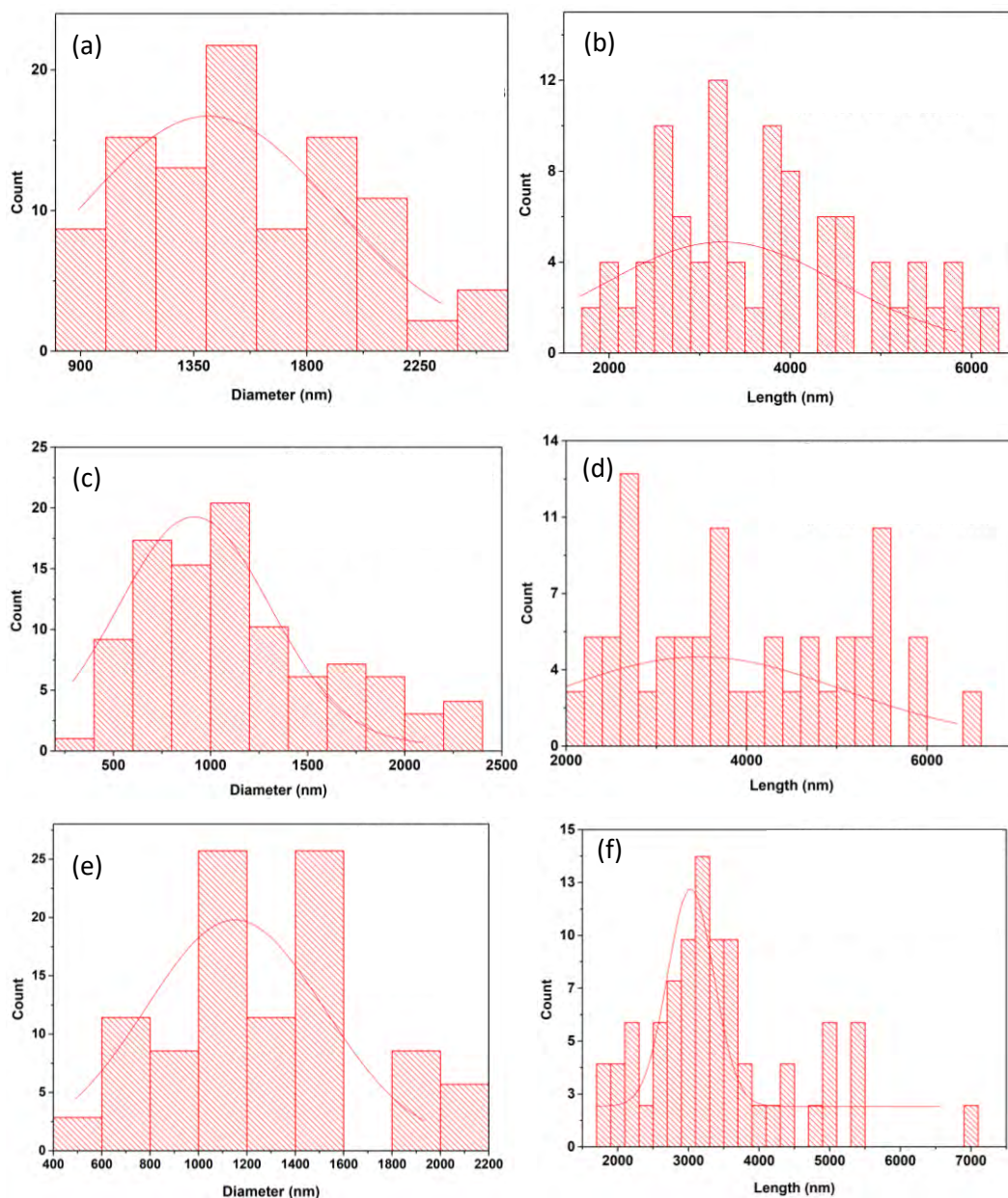


Fig. 4.6: Particle size distribution for (a, c, e) diameter and (b, d, f) length of ZnO nanorods formed by heating an equimolar (50 mM) mixture of HMT and ZAH (a) and (b) at 30%; (c) and (d) at 50%; (e) and (f) at 70% microwave power.

The size distribution for average diameter and length of the nanorods formed using ZAH and ZNH are shown in Figs. 4.6 to 4.7. When the microwave power increases from 30% to 70%, the average length increases from 1339 to 2414 nm for ZNH as precursor salt. Whereas, the average diameter decreases from 1471 to 1231 nm with microwave, for ZAH as precursor salt. The minimum average diameter (301 nm) with an average length of value 1365 nm was attained at 50% microwave power using ZNH precursor salt.

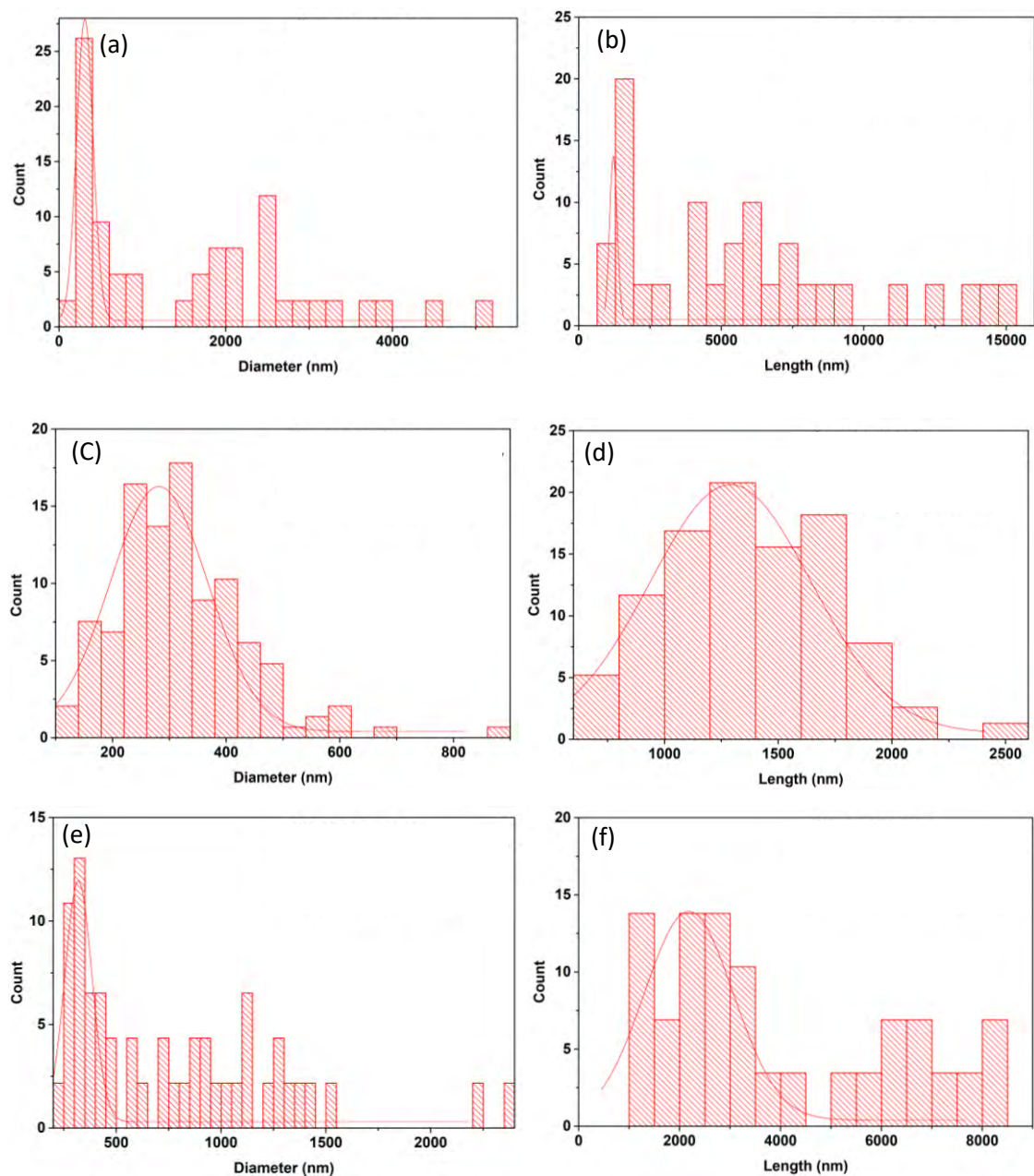


Fig. 4.7: Particle size distribution for (a, c, e) diameter and (b, d, f) length of ZnO nanorods formed by heating an equimolar (50 mM) mixture of HMT and ZNH: (a) and (b) at 30%; (c) and (d) at 50%; (e) and (f) at 70% microwave power.

Whereas, ZnO nanorods are synthesized at 50% percent using ZAH as precursor salt, have the maximum average length 3639 nm. Hence, it can be concluded that nanorods with good aspects ratio may be obtained at 50% microwave power by optimizing other synthesis parameter. The plots for average diameter and length as a function of microwave power are shown in Figs. 4.8 and 4.9.

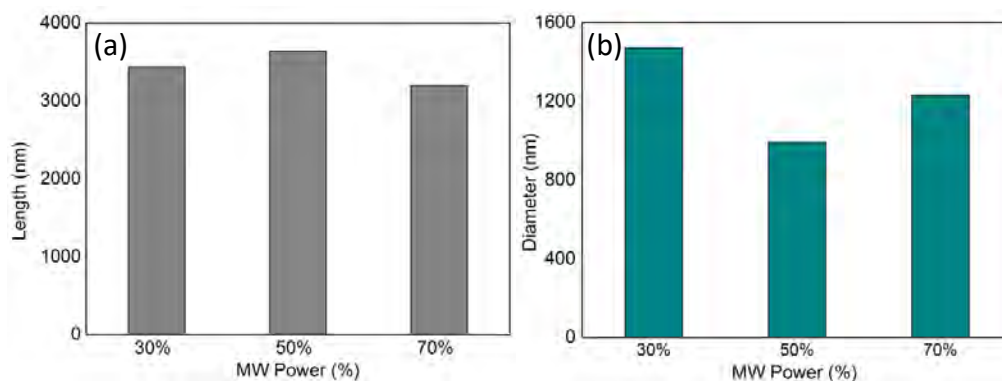


Fig. 4.8: The average (a) length and (b) diameter of ZnO nanorods formed by heating an equimolar (50 mM) mixture of HMT and ZAH using different microwave power.

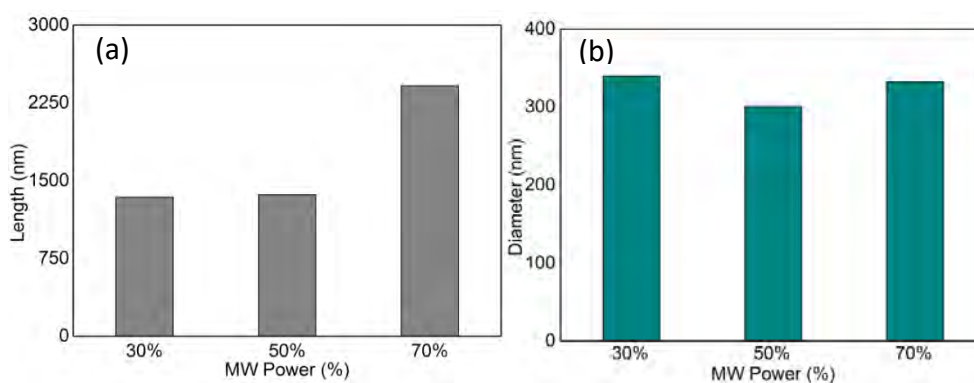


Fig. 4.9: The average (a) length and (b) diameter of ZnO nanorods formed by heating an equimolar (50 mM) mixture of HMT and ZNH using different microwave power.

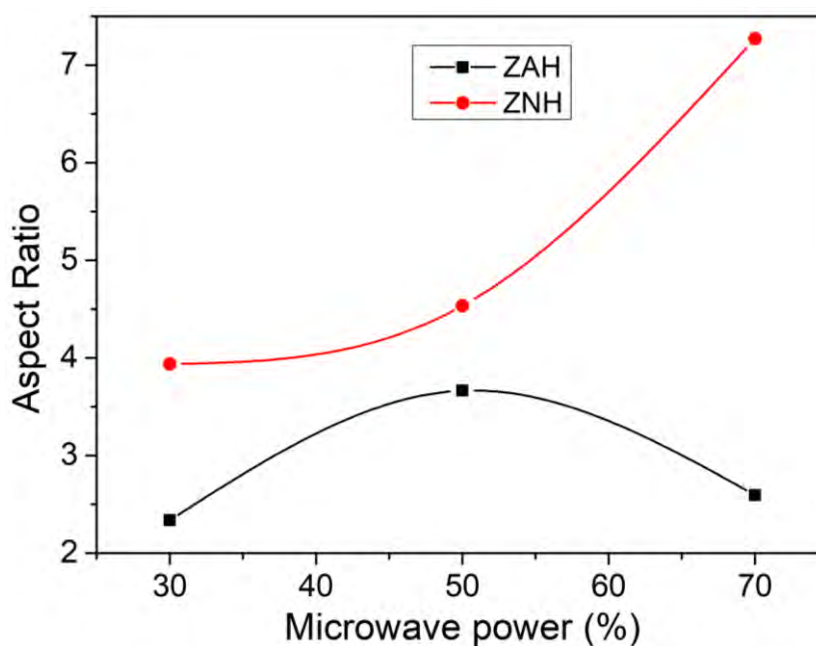


Fig. 4.10: Variation of aspect ratio with microwave power.

4.1.2 Effect of precursor

Two different precursors ZNH and ZAH are employed to synthesize ZnO nanorods. It is observed that the synthesized nanorods are of hexagonal prismatic rod shaped and morphology, size of the nanorods strongly depend on the source precursors as shown in Fig. 4.11. The nanorods formed by heating of equimolar HMTA and ZAH have an average diameter of 990 nm, which has been calculated from several SEM images using Gaussian distribution of the measured diameters. But the average diameter of the ZnO nanorods is observed to be reduced to about 300 nm when ZNH are used instead of ZAH as a precursor. It is conjectured that the precursor salt may influence both the nucleation and growth stages of the ZnO nanorods during the synthesis process, which also depends on material properties or reaction condition. With a fixed molar concentration of the different zinc source precursors the reaction is carried out keeping all other reaction conditions same. It is conjectured that, with same molar concentration of the precursor, ZNH based solution has higher tendency to form larger number of nuclei compared to the ZAH-based solution. As a result, the ZNH produce ZnO nanorods of smaller diameter. On the other hand, molar concentration of ZAH has influenced in the growth stage rather than the nucleation stage, which results in the formation of larger size of ZnO nanorods. The length to diameter aspect ratio of the ZnO nanorods is calculated to be 3.7 and 4.5, respectively for ZNH and ZAH precursor. In this research work a facile one step method is developed to synthesize ZnO nanorods with high aspect ratio. Smaller diameter may help to achieve a high aspect ratio value. At this stage, using 50% microwave power ZNH precursor salt provides the best result regarding the aspect ratio value. Therefore, to observe the effect of molar concentration and synthesis time ZAH is chosen as experimental precursor to produce further ZnO nanorods. For that, at 50% microwave power using ZNH precursor molar concentration and synthesis time is varied within selected range.

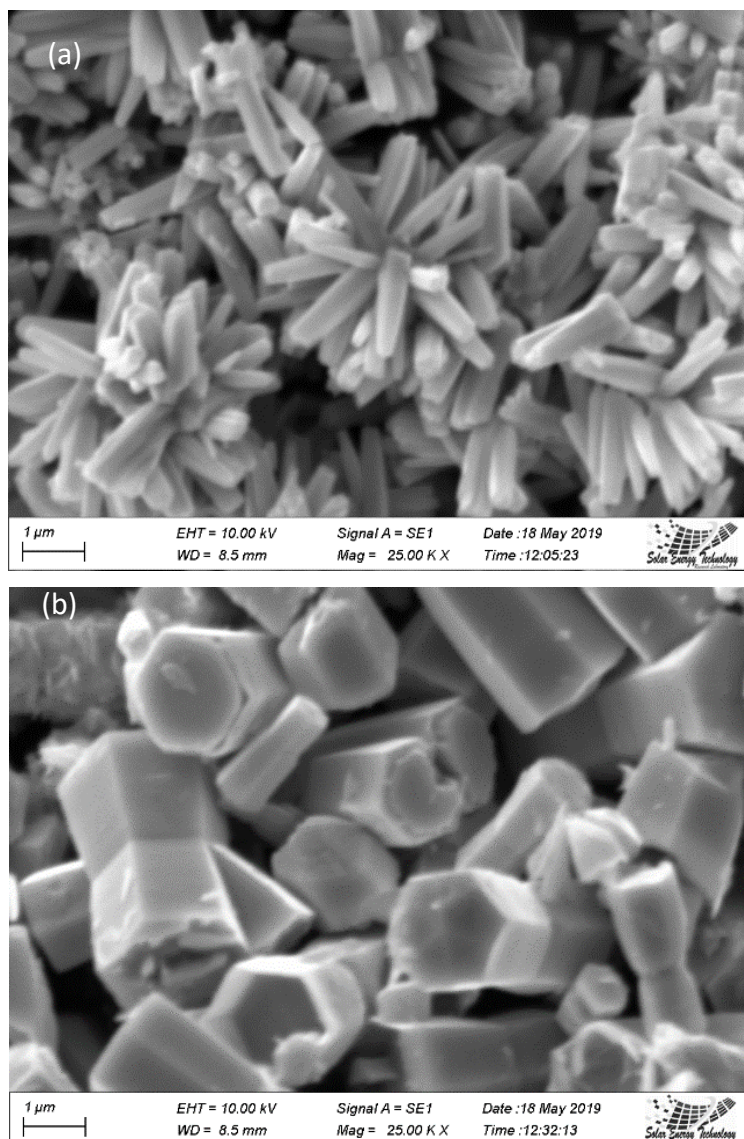


Fig. 4.11: SEM image of ZnO nanorods formed by heating an equimolar (50 mM) mixture of HMTA and (a) ZAH, (b) ZNH, with 50% microwave power.

4.1.3 Precursor concentration effect

The precursor concentration has been varied from 5 to 50 mM keeping the microwave power and precursor same. Figs. 4.12 and 4.13 show the SEM images of the synthesized ZnO nanorods corresponding to different molar concentration of precursor are presented. The gaussian distributions for measuring average diameter and length of the nanorods synthesized with different molar concentration of precursor salt are shown in Fig. 4.14. The bar diagram plots for average diameter and length as a function on precursor concentration are depicted in Fig. 4.15.

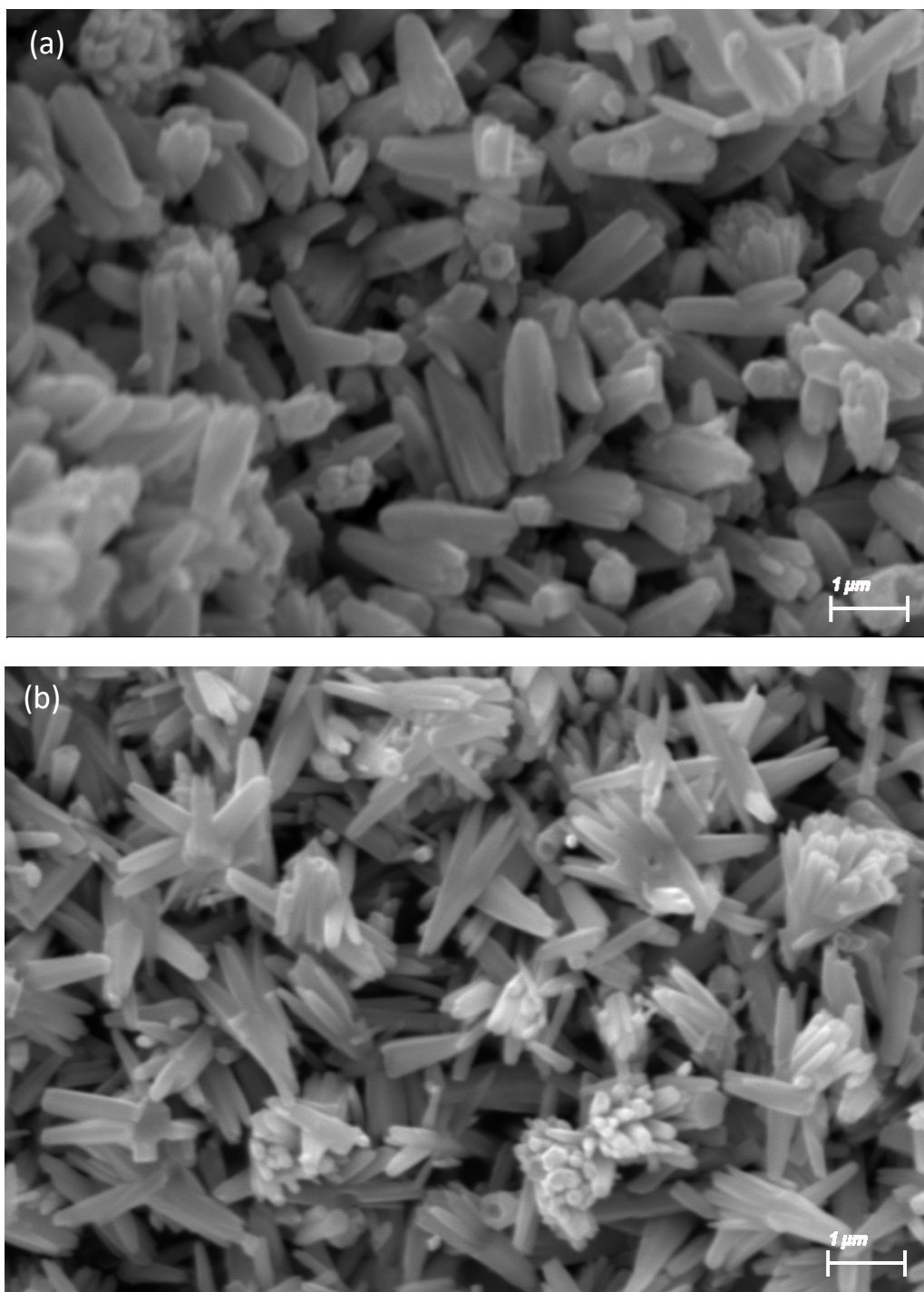


Fig. 4.12: SEM images ZnO nanorods formed by heating an equimolar mixture of HMT and ZNH with (a) 5 mM and (b) 10 mM precursor concentration.

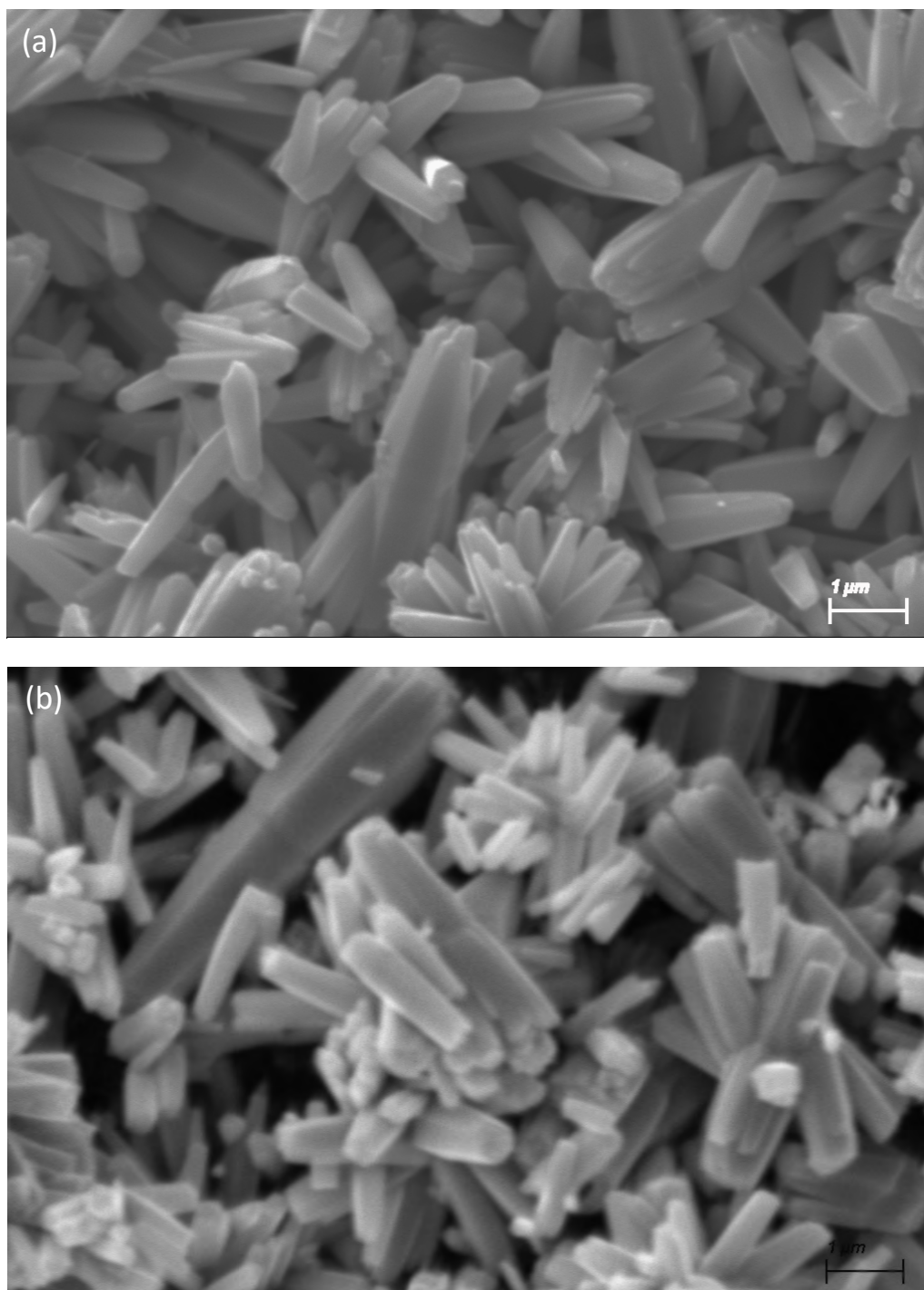


Fig. 4.13: SEM images ZnO nanorods formed by heating an equimolar mixture of HMT and ZNH, (a) 15 mM; (b) 50 mM precursor concentration.

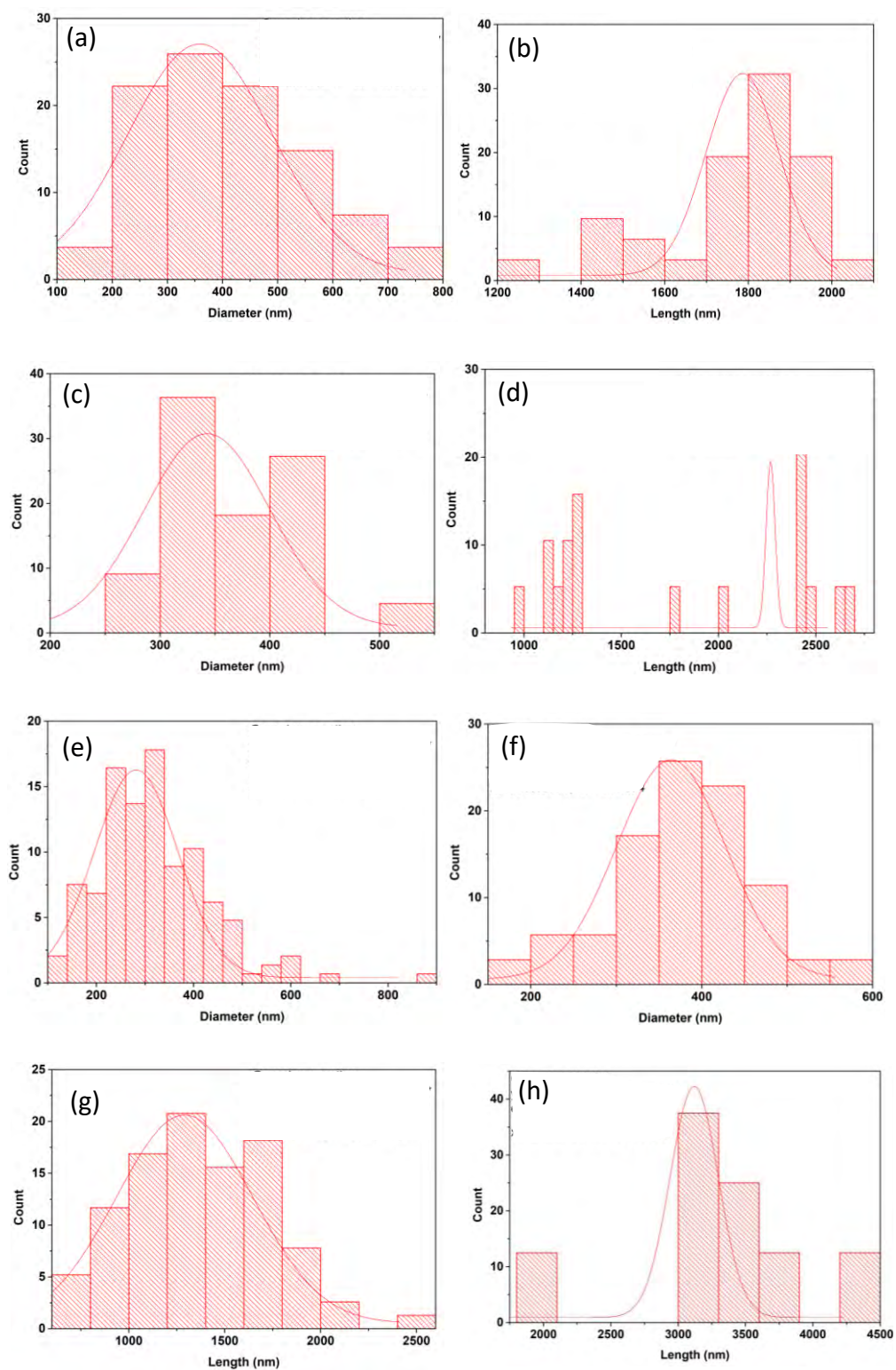


Fig. 4.14: Particle size distribution of ZnO nanorods formed by heating an equimolar mixture of HMT and ZNH, (a) and (b) 5 mM; (c) and (d) 10 mM; (e) and (f) 15 mM; (g) and (h) 50 mM precursor concentration.

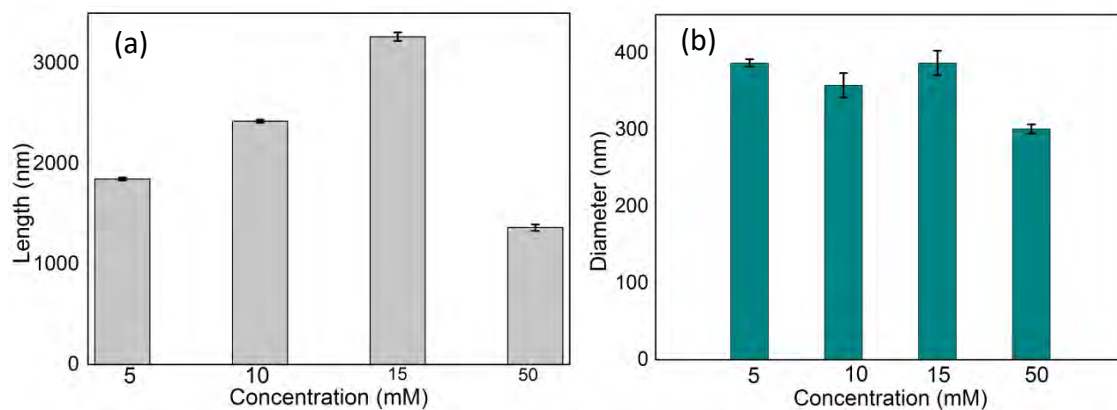


Fig. 4.15: The average (a) length and (b) diameter of the ZnO nanorods formed by heating an equimolar mixture of HMT and ZNH with different precursor concentration.

It is observed that when the concentration of the precursor solution is varied, the average diameter and length varies from 300 to 380 nm and from 1800 to 3500 nm, respectively. But average length of the ZnO nanorods is observed to be reduced to 1200 nm when precursor concentration become very high, which may be owing to three-dimensional branching in the nanorods as shown in Fig. 4.15 (b). This observation is in good agreement with the result reported in Ref. [20].

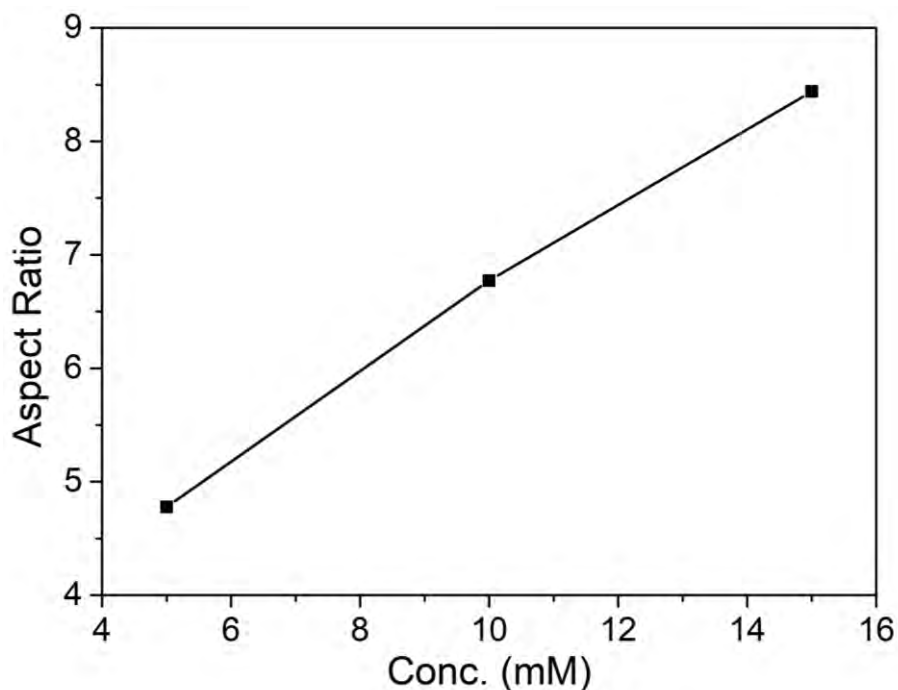


Fig. 4.16: Variation of aspect ratio with precursor concentration.

Fig. 4.16 gives a clear view, how the aspect ratio with precursor concentration. In this research, the precursor concentration was varied from 5 to 15 mM and the aspect ratio increases with the molar concentration. The maximum length of the ZnO nanorods are attained to be ~3100 nm at a precursor concentration of 15 mM, which is accompanied by an average diameter of about 390 nm, indicating a better aspect ratio (7.9) for ZnO nanorods. Also, it is observed that from the SEM images in Fig. 4.13, ZnO nanorods synthesized using a very high precursor concentration (50 mM) have branches.

At lower concentration of Zn^{2+} and OH^- , the concentration of growth unit and the collision rate of the growth unit are also less. This may facilitate the highly orientation growth of ZnO nanorods. When the concentrations of Zn^{2+} and OH^- become higher the nanorods are conjectured to be merged with each other due to the higher collision rate of growth units. As a result, the average length of the ZnO nanorods decreases for higher precursor concentration. Though, Fig. 4.13 confirms the branch formation at a very high precursor concentration, future research work needs to be done to find out the optimum condition by varying the precursor concentration chronologically.

4.1.4 Effect of synthesis time

The effect of growth-time for a certain concentration of precursor solution (15 mM) is demonstrated by SEM images as shown in Figs. 4.17 to 4.19. It can be clearly observed that the average length of the ZnO nanorods increases with growth time. It is conjectured that according to kinetics point of view prolonged synthesis duration provides enough time for orientational growth of the nanorods [20]. Branched ZnO nanorods is observed to be produced when the synthesis time is more than 20 min, because it is conjectured that during the prolonged synthesis time the already grown ZnO nanorods provide nucleation sites for the growth of new branches. Average diameter and length of the ZnO nanorods as a function of growth time are presented in Figs. 4.20 and 4.21. It is observed that average length of the ZnO nanorods increases dramatically from about 1.5 to 4 μm and the average diameter varies nonlinearly from about 400 to 500 nm. The maximum average length of 4 μm is accompanied by an average diameter of about 480 nm, indicating a better aspect ratio of 8.3 for ZnO nanorods. Fig. 4.23 is a plot of aspect ratio with varying synthesis time and shows that 20 min synthesis time is the optimum condition for 50% power level and 15 mM precursor concentration.

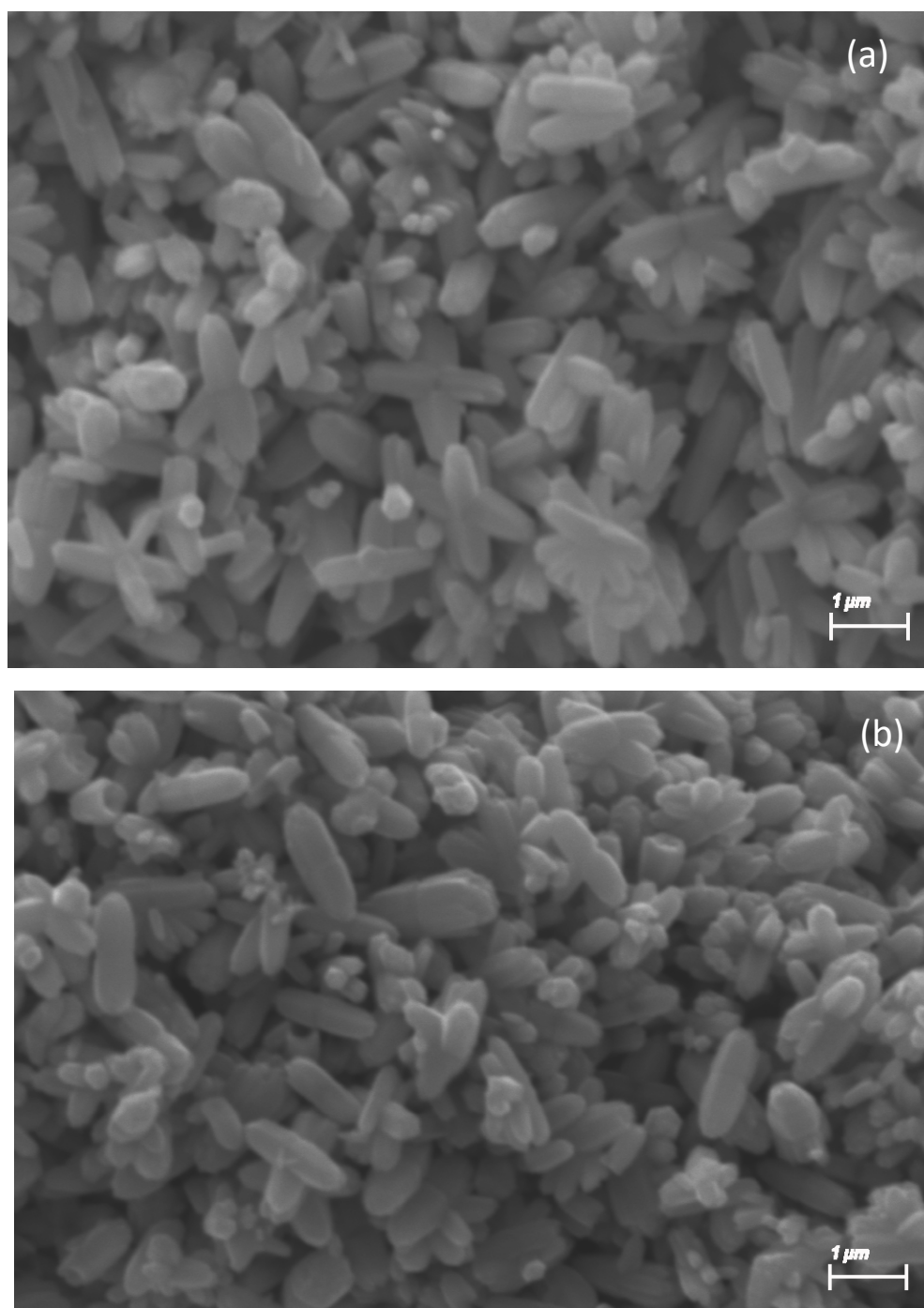


Fig. 4.17: SEM images ZnO nanorods formed by heating an equimolar mixture of HMT and ZNH for (a) 5 min; (b) 7 min.

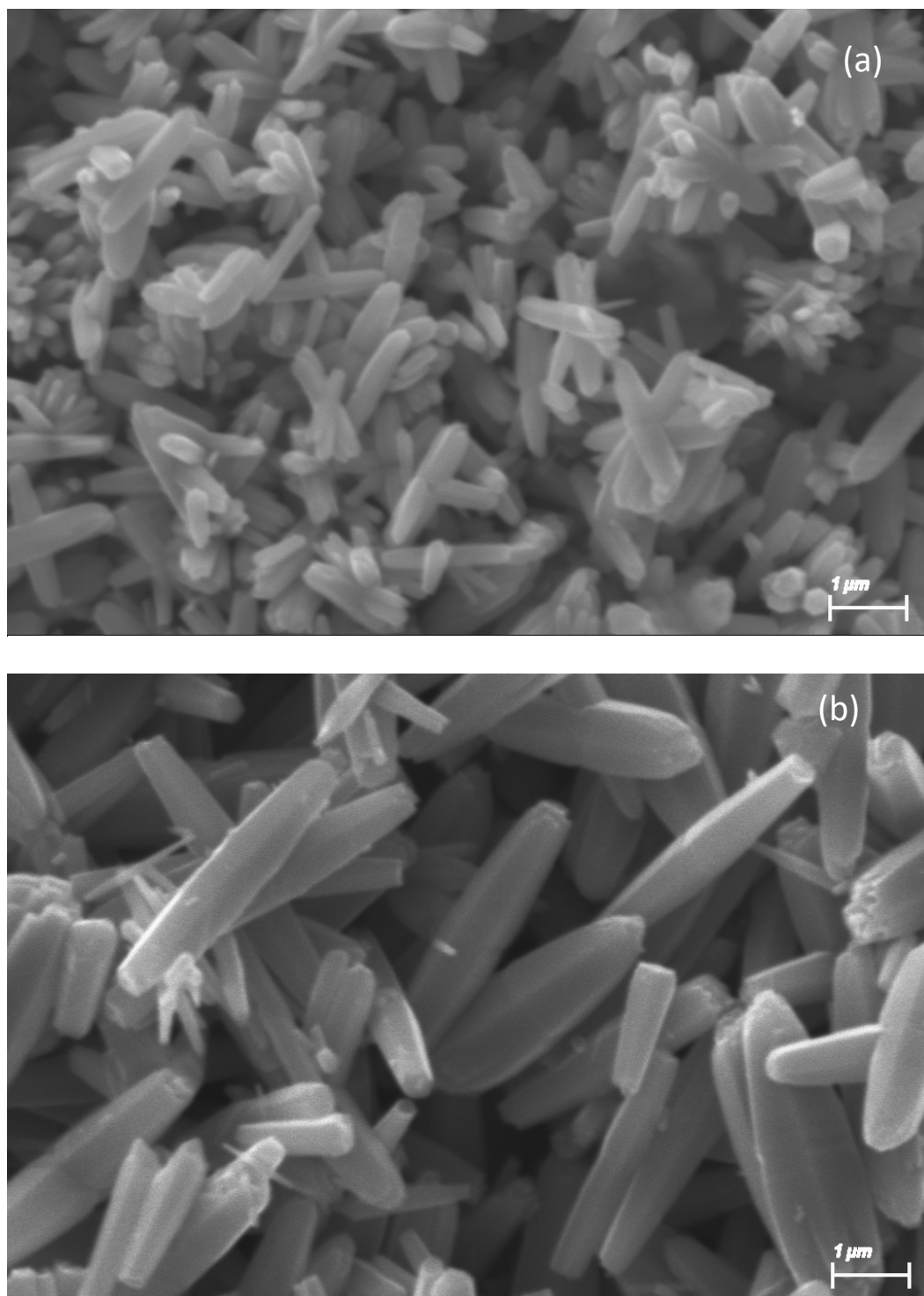


Fig. 4.18: SEM images ZnO nanorods formed by heating an equimolar mixture of HMT and ZNH for (a) 10 min; (b) 20 min.

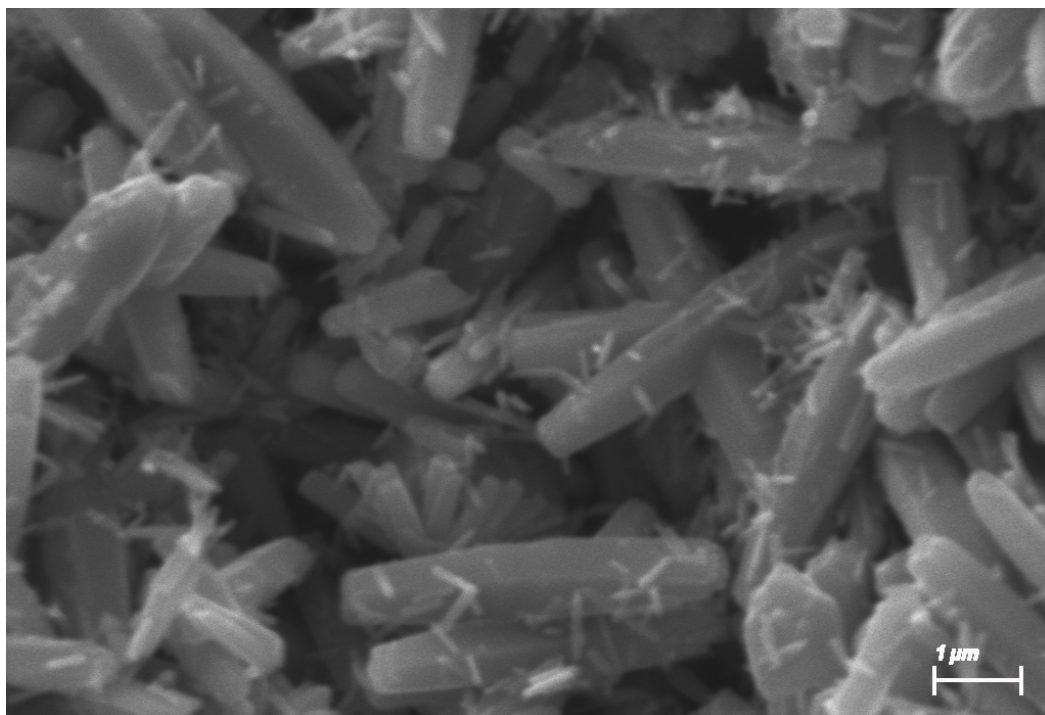


Fig. 4.19: SEM images ZnO nanorods formed by heating an equimolar mixture of HMT and ZNH for 30 min.

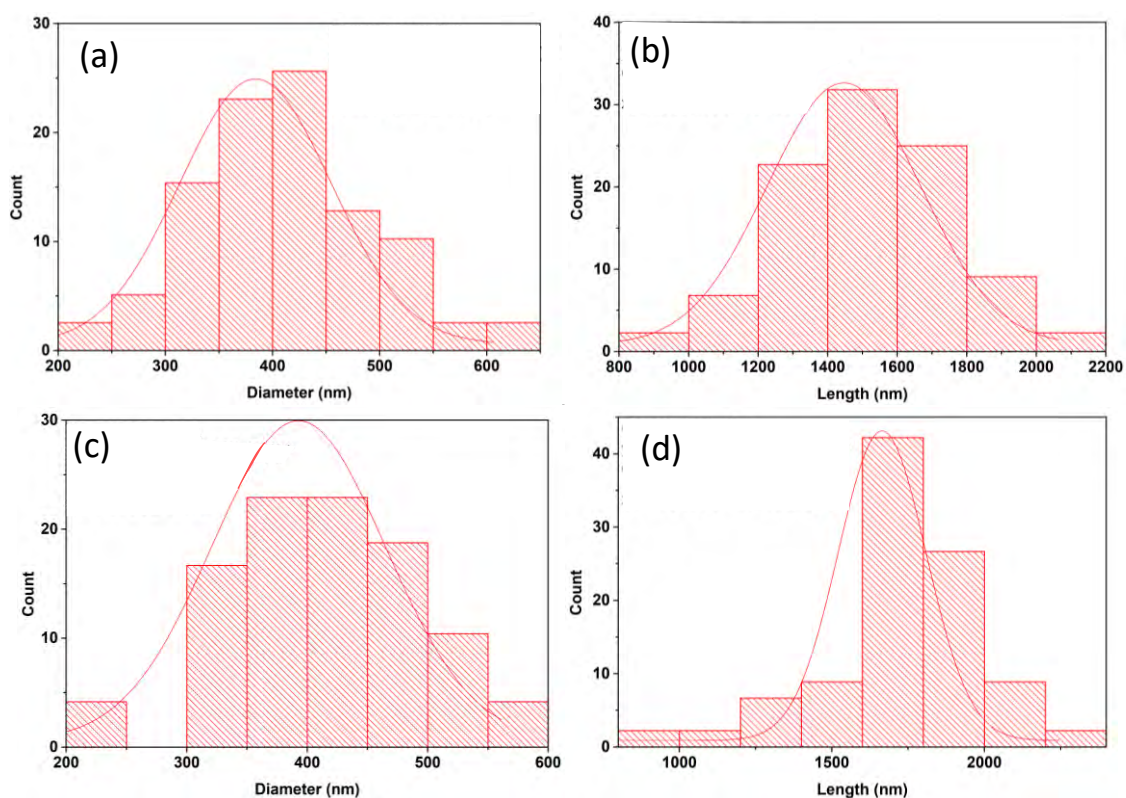


Fig. 4.20: Particle size distribution of (a, c) diameter and (b, d) length of the ZnO nanorods formed by heating an equimolar mixture of HMT and ZNH for (a) and (b) 5 min, (c) and (d) 7 min.

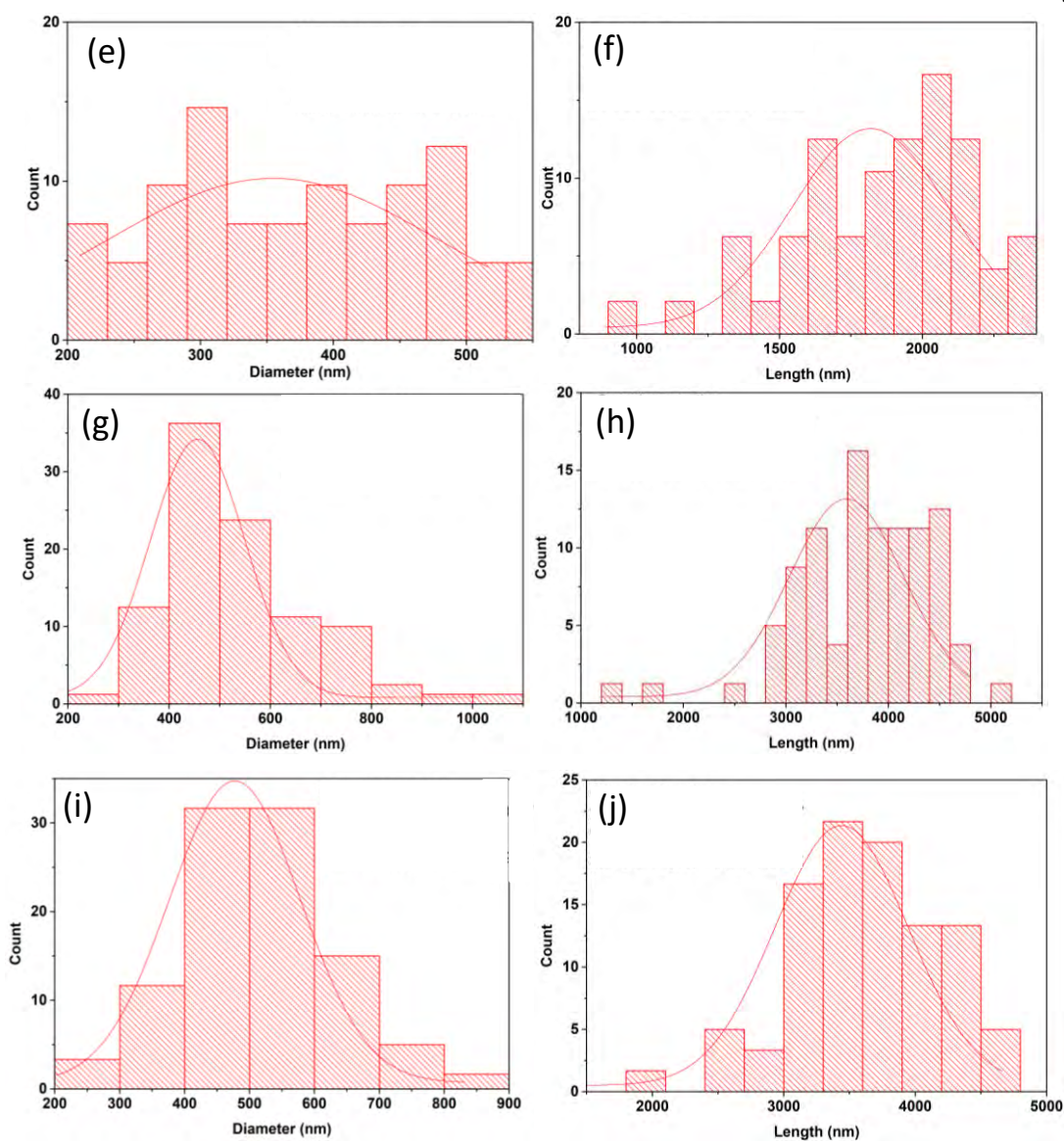


Fig. 4.21: Particle size distribution: Variation of (e, g, i) diameter and (f, h, j) length of the ZnO nanorods formed by heating an equimolar mixture of HMT and ZNH for (e) and (f) 10 min; (g) and (h) 20 min; (i) and (j) 30 min.

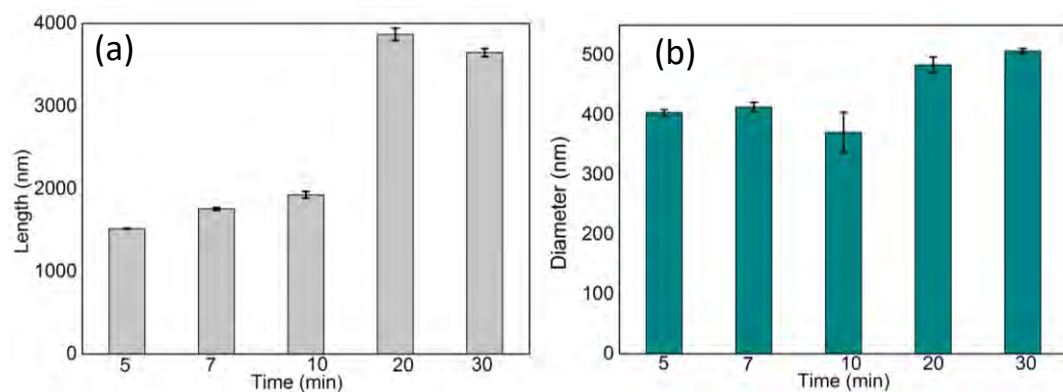


Fig. 4.22: The average (a) length and (b) diameter of ZnO nanorods formed by heating an equimolar mixture of HMT and ZNH for different synthesis time.

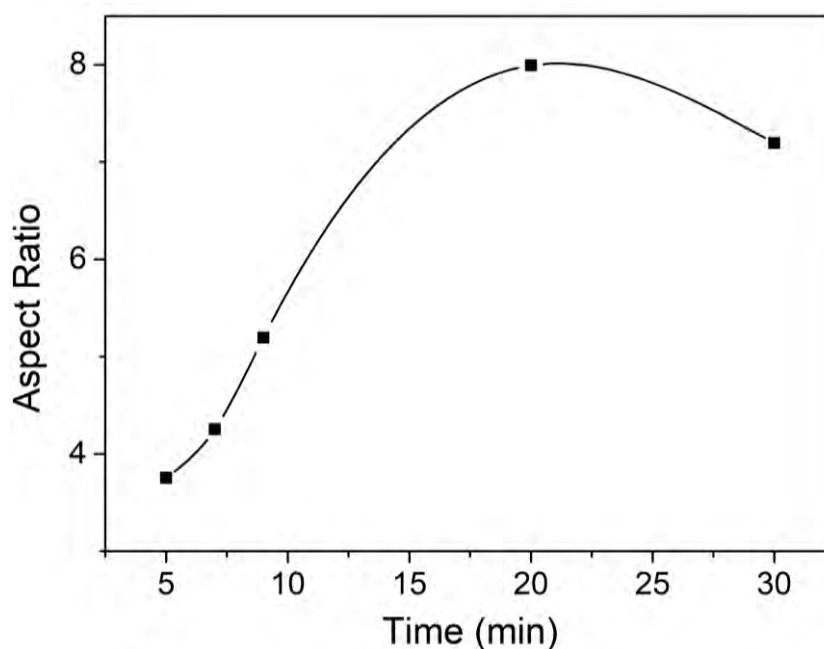


Fig. 4.23: Variation of aspect ratio with synthesis time.

4.1.5 Effect of surfactant

There is a clear change in morphology of the ZnO nanorods, when Triton-X is added as surfactant in the precursor solution. The distribution of ZnO nanorods is not homogenous and length of ZnO nanorods increases. Fig. 4.24 shows the SEM images of ZnO nanorods with different size and Table 4.1 summarizes the average length and diameter value of the ZnO nanorods. Optimum amount of surfactant may increase the aspect ratio of the synthesized nanorods.

Table 4.1: Average length and diameter of ZnO nanorods after adding surfactant.

Diameter, D (nm)	Length, L (nm)	Aspect ratio, L/D
1250	11000	8.8

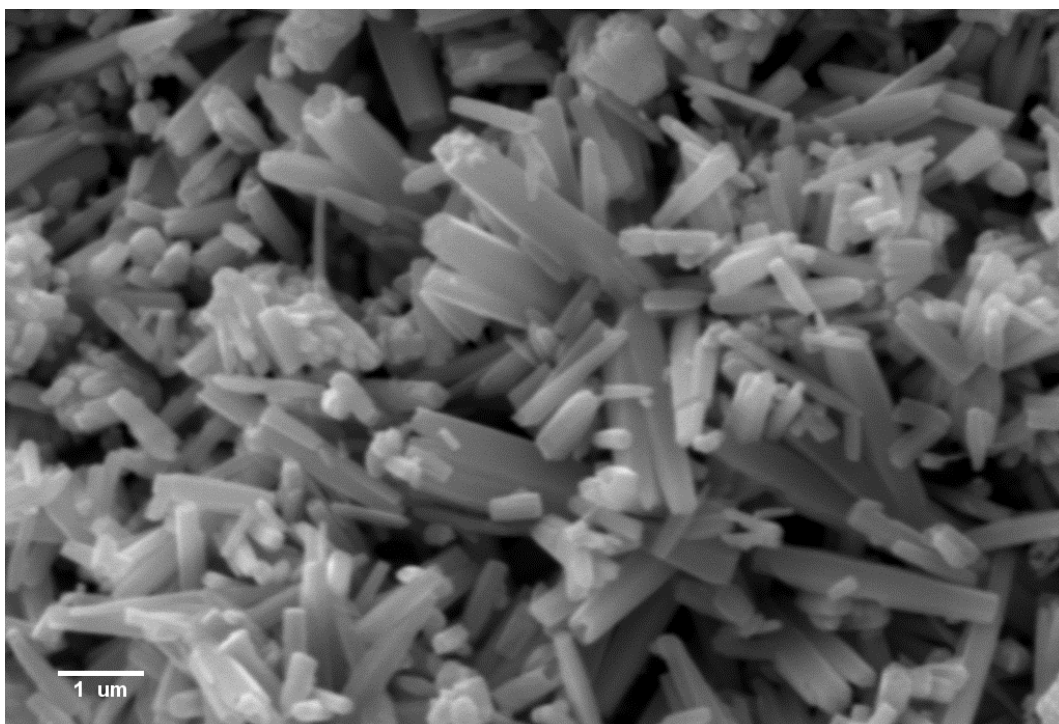


Fig. 4.24: Effect of addition of surfactant on the morphology of the ZnO nanorods.

4.1.6 Effect of heat treatment

ZnO nanorods are synthesized using 50% microwave irradiation with 15 mM precursor concentration and 20 min synthesis time and then sintered at the furnace to observe its effect on the size of the nanorods. From SEM images shown in Fig. 4.25, it is clear that the length of the ZnO nanorods increases with the sintering temperature up to 700 °C and forms nanobush instead of standalone nanorods. And, when the sintering temperature is gradually increased, the nanorods start to amalgamate with each other at a sintering temperature of 900°C. These SEM images of the sintered nanorods confirms the drastic change in the morphology of the synthesized ZnO nanorods with sintering temperature. Hence, it is discovered that the post synthesis temperature treatment is not a good option to obtain ZnO nanorods with high aspect ratio.

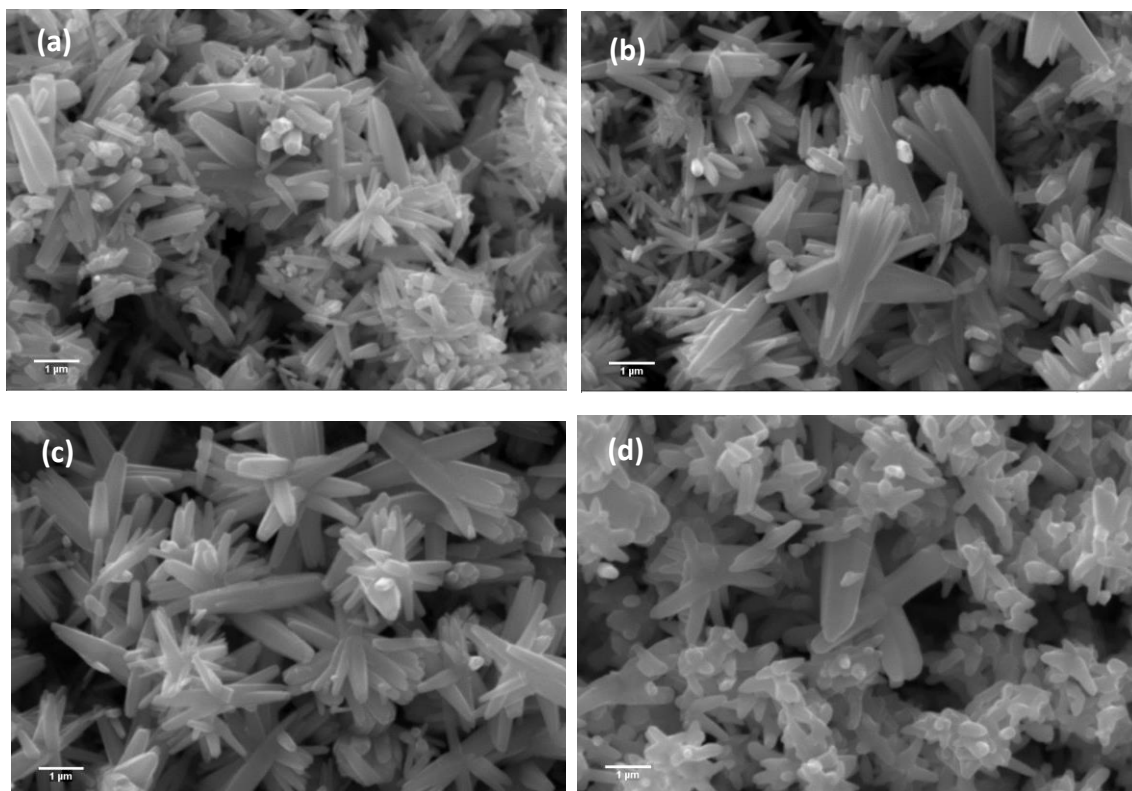


Fig. 4.25: Effects of heat treatment on the size of ZnO nanorods (a) as synthesized, and treated at (b) 500 °C (c) 700 °C (d) 900 °C.

4.2 Elemental Analysis

The elemental analysis revealed the presence of mainly Zn and O in the synthesized ZnO nanorods with no impurities. Fig. 4.26 shows the EDX pattern for ZnO nanorods synthesized using ZAH, with varying microwave power. All the samples have atomic percentage of Zn and O almost near the stoichiometric ratio [29].

Table 4.2: Elemental analysis of the nanorods produced using ZAH precursor with varying microwave power.

Precursor_MW_Conc._Time	Zn (at %)	O (at %)
ZAH_30%_50mM_20min	58.10	41.90
ZAH_50%_50mM_20min	59.37	40.63
ZAH_70%_50mM_20min	59.98	40.02

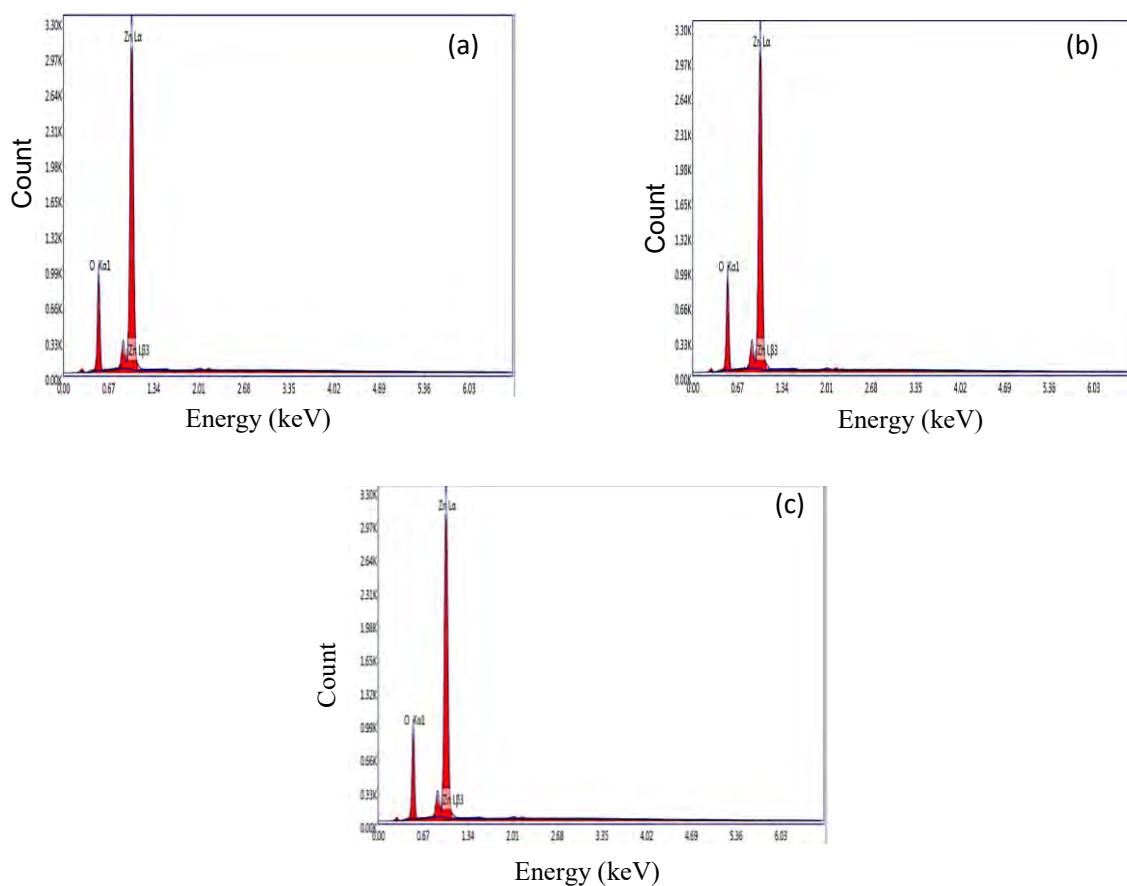


Fig. 4.26: EDX spectra of the ZnO nanorods synthesized using ZAH at (a) 30%, (b) 50% and (c) 70% microwave power.

Fig. 4.27 shows the EDX pattern for ZnO nanorods synthesized using ZNH and effect of variation of microwave power is summarized in Table 4.3. It is clear that, the ZnO nanorods synthesized at 50% microwave power provides the best result, regarding the standard stoichiometric ratio.

Table 4.3: Elemental analysis of the nanorods produced using ZNH precursor with different microwave power.

Precursor_MW_Conc._Time	Zn (at %)	O (at %)
ZNH_30%_50mM_20min	60.05	39.95
ZNH_50%_50mM_20min	58.67	41.33
ZNH_70%_50mM_20min	60.41	39.59

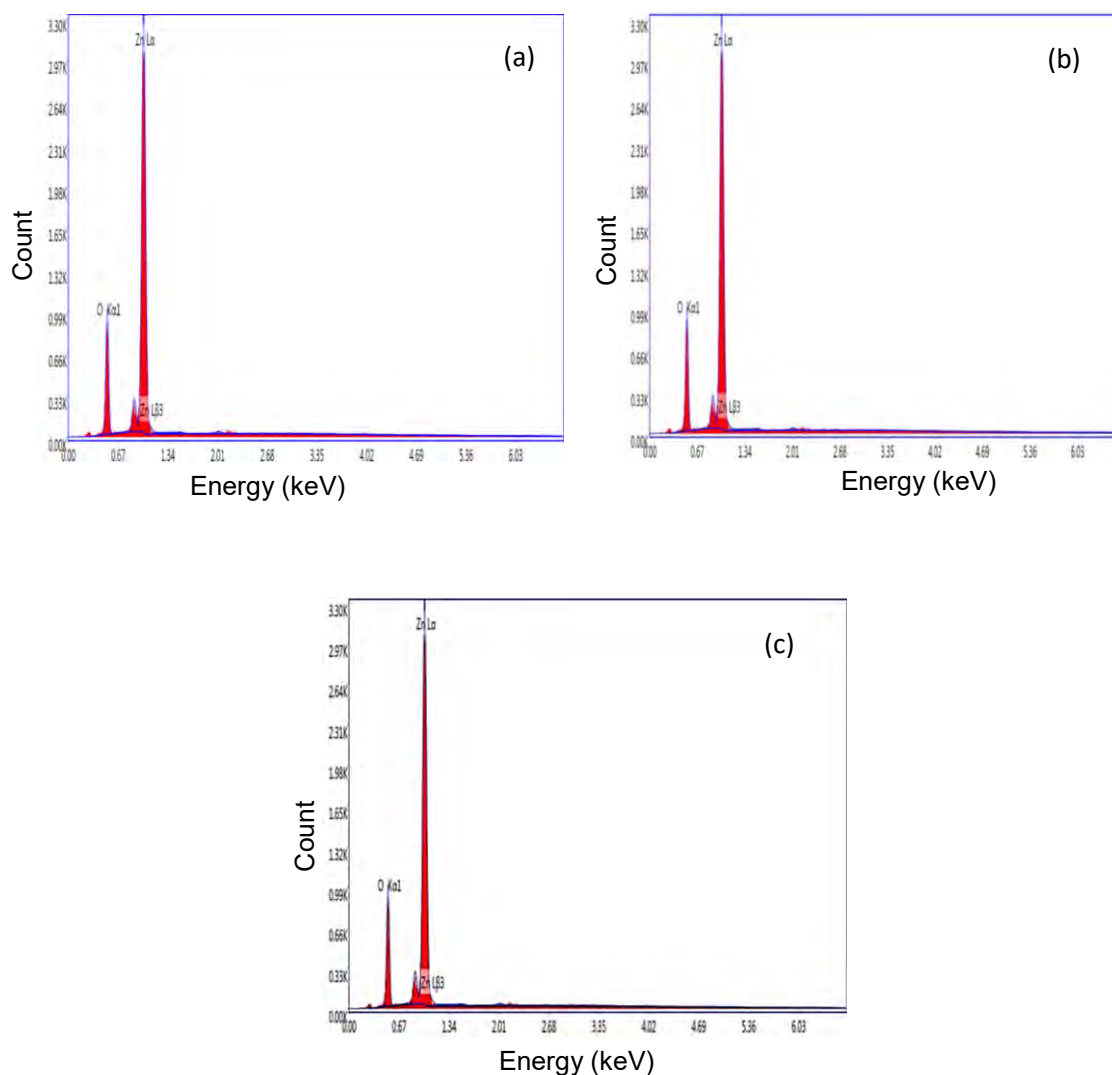


Fig. 4.27: EDX spectra of the ZnO nanorods synthesized using ZNH at (a) 30%, (b) 50% and (c) 70% microwave power.

Effect of synthesis time on the atomic percentage of Zn and O of the synthesized ZnO nanorods is shown in Fig. 4.28. All the data are summarized in Table. 4.4. It can be easily observed ZnO nanorods synthesize with synthesis time 7 min and 20 min have good stoichiometric ratio. No impurities were found in any sample and all the EDX pattern confirms the presence of Zn and O in the ZnO nanorods.

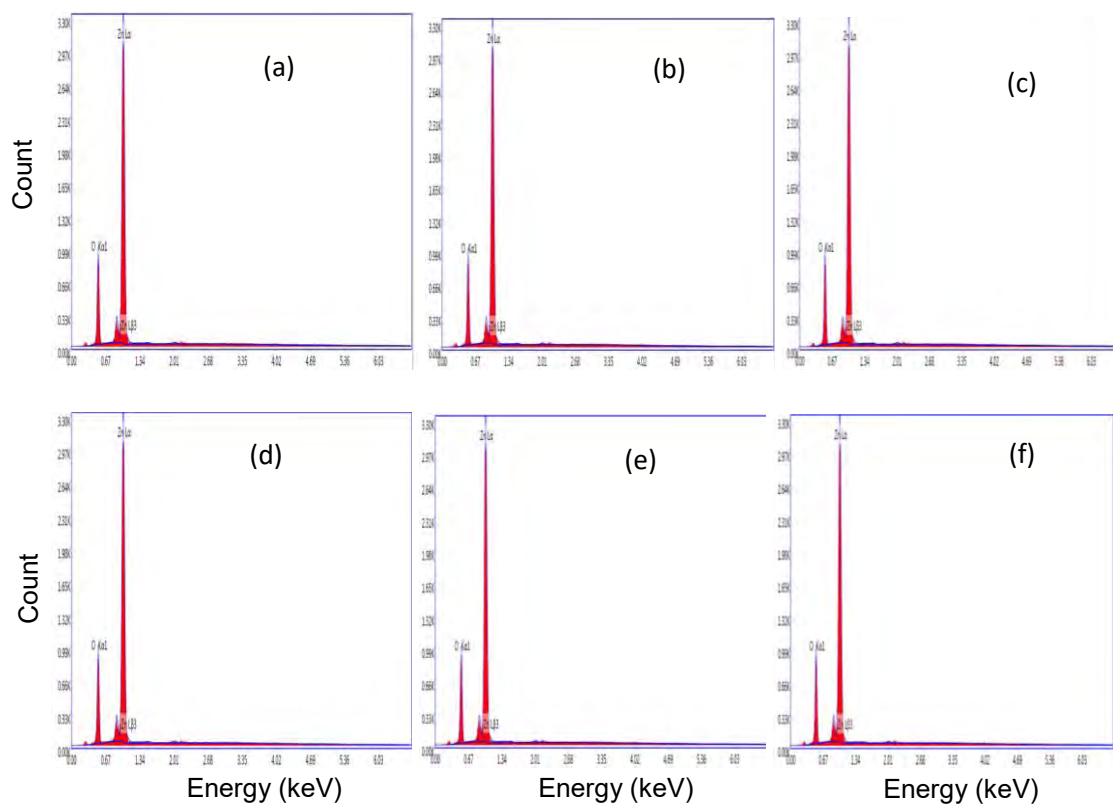


Fig. 4.28: Elemental analysis of the ZnO nanorods synthesized different synthesis time: (a) 5 min, (b) 7 min, (c) 10 min, (d) 15 min, (e) 20 min and (f) 30 min.

Table 4.4: Elemental analysis of the ZnO nanorods with varying synthesis time.

Precursor_MW_Conc._Time	Zn (at %)	O (at %)
ZNH_50%_15mM_5min	62.21	37.79
ZNH_50%_15mM_7min	59.16	40.84
ZNH_50%_15mM_10min	63.98	36.02
ZNH_50%_15mM_15min	67.50	32.50
ZNH_50%_15mM_20min	58.01	41.99
ZNH_50%_15mM_30min	60.27	39.73

4.3 Structural Property

The XRD spectra of the samples obtained with different precursor sources, precursor concentrations and synthesis duration are shown in Figs. 4.29 and 4.30. All the diffraction peaks are well matched with the hexagonal wurtzite structure of ZnO [JCPDS 36-1451] [27,28,46] and no diffraction peaks from impurities are detected.

XRD data gives information about samples in terms of peak position and intensity. The peak position is indicative of crystal structure. The peak intensity reflects the total scattering from each crystal planes, and depends on the distribution of atoms in the crystal structure. If crystalline nature increases, number of planes orientated in a particular direction increases and hence multiplicity increases, which lead to the increase in intensity. XRD spectra in Fig. 4.29 (a) shows that ZNH based ZnO nanorods have higher intensity of the (100), (002) and (101) diffraction peaks. SEM images also shows that ZnO nanorods synthesized using ZAH precursor are of larger sized compared to ZNH based ZnO nanorods. Larger sized ZnO nanorod may have larger number of crystal planes oriented in the same direction, that facilitates higher intensity of diffraction peaks.

The structural property also varies with precursor concentration. Fig. 4.29 (b) shows that, crystallinity increases with precursor concentration. This indicates that, strain and defects within the crystal reduces when the precursor concentration is increased gradually. As a result, there is an increase in diffraction peak intensity with precursor concentration when the other process parameters are kept fixed at optimum value.

Fig. 4.30 shows the XRD spectra for different synthesis time using ZNH precursor salt with a concentration of 15 mM. The intensity of the (100), (002) and (101) diffraction peaks increase with the synthesis time. It can be conjectured that longer synthesis time may have facilitated the reduction of defects within crystal. Also, the prolonged synthesis time provides the opportunity for the growth of larger number of oriented crystal planes to increase the total scattering from each crystal planes Overall, there is an increase in crystallinity with synthesis time could be observed from the XRD spectra.

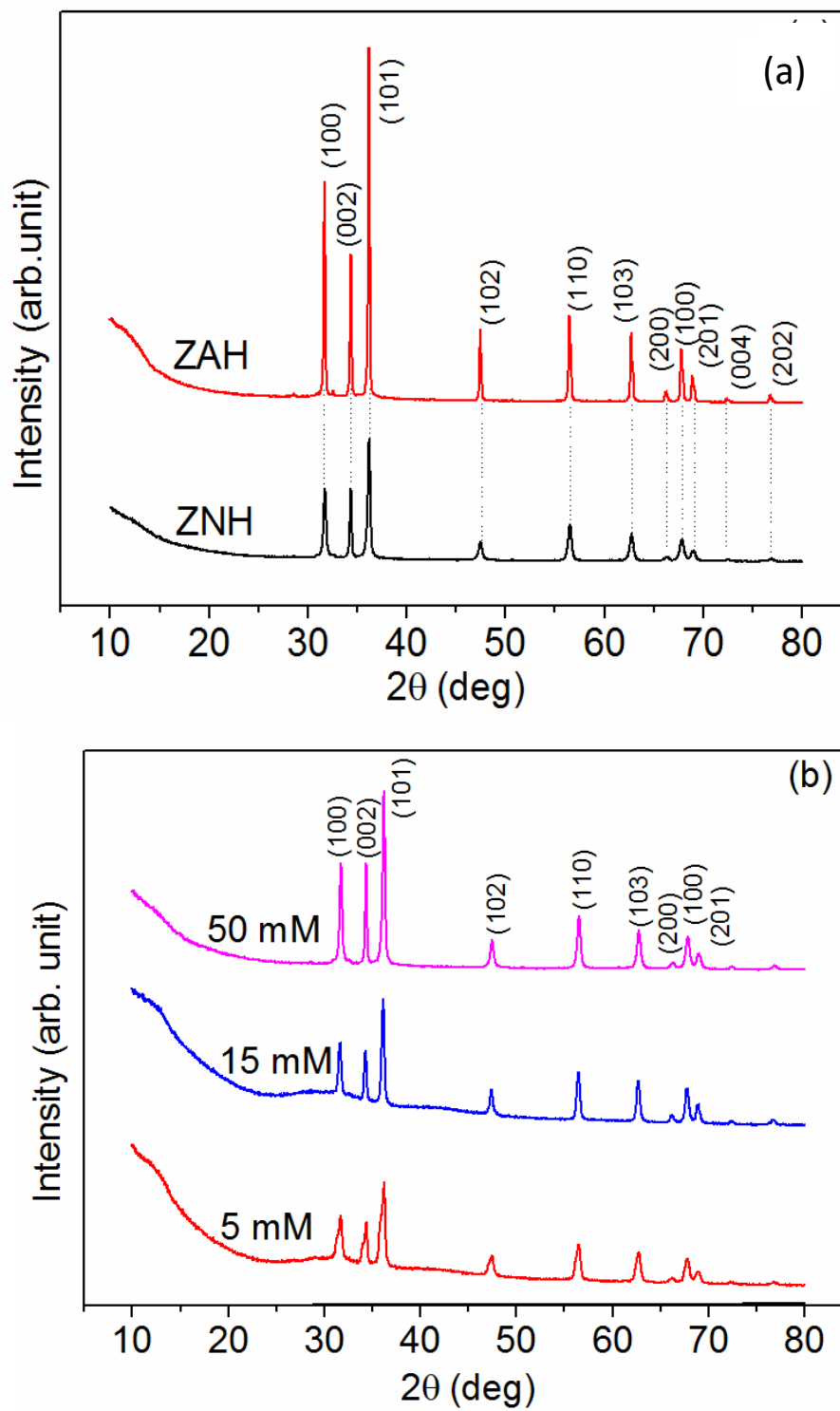


Fig. 4.29: XRD spectra of the ZnO nanorods synthesized (a) with different precursors, (b) at different concentrations.

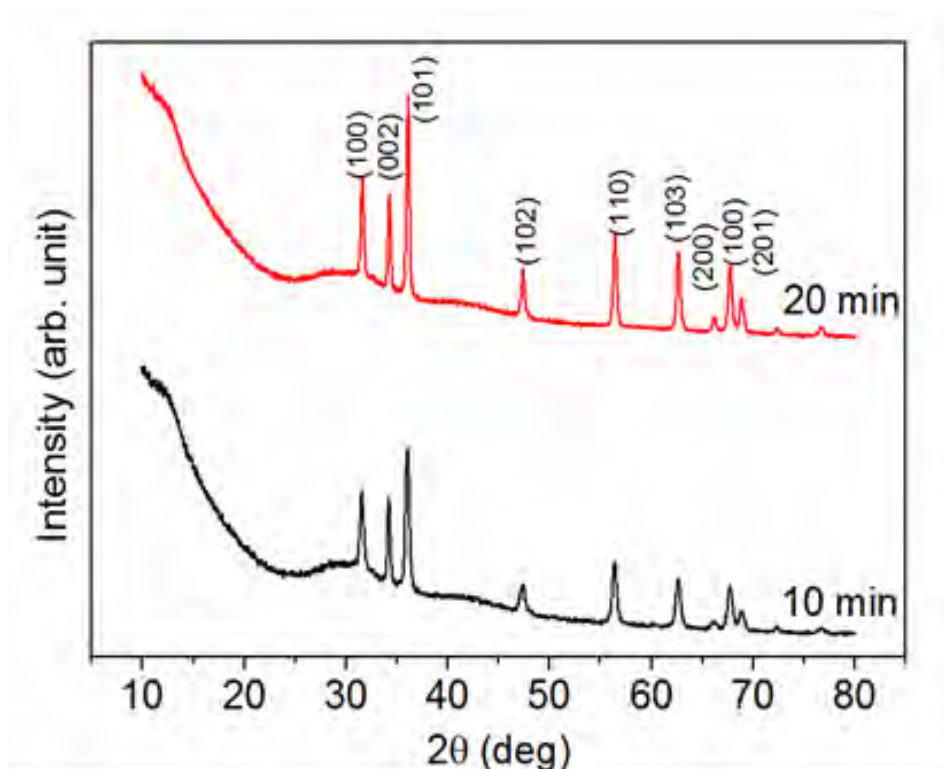


Fig. 4.30: XRD spectra of the ZnO nanorods synthesized for different synthesis time.

Table 4.5: Different structural parameters of the ZnO nanorods obtained from XRD studies.

Zinc Source	Molar Conc. (mM)	Synth. Time (min)	FWHM β ($^{\circ}$)	Lattice Parameter		Lattice strain ϵ_t
				a (\AA)	c (\AA)	
ZAH	50	20	0.187	3.25	5.22	0.143
ZNH	50	20	0.301	3.25	5.22	0.230
ZNH	15	20	0.338	3.27	5.23	0.223
ZNH	5	20	0.544	3.25	5.20	0.416
ZNH	15	10	0.435	3.27	5.24	0.334

To determine the crystal imperfection and distortion induced in the samples lattice strain (ε_l), which is caused by the varying displacement of the atoms with respect to their reference-lattice positions, is also calculated using the Williamson-Hall formula [28]:

$$\varepsilon_l = -\frac{\beta_{hkl}}{4 \tan \theta},$$

where θ and β have their usual significances. All the calculated values are listed in Table 4.5. It can be easily observed, the structural defects become lower in case of highly crystalline materials. Therefore, ZnO nanorods synthesized from ZAH precursor considered to have minimum strain.

4.4 Optical Property

The room temperature UV-vis absorption spectra of the ZnO nanorods synthesized with variation in microwave power, synthesis time, and precursor concentration are shown in Figs. 4.31 and 4.32. All the samples have wide strong absorption in the UV region. The absorption intensities for the ZnO nanorods with different microwave power are almost same, which is in agreement with the result obtained by Roza et al. [56].

The absorption intensity depends on the nanorod size, smaller particle size with lowest precursor concentration (5 mM) and shortest synthesis time (5 min) has higher intensity in absorption spectra. A slight blue shift in the absorption peak is also observed for ZnO nanorods synthesized from longer duration of heating of the precursor and higher precursor concentration, shown in Fig. 4.32. This result also supports the result reported in Ref. [20]. The absorption edge moves to a slightly higher energy, which could be attributed to the Burstein–Moss effect.

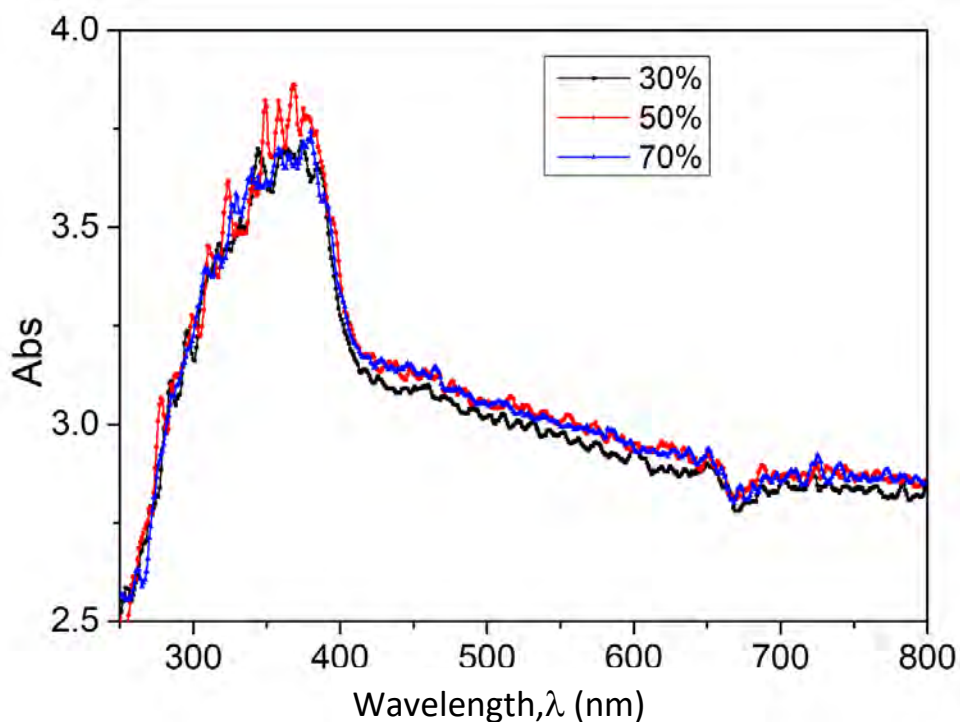


Fig. 4.31: UV-visible spectra of the ZnO nanorods obtained from different microwave powers.

In general, the generation of a Burstein–Moss shift depends upon the creation of a very high density of electrons (holes) in the conduction (valence) band such that the energy levels near the bottom of the band fill up. As a result, the Fermi energy level lies in the conduction band and all the energy levels below the Fermi level are occupied by electrons. In this situation an electron from the top of the valence band can only be excited into conduction band above the Fermi level, which involves higher energy. Consequently, there is a blue shift of the fundamental absorption edge [57]. As only the duration of synthesis time was elongated keeping the synthesis temperature (reaction conditions) same, a slight shift of absorption edge to a higher energy is observed as a result of some states close to the conduction band being populated. Gupta et al. [58] found a sharp absorption band-edge at 355 nm and the corresponding band gap value was calculated as 3.40 eV. Band gap value are calculated from absorption edge and Table 4.6 shows that all the samples have band gap near the standard value.

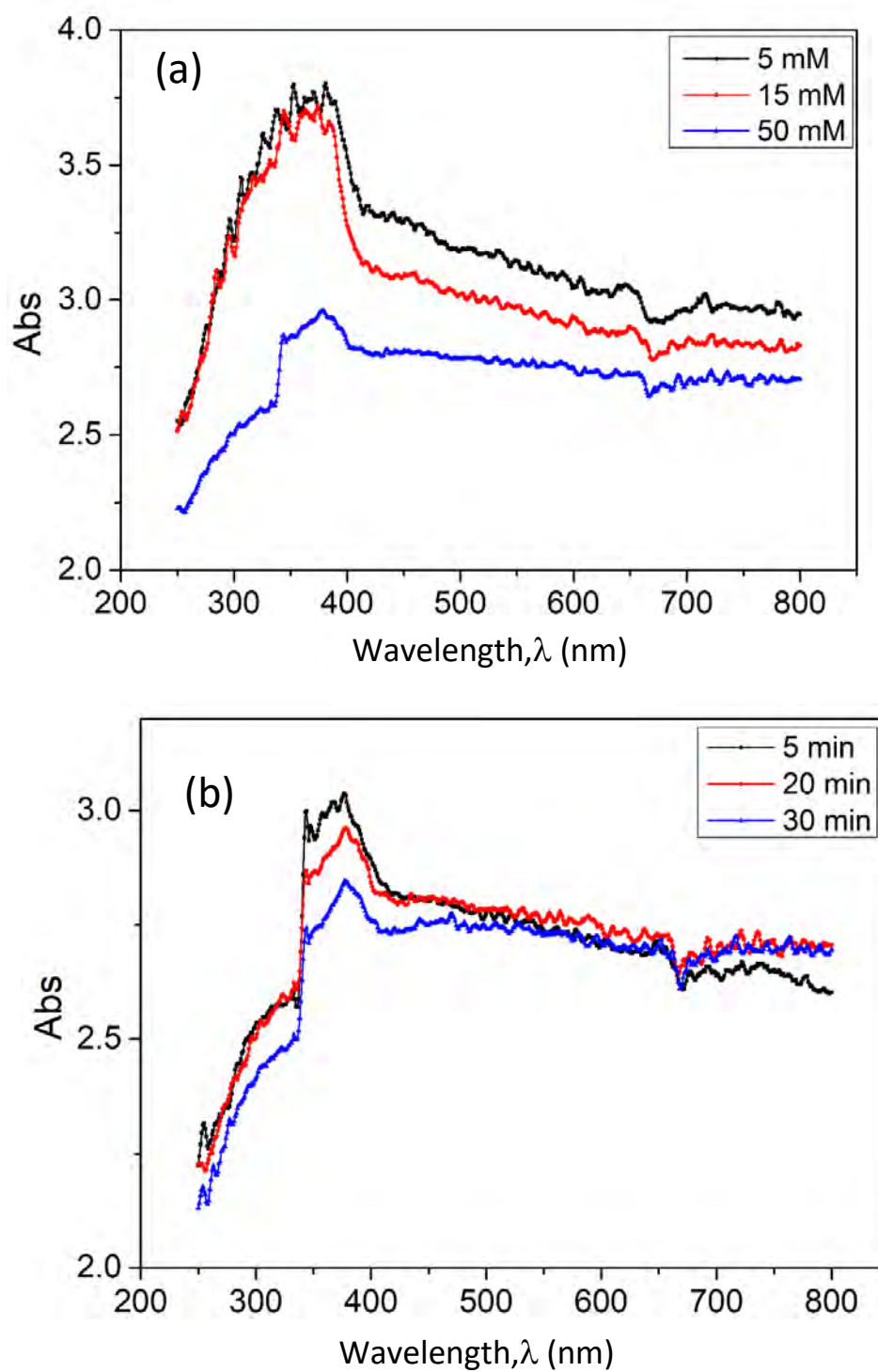


Fig. 4.32: UV-visible spectra of the ZnO nanorods obtained from different (a) precursor concentrations and (b) synthesis time.

Table 4.6: Energy band gap of the ZnO nanorods.

Sample	Absorption edge (nm)	Band gap (eV)
ZNH_70%_50 mM_20min	378	3.29
ZNH_50%_50 mM_20min	378	3.29
ZNH_50%_50 mM_20min	379	3.28
ZNH_70%_50 mM_20min	378	3.29
ZNH_50%_15 mM_20min	378	3.29
ZNH_50%_5 mM_20min	377	3.30
ZNH_50%_15 mM_30min	378	3.29
ZNH_50%_15 mM_20min	378	3.29
ZNH_50%_15 mM_5min	378	3.29

4.5 Dielectric Property

For dielectric measurement a tablet of 1.9 mm thickness and 12.45 mm diameter was prepared using a hydraulic press (MTI, YLJ-24, USA) with a pressure around 6 MPa. The prepared tablet was heat treated at 250° C for 2 hours to remove the PVA before measurement.

The dielectric constant is the ratio of the permittivity of a substance to the permittivity of free space. It is equal to the ratio of the capacitance of a capacitor filled with the given material to the capacitance of the same capacitor in vacuum without the dielectric material [43]. It is denoted by ϵ_r ,

$$\epsilon_r = \frac{C}{C_0}$$

$$C_0 = \frac{\epsilon_0 A}{d}$$

Where ϵ_0 is the permittivity in vacuum, 'A' and 'd' are the area and thickness of the dielectric, respectively.

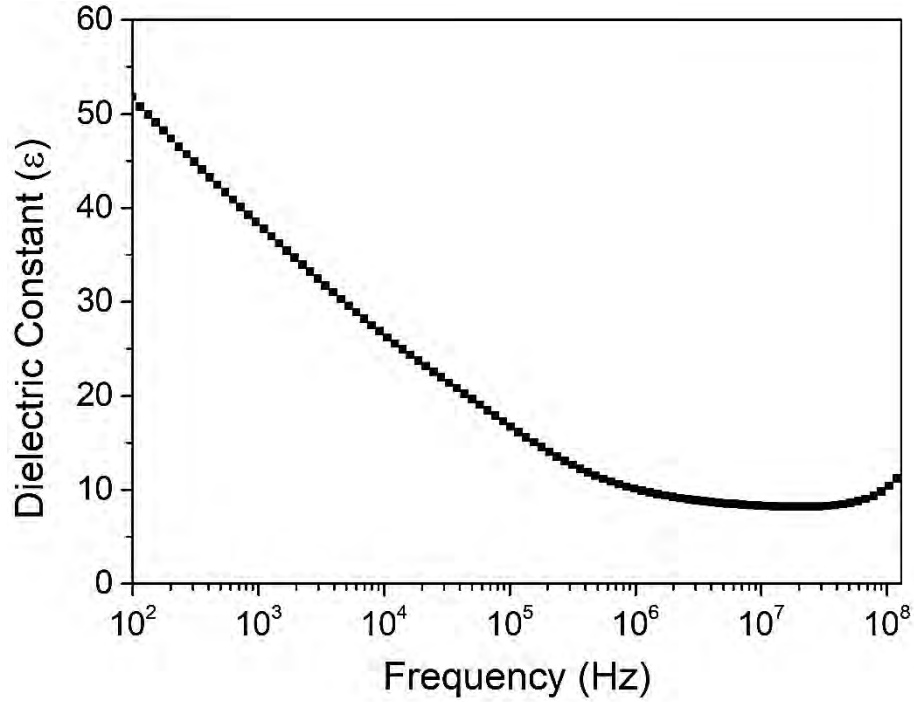


Fig. 4.33: Variation of dielectric constant of the ZnO nanorods with frequency.

The permittivity (ϵ) has the real and imaginary part such as,

$$\epsilon = \epsilon_r - j\epsilon_i$$

Where, ϵ_r and ϵ_i are the dielectric constant (relative permittivity) and dielectric loss factor. The ratio of the dielectric loss to the dielectric constant is known as loss tangent [59], which is calculated as,

$$\tan\delta = \frac{\epsilon_i}{\epsilon_r}$$

The nanorods has a high dielectric constant value at room temperature for lower frequency region which decreases with increasing frequency and attain a low constant value as shown in Fig. 4.33. The large value of dielectric constant of ZnO nanorods is a consequence of that, the nanoparticles of ZnO under the application of electric field act as a nano dipole. As the particle size is in nanometer order, the number of particles per unit volume is very large resulting in an increase in the dipole moment per unit volume and hence the high dielectric constant.

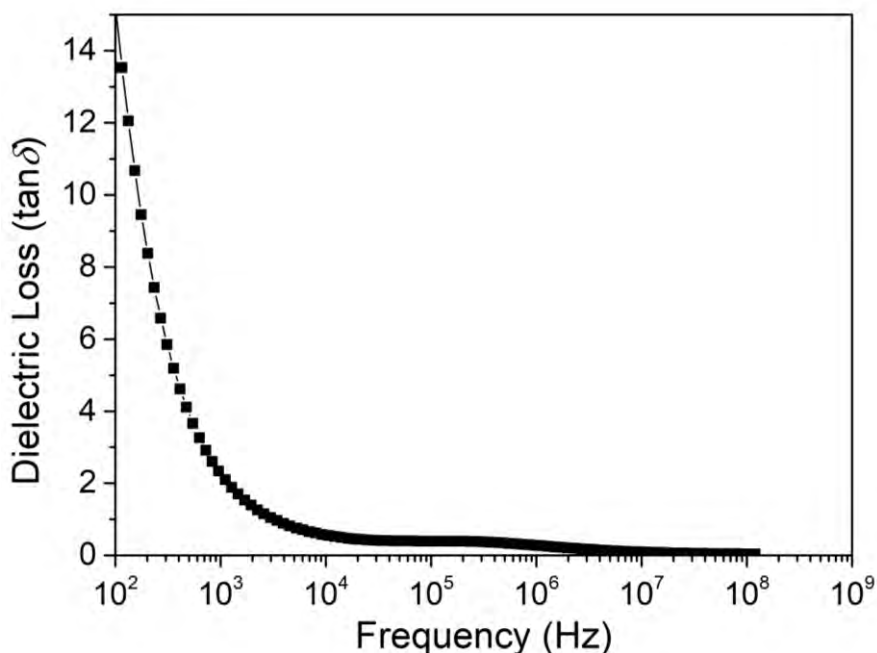


Fig. 4.34: Variation of dielectric loss of the ZnO nanorods with frequency.

However, at higher frequencies the nano dipoles fail to cope up with the rapid variation of the electric field and hence they show practically no dispersion which explains the exponential decrease in dielectric constant. Fig. 4.34 shows that dielectric loss also shows similar trend and it decreases to a very small value at higher frequencies. These results are in a well agreement with those reported by several research groups [60,61]. The high value of (ϵ) at low frequencies may be due to the presence of all the four polarizations namely space charge, orientation, electronic and ionic polarization and the low values at higher frequencies may be due to the loss of significance of these polarizations gradually. From the above studies it is observed that aspect ratio of the synthesized ZnO nanorods increases with precursor concentration (up to 15 mM) and synthesis time (up to 20 min). But there is a decrease in aspect ratio for higher precursor concentration and longer synthesis time. All samples have strong absorption in the UV region having a band gap between 3.19 and 3.30 eV. Maximum absorption edge depends on the size of the synthesized ZnO nanorods. Hexagonal wurtzite structure of is confirmed for all samples from the XRD spectra. The elemental analysis shows the presence of only Zn and O with atomic percentage almost near to the stoichiometric ratio.

CHAPTER 5

SUMMARY AND CONCLUSIONS

5.1 Summary

In this research work, a simple and low-cost route for the synthesis of ZnO nanorods has been reported. For that, a domestic microwave oven is customized for microwave assisted synthesis of ZnO nanorods.

Two different precursors (ZNH and ZAH) are employed to synthesize ZnO nanorods by varying the microwave power from 30% to 70% keeping the synthesis time and precursor concentration same. Maximum length of ZnO nanorods is obtained at 50% microwave power using ZAH precursor, whereas minimum diameter is also attained at 50% microwave power with ZNH precursor. It assumed that good length to diameter ratio could be attained at 50% microwave power.

It is observed that the synthesized nanorods are of hexagonal prismatic rod shaped, whose morphology and size depend strongly on the precursor sources. The nanorods formed by heating of equimolar HMTA and ZAH have an average diameter of 990 nm, which has been calculated from several SEM images and using Gaussian distribution of the measured diameters. The average diameter of the ZnO nanorods is observed to be reduced to about 300 nm when ZNH is used instead of ZAH as a precursor. The length to diameter aspect ratio of the ZnO nanorods is calculated to be 3.7 and 4.5, respectively for ZNH and ZAH precursors. Therefore, to observe the effect of molar concentration and synthesis time ZAH is chosen as the experimental precursor to produce further ZnO nanorods in this study.

The precursor concentration is varied from 5 to 50 mM, to discover the effect of precursor concentration. It is observed that when the concentration of the ZAH is increased from 5 to 50 mM, the average diameter and length varies respectively from 300 to 380 nm and from 1800 to 3500 nm. For the average length of the ZnO nanorods is observed to be reduced to 1200 nm when precursor concentration become high (50 mM). In this research, the maximum length of the ZnO nanorods is attained to be about 3100 nm at a precursor concentration of 15 mM, which is accompanied by an average diameter of about 390 nm, indicating a better aspect ratio of 7.9 for ZnO nanorods.

Synthesis time is also varied from 5 to 30 min for a constant precursor concentration (15 mM) to observe the effect of synthesis duration. It is observed that average length of the nanorods increases dramatically from about 1.5 to 4 μm and the average diameter varies nonlinearly from about 400 to 500 nm. The maximum average length of 4 μm is accompanied by an average diameter of about 480 nm, indicating a better aspect ratio of 8.3 for ZnO nanorods. It can be inferred for that 20 min is the optimum synthesis time for the 50% microwave power level and 15 mM precursor concentration.

Effect of sintering temperature is also observed and it is found that the length of the ZnO nanorod increases with sintering temperature. But, temperature treatment above 700 $^{\circ}\text{C}$ cause amalgamation of the nanorods.

The elemental analysis revealed the presence of mainly Zn and O in the synthesized ZnO nanorods with no impurities. All the samples have atomic percentage of Zn and O almost near the stoichiometric ratio.

All of the diffraction peaks in the XRD spectra indicates the hexagonal Wurtzite structure of the ZnO and no diffraction peaks from impurities are detected. It is observed that crystallinity of the ZnO nanorods increases with molar concentration and time.

Absorption intensity is related to the size of the ZnO nanorods. Smaller particle size facilitates higher absorption intensity within the UV region. A slight blue shift in the absorption peak is also observed for ZnO nanorods synthesized from longer duration of heating of the precursor and higher precursor concentration. The absorption edge moves to a slightly higher energy for prolonged synthesis time, which could be attributed to the Burstein–Moss effect. Energy band gaps for all the samples are observed to varies between 3.19 and 3.30 eV, which is well matched with the literature value.

The nanorods has a high dielectric constant value at room temperature in the lower frequency region, which decreases with increasing frequency and attain a low and constant value. The larger value of dielectric constant suggests that under the application of electric field the nanorods act as nano dipoles and larger the number of particles per unit volume higher the dipole moment per unit volume and hence higher the dielectric constant.

5.2 Conclusions

Hexagonal wurtzite structured ZnO nanorods with appropriate stoichiometric ratio are successfully synthesized with controlled size for different applications. The method is feasible for industrialization because it a very cheap and facile synthesis process to obtain ZnO nanorods within a very short time. Aspect ratio of the synthesized ZnO nanorods can be varied very easily with precursor concentration and synthesis time, therefore can be suitably used in water treatment and in gas sensors including antibacterial property-based purpose. All samples have strong absorption in the UV region having band gap around 3.37 eV, thus can be applicable as anti-UV agent in the textile industries and cosmetics sectors.

5.3 Future Scopes

- Research regarding the effect of variation of precursor concentration on synthesized nanorods may be studied in future.
- Basic precursors are used in this study. The addition of an appropriate surfactant or use of an efficient solvent to achieve higher aspect ratio of ZnO may be investigated.

References

- [1] Zhao, M., Wang, Z., and Mao, S. X., “Piezoelectric Characterization of Individual Zinc Oxide Nanobelt Probed by Piezoresponse Force Microscope,” *Nano Lett.*, vol. 4, pp. 587–590, 2004.
- [2] Lee, C. J., Lee, T. J., Lyu, S. C., Zhang, Y., Ruh, H., and Lee, H. J., “Field Emission From Well-Aligned Zinc Oxide Nanowires Grown at Low Temperature,” *Appl. Phys. Lett.*, vol. 81, pp. 3648–3650, 2002.
- [3] Comini, E., Faglia, G., Sberveglieri, G., Pan, Z., and Wang, Z. L., “Stable and Highly Sensitive Gas Sensors Based on Semiconducting Oxide Nanobelts,” *Appl. Phys. Lett.*, vol. 81, pp. 1869–1871, 2002.
- [4] Hughes, W. L., and Wang, Z. L., “Nanobelts as Nanocantilevers,” *Appl. Phys. Lett.*, vol. 82, pp. 2886–2888, 2003.
- [5] Grabowska, J., Nanda, K. K., McGlynn, E., Mosnier, J. P., Henry, M. O., Beaucamp, A., and Meaney, A., “Synthesis and Photoluminescence of ZnO Nanowires/Nanorods,” *J. Mater. Sci. Mater. Electron.*, vol. 16, pp. 397–401, 2005.
- [6] Grabowska, J., Nanda, K. K., McGlynn, E., Mosnier, J. P., and Henry, M. O., “Studying the Growth Conditions, the Alignment and Structure of ZnO Nanorods,” *Surf. Coat. Technol.*, vol. 200, pp. 1093–1096, 2005.
- [7] Ronning, C., Gao, P. X., Ding, Y., Wang, Z. L., and Schwen, D., “Manganese-Doped ZnO Nanobelts for Spintronics,” *Appl. Phys. Lett.*, vol. 84, pp. 783–785, 2004.
- [8] Grabowska, J., Meaney, A., Nanda, K. K., Mosnier, J. P., Henry, M. O., Duclère, J. R., and McGlynn, E., “Surface Excitonic Emission and Quenching Effects in ZnO Nanowire/Nanowall Systems: Limiting Effects on Device Potential,” *Phys. Rev. B - Cond. Matter Mater. Phys.*, vol. 71, pp. 1–7, 2005.
- [9] Xing, Y. J., Xi, Z. H., Xue, Z. Q., Zhang, X. D., Song, J. H., Wang, R. M., Xu, J., Song, Y., Zhang, S. L., and Yu, D. P., “Optical Properties of the ZnO Nanotubes Synthesized via Vapor Phase Growth,” *Appl. Phys. Lett.*, vol. 83, pp. 1689–1691, 2003.
- [10] Zheng, J. H., Jiang, Q., and Lian, J. S., “Synthesis and Optical Properties of Flower-Like ZnO Nanorods by Thermal Evaporation Method,” *Appl. Surf. Sci.*, vol. 257, pp. 5083–5087, 2011.
- [11] Kumar, S., Sahare, P. D., and Kumar, S., “Optimization of the CVD Parameters for ZnO Nanorods Growth: Its Photoluminescence and Field Emission Properties,” *Mater. Res. Bull.*, vol. 105, pp. 237–245, 2018.
- [12] Karaköse, E., and Çolak, H., “Structural and Optical Properties of ZnO Nanorods

- Prepared by Spray Pyrolysis Method,” *Energy*, vol. 140, pp. 92–97, 2017.
- [13] Worasawat, S., Masuzawa, T., Hatanaka, Y., Neo, Y., Mimura, H., and Pecharapa, W., “Synthesis and Characterization of ZnO Nanorods by Hydrothermal Method,” *Mater. Today Proc.*, vol. 5, pp. 10964–10969, 2018.
- [14] Sahoo, P., Sharma, A., and Thangavel, R., “Hydrothermal Synthesis, Structural and Optical Investigations of Undoped and Mg Doped ZnO Nanorods,” *AIP Conf. Proc.*, vol. 2100, 2019.
- [15] Napi, M. L. M., Sultan, S. M., Ismail, R., Ahmad, M. K., and Chai, G. M. T., “Optimization of a Hydrothermal Growth Process for Low Resistance 1D Fluorine-Doped Zinc Oxide Nanostructures,” *J. Nanomater.*, vol. 2019, 2019.
- [16] Zhao, X., Li, M., and Lou, X., “Sol-Gel Assisted Hydrothermal Synthesis of ZnO Microstructures: Morphology Control and Photocatalytic Activity,” *Adv. Powder Technol.*, vol. 25, pp. 372–378, 2014.
- [17] Jang, J. M., Kim, S. D., Choi, H. M., Kim, J. Y., and Jung, W. G., “Morphology Change of Self-Assembled ZnO 3D Nanostructures With Different pH in the Simple Hydrothermal Process,” *Mater. Chem. Phys.*, vol. 113, pp. 389–394, 2009.
- [18] Zhu, J., Zhang, J., Zhou, H., Qin, W., Chai, L., and Hu, Y., “Microwave-Assisted Synthesis and Characterization of ZnO-Nanorod Arrays,” *Trans. Nonferrous Met. Soc. China*, vol. 19, pp. 1578–1582, 2009.
- [19] Rana, A. U. H. S., Kang, M., and Kim, H. S., “Microwave-Assisted Facile and Ultrafast Growth of ZnO Nanostructures and Proposition of Alternative Microwave-Assisted Methods to Address Growth Stoppage,” *Sci. Rep.*, vol. 6, pp. 1–13, 2016.
- [20] Fang, M., and Liu, Z. W., “Controllable Size and Photoluminescence of ZnO Nanorod Arrays on Si Substrate Prepared by Microwave-Assisted Hydrothermal Method,” *Ceram. Int.*, vol. 43, pp. 6955–6962, 2017.
- [21] Chae, H. U., Rana, A. H. S., Park, Y.-J., and Kim, H.-S., “High-Speed Growth of ZnO Nanorods in Preheating Condition Using Microwave-Assisted Growth Method,” *J. Nanosci. Nanotechnol.*, vol. 18, pp. 2041–2044, 2017.
- [22] Tan, S. T., Umar, A. A., Yahaya, M., Yap, C. C., and Salleh, M. M., “Ultrafast Formation of ZnO Nanorods Via Seed-Mediated Microwave Assisted Hydrolysis Process,” *J. Phys. Conf. Ser.*, vol. 431, ArticleID: 012001, 2013.
- [23] Barreto, G. P., Morales, G., and Quintanilla, M. L. L., “Microwave Assisted Synthesis of ZnO Nanoparticles: Effect of Precursor Reagents, Temperature, Irradiation Time, and Additives on Nano-ZnO Morphology Development,” *J. Mater.*, vol. 2013, pp. 1–11, 2013.
- [24] Zhu, Z., Yang, D., and Liu, H., “Microwave-Assisted Hydrothermal Synthesis of ZnO Rod-Assembled Microspheres and Their Photocatalytic Performances,” *Adv.*

Powder Technol., vol. 22, pp. 493–497, 2011.

- [25] Brahma, S., Huang, J. -L., Liu, C. P., Kukreja, L. M., and Shivashankar, S. A., “Low Temperature and Rapid Deposition of ZnO Nanorods on Si (100) Substrate With Tunable Optical Emissions,” *Mater. Chem. Phys.*, vol. 140, pp. 634–642, 2013.
- [26] Dong, Z., Han, B., Qian, S., and Chen, D., “Fluorescent Properties of ZnO Nanostructures Fabricated by Hydrothermal Method,” *J. Nanomater.*, vol. 2012, ArticleID: 251276, 2012.
- [27] Bhat, D. K., “Facile Synthesis of ZnO Nanorods by Microwave Irradiation of Zinc-Hydrazine Hydrate Complex,” *Nanoscale Res. Lett.*, vol. 3, pp. 31–35, 2008.
- [28] Senthilkumar, N., Vivek, E., Shankar, M., Meena, M., Vimalan, M., and Potheher, I. V., “Synthesis of ZnO Nanorods by One Step Microwave-Assisted Hydrothermal Route for Electronic Device Applications,” *J. Mater. Sci. Mater. Electron.*, vol. 29, pp. 2927–2938, 2018.
- [29] Agarwal, S., Jangir, L. K., Rathore, K. S., Kumar, M., and Awasthi, K., “Morphology-Dependent Structural and Optical Properties of ZnO Nanostructures,” *Appl. Phys. A Mater. Sci. Process.*, vol. 125, pp. 1–7, 2019.
- [30] Alver, U., Kudret, A., and Kerli, S., “Influence of pH on Structural, Optical and Morphological Properties of ZnO Rod Arrays Fabricated by Hydrothermal Method,” *Optoelectron. Adv. Mater. Rapid Commun.*, vol. 6, pp. 107–109, 2012.
- [31] Kurda, A. H., Hassan, Y. M., and Ahmed, N. M., “Controlling Diameter, Length and Characterization of ZnO Nanorods by Simple Hydrothermal Method for Solar Cells,” *World J. Nano Sci. Eng.*, vol. 05, pp. 34–40, 2015.
- [32] Yuan, Z., Yu, J., and Jiang, Y., “Growth of Diameter-Controlled ZnO Nanorod Arrays by Hydrothermal Technique for Polymer Solar Cell Application,” *Energy Procedia*, vol. 12, pp. 502–507, 2011.
- [33] Lin, C. M., Cheng, N. J., Hung, S. C., and Li, Y. M., “Effect of Solution on One-Step Hydrothermal Growth of ZnO Nanorod Arrays and Its Application to Ultraviolet Photodetectors,” *J. Nano Res.*, vol. 40, pp. 46–57, 2016.
- [34] Majithia, R., Speich, J., and Meissner, K. E., “Mechanism of Generation of ZnO Microstructures by Microwave-assisted Hydrothermal Approach,” *Materials (Basel)*, vol. 6, pp. 2497–2507, 2013.
- [35] Ghosh, S., and Chakraborty, J., “Rapid Synthesis of Zinc Oxide Nanoforest: Use of Microwave and Forced Seeding,” *Mater. Res. Express*, vol. 3, pp. 1–9, 2016.
- [36] Pimentel, A., Nunes, D., Duarte, P., Rodrigues, J., Costa, F. M., Monteiro, T., Martins, R., and Fortunato, E., “Synthesis of Long ZnO Nanorods Under Microwave Irradiation or Conventional Heating,” *J. Phys. Chem. C*, vol. 118, pp. 14629–14639, 2014.

- [37] Garino, N., Limongi, T., Dumontel, B., Canta, M., Racca, L., Laurenti, M., Castellino, M., Casu, A., Falqui, A., and Cauda, V., "A Microwave-Assisted Synthesis of Zinc Oxide Nanocrystals Finely Tuned for Biological Applications," *Nanomater.*, vol. 9, pp. 1–17, 2019.
- [38] Yalcin, M., "Microwave-Assisted Synthesis of ZnO Nanoflakes: Structural, Optical and Dielectric Characterization," *Mater. Res. Exp.*, vol. 7, 2020.
- [39] Sadhukhan, P., Kundu, M., Rana, S., Kumar, R., Das, J., and Sil, P. C., "Microwave Induced Synthesis of ZnO Nanorods and Their Efficacy as a Drug Carrier With Profound Anticancer and Antibacterial Properties," *Toxicol. Reports*, vol. 6, pp. 176–185, 2019.
- [40] Liu, J., She, J., Deng, S., Chen, J., and Xu, N., "Ultrathin Seed-Layer for Tuning Density of ZnO Nanowire Arrays and Their Field Emission Characteristics," *J. Phys. Chem. C*, vol. 112, pp. 11685–11690, 2008.
- [41] Weintraub, B., Chang, S., Singamaneni, S., Han, W. H., Choi, Y. J., Bae, J., Kirkham, M., Tsukruk, V. V., and Deng, Y., "Density-Controlled, Solution-Based Growth of ZnO Nanorod Arrays Via Layer-By-Layer Polymer Thin Films for Enhanced Field Emission," *Nanotechnol.*, vol. 19, 2008.
- [42] Xu, S., Wei, Y., Liu, J., Yang, R., and Wang, Z. L., "Integrated Multilayer Nanogenerator Fabricated Using Paired Nanotip-to-Nanowire Brushes," *Nano Lett.*, vol. 8, pp. 4027–4032, 2008.
- [43] Sun, H., Luo, M., Weng, W., Cheng, K., Du, P., Shen, G., and Han, G., "Position and Density Control in Hydrothermal Growth of ZnO Nanorod Arrays Through Pre-Formed Micro/Nanodots," *Nanotechnol.*, vol. 19, 2008.
- [44] Zeng, H., Cui, J., Cao, B., Gibson, U., Bando, Y., and Golberg, D., "Electrochemical Deposition of ZnO Nanowire Arrays: Organization, Doping, and Properties," *Sci. Adv. Mater.*, vol. 2, pp. 336–358, 2010.
- [45] Izaki, M., Watanabe, M., Aritomo, H., Yamaguchi, Ippei Shunsuke, Asahina Shinagawa, Tsutomu Chigane, M., Inaba, M., and Tasaka, A., "Zinc Oxide Nano-Cauliflower Array with Room Temperature Ultraviolet Light Emission," *Cryst. Growth Desgn*, vol. 8, pp. 1418–1421, 2008.
- [46] Yu, L., Zhang, G., Li, S., Xi, Z., and Guo, D., "Fabrication of Arrays of Zinc Oxide Nanorods and Nanotubes in Aqueous Solution Under an External Voltage," *J. Cryst. Growth*, vol. 299, pp. 184–188, 2007.
- [47] Zheng, M. J., Zhang, L. D., Li, G. H., and Shen, W. Z., "Fabrication and Optical Properties of Large-Scale Uniform Zinc Oxide Nanowire Arrays by One-Step Electrochemical Deposition Technique," *Chem. Phys. Lett.*, vol. 363, pp. 123–128, 2002.
- [48] Vayssieres, L., "Growth of Arrayed Nanorods and Nanowires of ZnO from

- Aqueous Solutions,” *Adv. Mater.*, vol. 15, pp. 464–466, 2003.
- [49] Cheng, C., Yan, B., Wong, S. M., Li, X., Zhou, W., Yu, T., Shen, Z., Yu, H., and Fan, H. J., “Fabrication and SERS Performance of Silver-Nanoparticle-Decorated Si/ZnO Nanotrees in Ordered Arrays,” *ACS Appl. Mater. Interf.*, vol. 2, pp. 1824–1828, 2010.
- [50] Greene, L. E., Law, M., Goldberger, J., Kim, F., Johnson, J. C., Zhang, Y., Saykally, R. J., and Yang, P., “Low-Temperature Wafer-Scale Production of ZnO Nanowire Arrays,” *Angew. Chemie - Int. Ed.*, vol. 42, pp. 3031–3034, 2003.
- [51] Qin, Y., Wang, X., and Wang, Z. L., “Microfibre-Nanowire Hybrid Structure for Energy Scavenging,” *Nature*, vol. 451, pp. 809–813, 2008.
- [52] Bae, J., Song, M. K., Park, Y. J., Kim, J. M., Liu, M., and Wang, Z. L., “Fiber Supercapacitors Made of Nanowire-Fiber Hybrid Structures for Wearable/Flexible Energy Storage,” *Angew. Chem. - Int. Ed.*, vol. 50, pp. 1683–1687, 2011.
- [53] Xu, S., and Wang, Z. L., “One-Dimensional ZnO Nanostructures: Solution Growth and Functional Properties,” *Nano Res.*, vol. 4, pp. 1013–1098, 2011.
- [54] Yamabi, S., and Imai, H., “Growth Conditions for Wurtzite Zinc Oxide Films in Aqueous Solutions,” *J. Mater. Chem.*, vol. 12, pp. 3773–3778, 2002.
- [55] Thein, M. T., Pung, S. Y., Aziz, A., and Itoh, M., “The Role of Ammonia Hydroxide in the Formation of ZnO Hexagonal Nanodisks Using Sol–Gel Technique and Their Photocatalytic Study,” *J. Exp. Nanosci.*, vol. 10, pp. 1068–1081, 2015.
- [56] Roza, L., Fauzia, V., and Rahman, M. Y. A., “Tailoring the Active Surface Sites of ZnO Nanorods on the Glass Substrate for Photocatalytic Activity Enhancement,” *Surf. Interf.*, vol. 15, pp. 117–124, 2019.
- [57] Bashar, M. S., Matin, R., Sultana, M., Siddika, A., Rahaman, M., Gafur, M. A., and Ahmed, F., “Effect of Rapid Thermal Annealing on Structural and Optical Properties of ZnS Thin Films Fabricated by RF Magnetron Sputtering Technique,” *J. Theor. Appl. Phys.*, vol. 14, pp. 53–63, 2020.
- [58] Gupta, M. K., Sinha, N., Singh, B. K., Singh, N., Kumar, K., and Kumar, B., “Piezoelectric, Dielectric, Optical and Electrical Characterization of Solution Grown Flower-Like ZnO Nanocrystal,” *Mater. Lett.*, vol. 63, pp. 1910–1913, 2009.
- [59] Sharma, J., Chand, N., and Bapat, M. N., “Effect of Cenosphere on Dielectric Properties of Low Density Polyethylene,” *Results Phys.*, vol. 2, pp. 26–33, 2012.
- [60] Sakthivel, P., Fernandez, A. C., and Jesudurai, J., “Hydrothermal Synthesis of Zinc Oxide – Aluminium Oxide Nanocomposite,” *Nanocompos. Mater.*, vol. 50, pp. 10558–10560, 2012.

- [61] Yu, J., Wu, W., Dai, D., Song, Y., Li, C., and Jiang, N., “Crystal Structure Transformation and Dielectric Properties of Polymer Composites Incorporating Zinc Oxide Nanorods,” *Macromol. Res.*, vol. 22, pp. 19–25, 2014.